TÜRKİYE CUMHURİYETİ
ADANA ALPARSLAN TÜRKEŞ SCIENCE AND TECHNOLOGY UNIVERSITY

GRADUATE SCHOOL
BIOENGINEERING DEPARTMENT

ENGINEERING OF A NOVEL 3-DIMENSIONAL GLIOBLASTOMA CELL CULTURE SYSTEM

MERYEM DAMLA ÖZDEMİR

M.Sc.

ADANA 2022

TÜRKİYE CUMHURİYETİ
ADANA ALPARSLAN TÜRKEŞ SCIENCE AND TECHNOLOGY UNIVERSITY

GRADUATE SCHOOL
BIOENGINEERING DEPARTMENT

ENGINEERING OF A NOVEL 3-DIMENSIONAL GLIOBLASTOMA CELL CULTURE SYSTEM

MERYEM DAMLA ÖZDEMİR

M.Sc.

THESIS ADVISOR
ASSOC.PROF. DR. DİLEK GÖKTÜRK

SECOND ADVISOR
PROF. DR. GÖZDE BAYDEMİR PEŞİNT

ADANA, 2022

DECLARATION OF CONFORMITY TO SCIENTIFIC ETHICS

In this thesis study, which was prepared following the thesis writing rules of Adana Alparslan Türkeş Science and Technology University Institute of Graduate School, I declare that I provide all the information, documents, evaluations, and results in accordance with scientific ethics and moral codes without resorting to any means or assistance that would be contrary to scientific ethics and traditions. I also declare that I refer to all of the articles I used in this study with appropriate references and accept all moral and legal consequences if a situation is found contrary to my statement regarding my work.

12/12/2022

M. Damla ÖZDEMİR

ÖZET

YENİ BİR 3 BOYUTLU GLİOBLASTOMA HÜCRE KÜLTÜRÜ SİSTEMİNİN GELİŞTİRİLMESİ

M.Damla ÖZDEMİR

Yüksek Lisans, Biyomühendislik Anabilim Dalı

Danışman: Doç. Dr. Dilek GÖKTÜRK

II. Danışman: Prof. Dr. Gözde BAYDEMİR PEŞİNT

Aralık 2022, 79 sayfa

Glioblastoma (GBM) oldukça agresif, ölümcül ve kötü prognozludur. GBM için uygulanan tedaviler, tümörün istilacılığı ve heterojenliği nedeniyle sıklıkla başarısız olur. Ayrıca tedavinin ilerlemesini engelleyen, ilaç direnç mekanizmalarından sorumlu pek çok moleküler değişiklik vardır. Bu nedenle, bu mekanizmaların araştırılması ve GBM biyolojisinin anlaşılması, yeni tedaviler geliştirebilmek için çok önemlidir. 3D GBM hücre kültürü modelleri, GBM biyolojisini ve ilaç direnci mekanizmasını incelemek için kullanılabilir.

Bu çalışmada GBM'nin ilaç direnç mekanizmasını araştırmak ve tümör biyolojisini anlamak için yeni bir 3D GBM hücre kültürü modeli oluşturulması amaçlanmıştır. Bu amaçla pHEMA-jelatin esaslı kriyojeller, 3 farklı kriyojelasyon sıcaklığında (-12 ^{o}C, -16 ^{o}C ve -20 ^{o}C) ve 3 farklı jelatin konsantrasyonu ile (0.2g, 0.3g, 0.4g) başarıyla sentezlenmiştir. Kriyojeller için karakterizasyon çalışmaları ve in vitro hücre çalışmaları yapılmıştır. Yapılan analizlere göre sentezlenen kriyojellerin tamamı gözeneklilik, şişme özelliği ve biyouyumluluk açısından yapı iskelesi olarak kullanıma uygun bulunmuştur. GBM hücrelerinin ilaç yanıtlarını araştırmak için -16 ^{o}C'de 0,4 g jelatin konsantrasyonu ile sentezlenen pHEMA-jelatin bazlı kriyojel, en iyi hücre canlılık sonucunu verdiği için tercih edilmiştir. GBM hücrelerinin, in vivo koşullara benzer şekilde, 2D kültürlenmiş hücrelere göre ilaçlara karşı daha fazla direnç gösterdiği görülmüştür.

Anahtar Kelimeler: 3D hücre kültürü, Glioblastoma, Kriyojel doku iskelesi, Jelatin, pHEMA.

ABSTRACT

ENGINEERING OF A NOVEL 3-DIMENSIONAL GLIOBLASTOMA CELL CULTURE SYSTEM

M.Damla ÖZDEMİR

M.Sc., Department of Bioengineering

Supervisor: Assoc. Prof. Dr. Dilek GÖKTÜRK

Co-Supervisor: Prof. Dr. Gözde BAYDEMİR PEŞİNT

December 2022, 79 pages

Glioblastoma (GBM) is considerably aggressive, lethal, and has a poor prognosis. The therapies applying for GBM often fail because of the invasiveness and heterogeneity of the tumor. In addition, there are many molecular alterations responsible for the drug resistance mechanisms that hinder the success of treatment. Therefore, investigating these mechanisms and understanding GBM biology is crucial for developing new treatments. 3D GBM cell culture models can be used to study GBM biology and drug resistance mechanism.

In this study, it is aimed to establish a novel 3D GBM cell culture model to investigate the drug resistance mechanism and to understand the tumor biology of GBM. For this purpose, pHEMA-gelatin-based cryogels were synthesized at 3 different cryogelation temperatures (-12 ^{o}C, -16 ^{o}C, and -20 ^{o}C) and with 3 different gelatin concentrations (0.2g, 0.3g, 0.4g). The characterization studies of cryogels and in vitro cell studies were performed. According to the analyses performed, all of the synthesized cryogels were found suitable for use as scaffolds in terms of porosity, swelling characteristics, and non-cytotoxicity. To investigate the drug responses of GBM cells, a pHEMA-gelatin-based cryogel synthesized at -16 ^{o}C with 0,4 g gelatin concentration was preferred because it gave the best cell viability results. It was observed that the GBM cells showed greater resistance to drugs than 2D cultured cells, similar to in vivo conditions.

Keywords: 3D cell culture, Cryogel tissue scaffold, Gelatin, Glioblastoma, pHEMA.

Dedication

For my lovely nephew who is the next engineer of my family

ACKNOWLEDGEMENTS

I would first like to express my deepest gratitude to my supervisors; Assoc. Prof. Dr. Dilek GÖKTÜRK and Prof. Dr. Gözde BAYDEMİR PEŞİNT. The doors to their offices were always open whenever I ran into a trouble spot or had a question about my research or writing. They consistently assured me that the paper was my own work but steered me in the right direction whenever they thought I needed it. Their kind discussion and suggestions made it possible for my thesis work to be well-appointed.

I am grateful to the juries for agreeing to be the members of the jury for my thesis.

I would like to declare my thanks to Assoc. Prof. Dr. Sibel ÖZDAŞ who provided me with materials and equipment during my thesis work.

I also would like to express my gratitude to my colleague Res. Asst. Okan ZENGER who helped me with the cryogel synthesis.

My sincere thanks also go to all academicians at ATU Bioengineering department who do not spare their support whenever I need them.

Last but not least; I would like to thank my family; my parents and all of my family members for supporting me spiritually throughout the writing of this thesis and over my life in general. I would like to express my special thanks to my lovely parents, sister and fiancé for their endless love, faith and encouragement that helped me, continually, to move forward. This accomplishment would not have been possible without them.

TABLE OF CONTENTS

CERTIFICATION OF APPROVAL Hata! Yer işareti tanımlanmamış.
DECLARATION OF CONFORMITY TO SCIENTIFIC ETHICS **i**
ÖZET **ii**
ABSTRACT **iii**
Dedication **iv**
TABLE OF CONTENTS **vi**
LIST OF FIGURES **viii**
LIST OF TABLES **x**
LIST OF ABBREVIATION **xi**
LIST OF NOMENCLATURE **xii**
1. INTRODUCTION **1**
2. THEORETICAL FOUNDATIONS AND LITERATURE REVİEW **4**
2.1. Gliomas and Glioblastoma 4
2.1.1 Diagnosis and treatment of GBM 5
2.1.2 Genetics and subtypes of GBM 7
2.1.3 Tumor microenvironment of GBM and immune escape 13
2.1.4 Angiogenesis, invasion, and apoptosis in GBM 17
2.2. Tissue Engineering and Scaffolds 20
2.2.1 Chemical composition and production techniques of scaffolds 23
2.2.1.1 Cryogelation 28
2.2.1.2 pHEMA 30
2.2.1.3 Gelatin 31
2.2.2 3D cell cultures and tumor models 32
3. METHODOLOGY **40**
3.1. Synthesis And Characterization of pHEMA-Gelatin Cryogels 40
3.1.1. Chemical structure analyses 41
3.1.2. Morphology analyses 42
3.1.3. Swelling ratio and porosity assay 42
3.1.4. Polymerization yield 42
3.2. In Vitro Cell Studies 43
3.2.1. Cells and culture conditions 43

3.2.2. Sterilization of Scaffolds 43
3.2.3. Cytotoxicity Assay 43
3.2.4. Cell attachment analysis 44
3.2.5. Migration assay 44
3.2.6. Drug response assay 45
3.3. Statistical Analyses 47
4. ANALYSIS AND DISCUSSION 48
4.1. Synthesis and Characterization of pHEMA-Gelatin Cryogels 48
4.1.1. Chemical structure analyses 48
4.1.2. Morphology Analyses 49
4.1.3. Swelling ratio and porosity assay 52
4.1.4. Polymerization yield 55
4.2. In Vitro Cell Studies 55
4.2.1. Cytotoxicity Assay 55
4.2.1.1. Direct cytotoxicity 55
4.2.1.2. Indirect cytotoxicity 58
4.2.2. Cell attachment 58
4.2.3. Migration assay 61
4.2.4. Drug response assay 62
5. CONCLUSION 67
REFERANCES 68
APPENDİX
CURRICULUM VITAE

LIST OF FIGURES

Figure 2.1. The list of the several gene mutations detected in GBM……..…8
Figure 2.2. Genetic alterations leading to GBM carcinogenesis……..……...10
Figure 2.3. Successive genetic alterations detected in the pathogenesis of various glioblastoma subtypes……...11
Figure 2.4. The immune cells participated GBM tumor microenvironment..... 14
Figure 2.5. Potential Lineage Associations for Formation and ontogeny of Brain Cancer-Propagating Cells (BCPCs), and production of Glioblastoma (GBM) Tumors..... 17
Figure 2.6. The migration routes of GBM tumor cells……..….19
Figure 2.7. The condition of proteins involved in the apoptotic process in GBM. 20
Figure 2.8. Some of the biomaterials used in scaffold production…….……24
Figure 2.9. The schematic representation of cryogelation process 29
Figure 2.10. The chemical structure of HEMA..... 31
Figure 2.11. In 2D cell culture systems, cells adhere to the surface of a plastic or glass petri dish and therefore cell-cell and cell-environment interactions is restricted, while the 3D cell culture system provides rich interactions……..……...33
Figure 2.12. A general overview of 3D cell culture models; (A) scaffold-based model which depends on an extrinsic supporting material, (B) scaffold-free model that cells are grown self-assembly as spheroids or clusters, and (C) hybrid model……...……..36
Figure 3.1. The methods applied in this study. 40
Figure 3.2. GBM cells were cultured as hanging drop, 2D, and 3D for migration assay. 45
Figure 3.3. The schematic representation of 24 well plates 46
Figure 4.1. The optical photographs of synthesized pHEMA-gelatin-based cryogels..... 48
Figure 4.2. The FTIR spectra of cryogels coded as 162, 163 and 164…….49
Figure 4.3. The SEM images of pHEMA-gelatin based cryogels……50
Figure 4.4. The pore sizes of cryogels determined by the ImageJ software 51
Figure 4.5. The optical photographs of synthesized pHEMA-gelatin-based cryogels. 52
Figure 4.6. The swelling ratio of pHEMA-gelatin-based cryogels 53
Figure 4.7. The viabilities (%) of MEF cells seeded as 2D (control) and seeded onto pHEMA-gelatin based cryogel scaffolds (202, 203, 204, 122,123, 124, 162, 163, 164) according to neutral red assay results…….……..…56
Figure 4.8. The viabilities (%) of GBM cells seeded as 2D (control) and seeded onto pHEMA-gelatin based cryogel scaffolds (202, 203, 204, 122,123, 124, 162, 163, 164) according to neutral red assay results…….……..…57
Figure 4.9. The indirect cytotoxicity assay results of pHEMA-gelatin based cryogel scaffold coded as 164 on MEF cells……..……58
Figure 4.10. The SEM images of one day cultured GBM cells on pHEMA-gelatin based cryogels. 59
Figure 4.11. The SEM images of GBM cells cultured on cryogel coded as 164. 60
Figure 4.12. The DAPI staining images of GBM cells cultured on cryogel coded as 164. 61
Figure 4.13. The DAPI satining images of one day cultured cells for migration assay…….. 62

Figure 4.14. The neutral red cell viability assay results of (a) temozolomide and (b) etoposide given cells..... 62
Figure 4.15. The neutral red cell viability assay results of temozolomide and etoposide given cells ...……...…63
Figure 4.16. The DAPI staining images of one day cultured GBM cells with etoposide and temozolomide..... 65

LIST OF TABLES

Table 2.1. The features of primary and secondary glioblastoma 9
Table 2.2. GBM subtypes and genetic markers 12
Table 2.3. The cell types presented in the GBM tumor microenvironment 13
Table 2.4. The immune system factors included in TME of GBM 15
Table 2.5. The features of an ideal tissue scaffold 22
Table 2.6. The advantages and disadvantages of natural and synthetic biomaterials used in production of scaffolds 25
Table 2.7. Conventional techniques that used for tissue scaffold production 26
Table 2.8. Rapid prototyping techniques that used for tissue scaffold production 27
Table 2.9. Various applications for cryogels 30
Table 2.10. The important characteristics of 2D and 3D cell cultures 34
Table 2.11. Certain studies about 3D GBM cell culture 38
Table 3.1. The temperatures and the gelatin quantities of cryogels. 41
Table 4.1. Calculated swelling ratio, swelling degree, macroporosity and polymerization yield values of cryogels. 54

LIST OF ABBREVIATION

pHEMA	: Poly (2-Hydroxyethyl Methacrylate)
GBM	: Glioblastoma
MEF	: Mouse Embryonic Fibroblast
TMZ	: Temozolomide
FTIR	: Fourier Transform Infrared Spectroscopy
SEM	: Scanning Electron Microscopy
PBS	: Phosphate-Buffered Saline
DMEM	: Dulbecco's Modified Eagle's Medium
FBS	: Fetal Bovine Serum
NR	: Neutral Red Cell Viability Assay
2D	: 2 Dimensional
3D	: 3 Dimensional
IC_{50}	: Half-Maximal Inhibitory Concentration
DAPI	: 4',6-diamidino-2-phenylindole, dihydrochloride

LIST OF NOMENCLATURE

μL	: Microliter
mL	: Milliliter
μM	: Micromolar
Min	: Minute
mm	: Milimeter
m_d	:Dry Weight Of Cryogels
m_w	: Wet Weight Of Cryogels
m_s	: Squeezed Weight Of Cryogels
m_t	: Total Monomer Mass Of Cryogels

1. INTRODUCTION

Cancer became the leading cause of death in this era. Research conducted by the World Health Organization (WHO) on 36 types of cancer in 185 countries revealed that there were 19 292 789 cancer cases and 9 958 133 cancer-related deaths in 2020. 308 102 of these cancer cases were brain and central nervous system cancers, and 251 329 people died due to brain and central nervous system cancers in 2020 (Sung et al., 2021). Malignant gliomas which are the tumors of the Central Nervous system constitute 2.5% of worldwide cancer deaths. Glioblastoma (GBM) is comprised the 50% of all gliomas and sorted as grade IV glioma by WHO (Behnan, Finocchiaro, & Hanna, 2019; Silantyev et al., 2019; Xiong et al., 2019). GBM is counted as one of the most lethal types of cancer with a worldwide frequency of 3-10 per 100,000 people in a year (Bailly et al., 2019; Korbecki et al., 2018). GBM is characterized by being highly invasive, vascular, and heterogenic and having a very poor prognosis (Caspani, Crossley, Redondo-Garcia, & Martinez, 2014; Logun et al., 2016). Patients having GBM are usually treated by surgical resection in combination with radiotherapy or chemotherapy (Korbecki et al., 2018). However, the surgical and medical treatments of GBM have not enough effectiveness due to reasons such as the heterogeneity, and the invasiveness of the tumor (Caspani et al., 2014; Cenciarini et al., 2019). GBM gains resistance to therapy because of the several molecular alterations and many factors such as unrestrained cellular proliferation, vascularization, migration, and contribution of cancer stem-like cells (Cenciarini et al., 2019; Elkamhawy et al., 2015; Taylor, Brzozowski, & Skelding, 2019). Thus, it is of vital importance to develop novel approaches to be able to fight this lethal tumor.

Initially, 2D cell culture models were used in cancer studies.The 2D model, however, is insufficient to understand molecular changes in tumors and identify the mechanisms of chemo-resistances. The 3D model has gained popularity as an option for cancer studies (Chaicharoenaudomrung, Kunhorm, & Noisa, 2019; Langhans, 2018). When compared to 2D models, 3D models have many advantages. In comparison to 3D cell culture, 2D is simpler, less expensive, offers higher performance, and requires less time to complete. However, the tissue matrix, which is known to control tumor growth, is absent in 2D culture. The cells in the monolayer have unfettered access to the medium's components because the 2D model does not account for a diffusion gradient of medicines, oxygen, nutrients, and wastes. Due to

the organic nature of the tumor mass, the availability of oxygen, nutrients, metabolites, and signal molecules for cancer cells in vivo is more variable. It is possible to create a diffusion gradient with a 3D cancer cell culture model that offers cells a microenvironment similar to that found in vivo (Chaicharoenaudomrung et al., 2019; Kapałczyńska et al., 2018). Additionally, the cancer cells in 3D culture have similar drug resistance characteristics to the cancer cells in vivo. As a result, the 3D cell culture model allows for the in vitro replication of a number of variables influencing the in vivo effectiveness of anti-cancer medications (Chaicharoenaudomrung et al., 2019; Lovitt, Shelper, & Avery, 2014).

The 3D cell culture can be implemented using a scaffold. There are various ways to create different scaffolds utilizing synthetic or natural biomaterials (Zhu & Chen, 2013). Among these methods, the recently developed cryogelation method is very popular. Cryogel tissue scaffolds with macroporous morphology and tunable pore diameter, which are recognized in tissue engineering and regenerative medicine, can be synthesized using the cryogelation method (Kao, Kuo, Chen, & Chen, 2019). Cryogels find their place in many tissue engineering applications as tissue scaffolds because they have important properties such as a highly porous structure, pore interconnectivity, mechanical stability and flexibility, and good swelling in an aqueous solution (Memic et al., 2019; Rogers & Bencherif, 2019).

A non-toxic synthetic polymer known as poly (2-hydroxyethyl methacrylate) or pHEMA which is created by the cross-linking of hazardous HEMA monomers and has a great potential as a scaffold due to its excellent biological and mechanical features. pHEMA is a neutral hydrophilic, nondegradable, optically transparent, swelling, and inert biomaterial that possesses biocompatibility and mechanical properties resembling living tissues. Also, it is easy synthesized and its most of physical properties can be easily manipulated by cross-linking or co-polymerization techniques (García-Couce et al., 2021; Tabatabaee, Baheiraei, & Salehnia, 2022; Zasońska et al., 2021). Despite all these positive properties, pHEMA has a weakness about cell adhesion. Although this weakness can be an impediment for tissue engineering in some applications, it can be easily resolved with the combination of some natural polymers (Peng et al., 2022; Tabatabaee et al., 2022). In this study, gelatin, a natural polymer, was used together with pHEMA for scaffold construction to increase cell adhesion. Gelatin is a natural polymer acquired from collagen which is the major structural component of ECM. Due to its biocompatibility, biodegradability, lack of immunogenicity, low cost, and

ease of production, gelatin is frequently used as a biomaterial. Gelatin's superior cell adhesion, improved cell proliferation, and accelerated cell migration are other significant characteristics. Low mechanical stability is a drawback for gelatin; however, the mechanical characteristics of the scaffold can be enhanced by using gelatin with a different biomaterial (Fan, Staufer, & Accardo, 2019; Kim et al., 2017; Mehrotra, Dwivedi, Nandana, & Singh, 2020; Tabatabaee et al., 2022; C. Y. Wang et al., 2020).

The aim of this study is establishing a novel 3D glioblastoma model by utilizing the unique properties of the pHEMA-gelatin-based cryogel to be able to investigate drug resistance mechanism and GBM biology and to compare them with 2D. There are limited studies in the literature about the 3D GBM model created with cryogel scaffolds. The innovative aspect of this study will be the establishment of a novel 3D GBM cancer cell culture system.

2. THEORETICAL FOUNDATIONS AND LITERATURE REVİEW

2.1. Gliomas and Glioblastoma

Glioma is the neuroectodermal tumor of the Central Nervous System (CNS) which constitutes 2.5% of worldwide cancer deaths. Gliomas are the most prevalent solid tumors in youngsters, even though they are most commonly encountered in people over 55 years old. Besides they are the third leading cause of cancer death for people aged 15 to 34 and unfortunately, the incidence of tumors has been continuously increasing over the last 30 years. Gliomas, which constitute approximately 80% of all brain tumors, are of ependymal, oligodendroglial, and astrocytic origin. Although all gliomas arise from neuroepithelial tissue, they differ greatly in the age of beginning, severity, histological characteristics, and potential to grow and spread (Behnan et al., 2019; Ohgaki & Kleihues, 2005; Silantyev et al., 2019; Sontheimer, 2008). The WHO classified gliomas into four primary categories (grades I–IV), based on histological characteristics (cellularity, mitotic patterns, necrosis, and vascular propagation) and astrocytic and oligodendroglial phenotype. Grade I gliomas are pilocytic astrocytomas that most commonly affect young persons; grade II gliomas comprise oligodendrogliomas and astrocytomas (mixed oligoastrocytomas), grade III gliomas include anaplastic astrocytomas and anaplastic oligodendrogliomas, and grade IV gliomas are glioblastoma. While these 4 primary categories are also a measure of the aggressiveness of tumors, astrocytomas have a worse prognosis than oligodendrogliomas of the same grade. Glioblastoma, the grade IV glioma, is the most aggressive type of glioma (Behnan et al., 2019; Shapiro, 1998).

Glioblastoma (GBM) originated from irregular astrocytes and other glial cells. It is the most prevalent and malignant type of glioma in adults and constitutes 60% of all primary brain tumors. Although the global frequency of GBM is lower than 6 per 100.000, it proceeds with a highly poor prognosis and is responsible for 2,5% of cancer-caused fatalities (Lenin et al., 2021; Qiu, Shi, & Jiang, 2017; Yeo, Brown, Gargett, & Ebert, 2021). GBM may affect people of various ages, although the most prevalent age group is between the ages of 55 and 64. Interestingly males are more susceptible to GBM than females (1,6:1), just as Caucasians are more susceptible than others (di Filippo, Duarte, Luiz, de Araújo, & Chorilli, 2021; Hanif,

Muzaffar, Perveen, Malhi, & Simjee, 2017). The general symptoms of GBM include headaches, nausea and vomiting, visual field defect, blurred vision, memory loss, urinary incontinence, cognition impairments, and personality changes. Seizures, a common sign of progressive GBM, are seen in 25% of patients and when the tumor develops to a particularly big size, patients may rapidly get unconscious (di Filippo et al., 2021; Hsu et al., 2021; Qiu et al., 2017). Intrinsically the symptoms of GBM patients mostly vary depending on the destruction grade of the brain tissue and the size and location of the tumor. The necrosis on the destructed brain tissue causes symptoms including cognitive impairments and focal neural deficit (40-60%). These symptoms may change according to the areas of the brain impacted by the tumor. For instance, whereas the patients who have a tumor located in their temporal lobe suffer from visual and hearing problems, patients with a tumor located in their frontal lobe show cognition impairments, and personality changes (20-40%). Gait imbalance and incontinence can arise when the tumor reaches a huge mass and size. Also, the increments of the tumor size and of edema surrounding the tumor cause the increments in intracranial pressures leading the headaches which are common in 30-50 percent of GBM patients (Hanif et al., 2017).

2.1.1 Diagnosis and treatment of GBM

The absence of appropriate diagnostic techniques is one of the most serious challenges in glioblastoma care. Neuroimaging, as well as histological and molecular categorization, are standard diagnostic methods in patients with primary brain tumors. However, these methods might be used when the tumor is already in the late phase. The main reason for the late diagnosis is that the spread of a typical brain tumor is very slow, which provides a slow adaptation to tumor-induced compressions and deformations. Therefore, although there are obvious morphological indicators of tumor spread into brain tissue, clinical symptoms may be completely absent (Bjorland, Fluge, Gilje, Mahesparan, & Farbu, 2021; Silantyev et al., 2019).

The general strategy for GBM treatment is the combination of surgical resection, radiation, and chemotherapy. Unfortunately, the excessive proliferation and invasion ability of GBM cells often results in ineffective surgical resection and the inability of radiation to focus. Because of the aggressiveness and invasiveness of GBM, even after surgery, there may be

cancerous cells that cause the advancement or recurrence of the tumor (di Filippo et al., 2021; Lah Turnšek et al., 2021). After surgery, the standard treatment of GBM, also known as the Stupp protocol, includes the daily chemotherapy agent Temozolomide (TMZ) (75 mg/m² body surface, until the last day of radiotherapy) with concurrent radiotherapy (60 Gy) followed by six courses of adjuvant TMZ therapy (50 to 200 mg/ m², for 5 days during each 28-day courses) (Stupp et al., 2005). TMZ, known as DNA alkylating substance, is the first preferred chemotherapeutic for GBM treatment. It alkylates O-6 or N-7 guanine or N-3 adenine of DNA which induces mismatching of DNA during replication and resulted in cycle arrest and apoptosis (Burster et al., 2021; Li, Zhang, Kiang, Cheng, & Leung, 2018). The alkylating agents used for GBM therapy, other than TMZ are chloroethylating drugs including carmustine and lomustine. It has been proven that alkylating agents extend patient life by inducing apoptosis of cancer cells, but the concomitant effect on healthy cells generates side effects that restrict tolerable dosages. TMZ shows relatively lower side effects and has therefore become the standard therapy of GBM in combination with radiotherapy, mostly in developed countries that can afford the high cost of TMZ. However, treatment with TMZ or other chemotherapeutics mostly cannot be effective enough due to drug resistance that results from many different mechanisms (Burster et al., 2021; Yool & Ramesh, 2020). In case of no response to chemotherapy with alkylating agents, the therapy may be conducted with secondary cytotoxic drugs such as carboplatin, oxaliplatin irinotecan, and etoposide. These drugs, like TMZ, are effective in reducing cancerous cells via altering the DNA (Yool & Ramesh, 2020). Etoposide, which is an extensively used anticancer drug, has the potential to be effective in GBM therapy. It is one of the DNA topoisomerase II inhibitors that leads to the breaking of double-strand DNA and prevents DNA synthesis. In addition, etoposide can encourage p53 and Bax formation, which leads to apoptosis through suppression of cell cycle and acceleration of cytochrome c releasing from mitochondria, respectively. However, access of etoposide to the brain parenchyma is severely prevented by the blood-brain barrier, which restricts access to the central nervous system of nearly all large compounds (>400 Da) and 98% of small molecule drugs (Klasen et al., 2014; Kuo & Chen, 2015; Yadav et al., 2015). Besides these drugs used in GBM therapy, several anti-angiogenic agents, and antibodies for EGFR (epidermal growth factor receptor) and other tyrosine kinase receptors are also attempted (Yool & Ramesh, 2020).

One another method newly used for GBM treatment is tumor treating field (TTF) which transmits electric fields to the tumor from an electrode placed on the patient's scalp to hinder cancer cell proliferation. TTFs induce apoptosis in cancer cells by interrupting the generation of the mitotic spindle during cell division and causing damage to the cell structure. TTFs disrupt cell division while leaving nondividing cells unaffected, making them a cancer-specific treatment. TTFs in conjunction with traditional chemotherapy and radiation have shown to be extremely effective with few adverse effects (Khaddour, Johanns, & Ansstas, 2020; Seker-Polat, Degirmenci, Solaroglu, & Bagci-Onder, 2022).

The currently available treatments of GBM cannot be curative exactly, but just extend the life of patients. The majority of patients diagnosed with GBM can maintain life for up to 15 months even though accomplished treatment strategies. Broadly, treatment with TMZ prolongs the life expectancy of GBM patients from 12.1 to 14.6 months. Only 30% of patients can survive for 2 years, 5% for 5 years, and 2% for 10 years (Behl et al., 2021; Burster et al., 2021; Khaddour et al., 2020). Present GBM treatments cannot be successful exactly due to drug resistance and the heterogeneity of the tumor. GBM often comes up as the various grades of the same tumor, with cell differentiation indicating the presence of diverse cell populations with varying susceptibility to treatment (Bolcaen et al., 2021).

2.1.2 Genetics and subtypes of GBM

GBM has a variety of genetic and molecular alterations that produce changes in numerous signaling processes, leading to the growth of the tumor. Through the use of next-generation sequencing technologies, characteristic molecular patterns of GBM tumors have been revealed, particularly in uncontrolled tumors. Mutations in various genes have been discovered in GBM such as epidermal growth factor receptor (EGFR), tumor suppressor P53 (TP53), phosphatase and tensin homolog (PTEN), etc. (figure 2.1) (di Cintio et al., 2020).

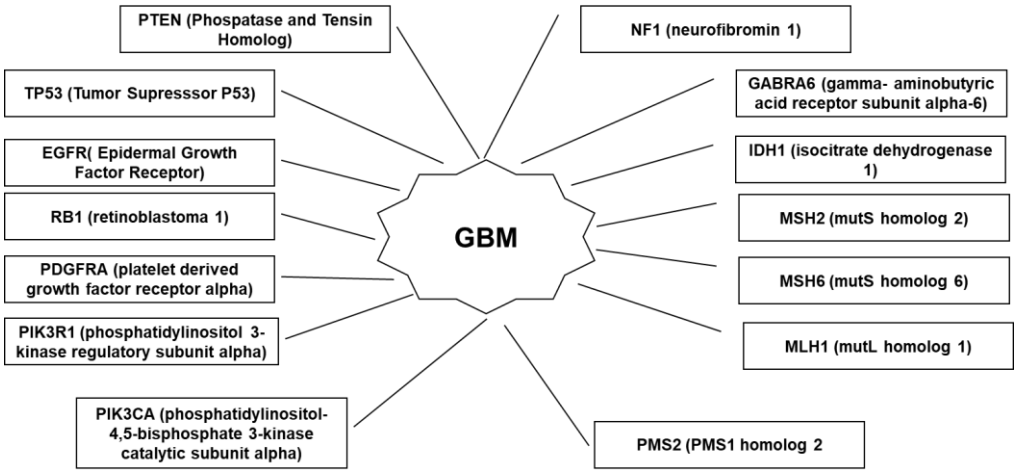

Figure 2.1. The list of the several gene mutations detected in GBM.

GBM is divided into 2 subgroups: primary and secondary GBM (table 2.1). Primary GBM constitutes 90 percentages of all GBM cases and particularly occurs in older patients (≥62 years) while secondary GBM which is formed by the transformation of astrocytoma and anaplastic astrocytoma to a more malignant degree of anaplasia mostly occurs at younger ages (~45 years) (Behl et al., 2021; Ghosh, Nandi, & Bhattacharjee, 2018).

Table 2.1. The features of primary and secondary glioblastoma (Silantyev et al., 2019).

Status/Feature	Primary Glioblastoma	Secondary Glioblastoma
Positive status mutation of IDH gene	<5%	~80%
Preceding cancer disease	Not identified; detected for the first time (de novo)	Diffuse astrocytoma; anaplastic astrocytoma
The percentages of all detected glioblastoma	90%	<10%
The average of diagnosis	62	44
Sex ratio (M:W)	1.42:1	1.05:1
Median overall survival • Surgical treatment and radiotherapy • Surgical treatment radiotherapy and chemotherapy	 9.9 months 15 months	 24 months 31 months
Localization	Supratentorial	Predominantly frontal
Necrosis	Extensive	Limited
TERT promoter mutation	72%	26%
TP53 mutation	27%	81%
ATRX mutation	Rarely	71%
EGFR mutation	35%	Rarely
PTEN mutation	25%	Rarely

Primary and secondary GBM are similar in regard to morphology but the genetic signatures and molecular pathways that contribute to growth and progression show alterations. In primary GBMs, majorly there are amplification and/or overexpression of EGFR and MDM2, mutation of PTEN, deletion or mutation of homozygous CDK4, deletion of p16 and alterations in chromosome 10. On the other hand, TP53, ATRX, and IDH mutations are generally seen in secondary GBMs (figure 2.2) (Behl et al., 2021; von Neubeck, Seidlitz, Kitzler, Beuthien-Baumann, & Krause, 2015).

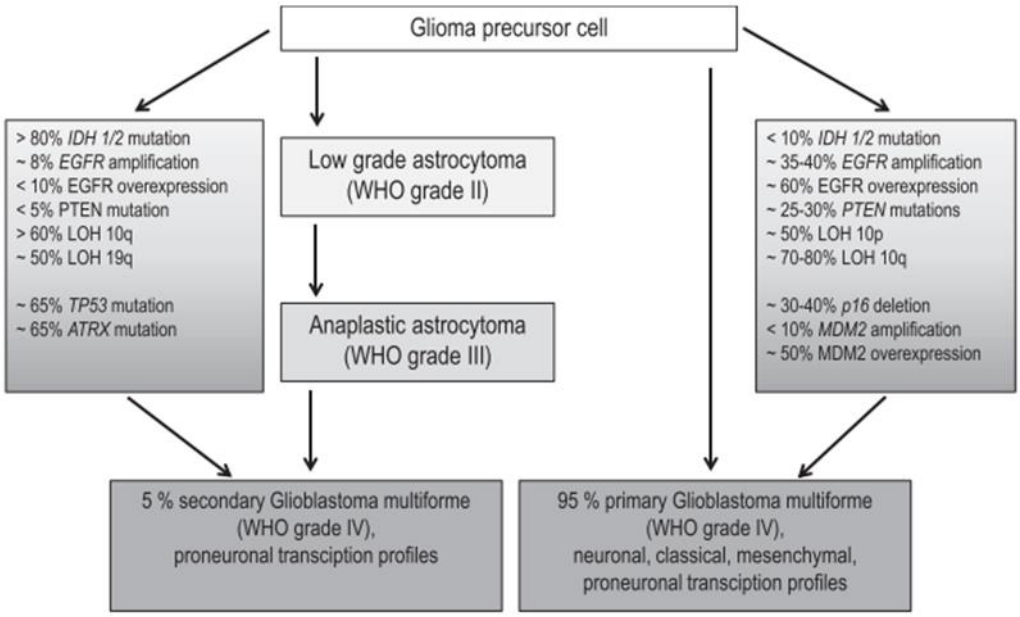

Figure 2.2. Genetic alterations leading to GBM carcinogenesis (von Neubeck et al., 2015).

The Cancer Genome Atlas (TCGA) clustered primary GBM into 4 molecular subtypes according to genetic patterns, DNA copy number, and somatic mutations which was determined the via transcriptomic studies. These subtypes are classical, proneural, neural, and mesenchymal (table 2.2 and figure 2.3) (Lah Turnšek et al., 2021; Lenin et al., 2021).

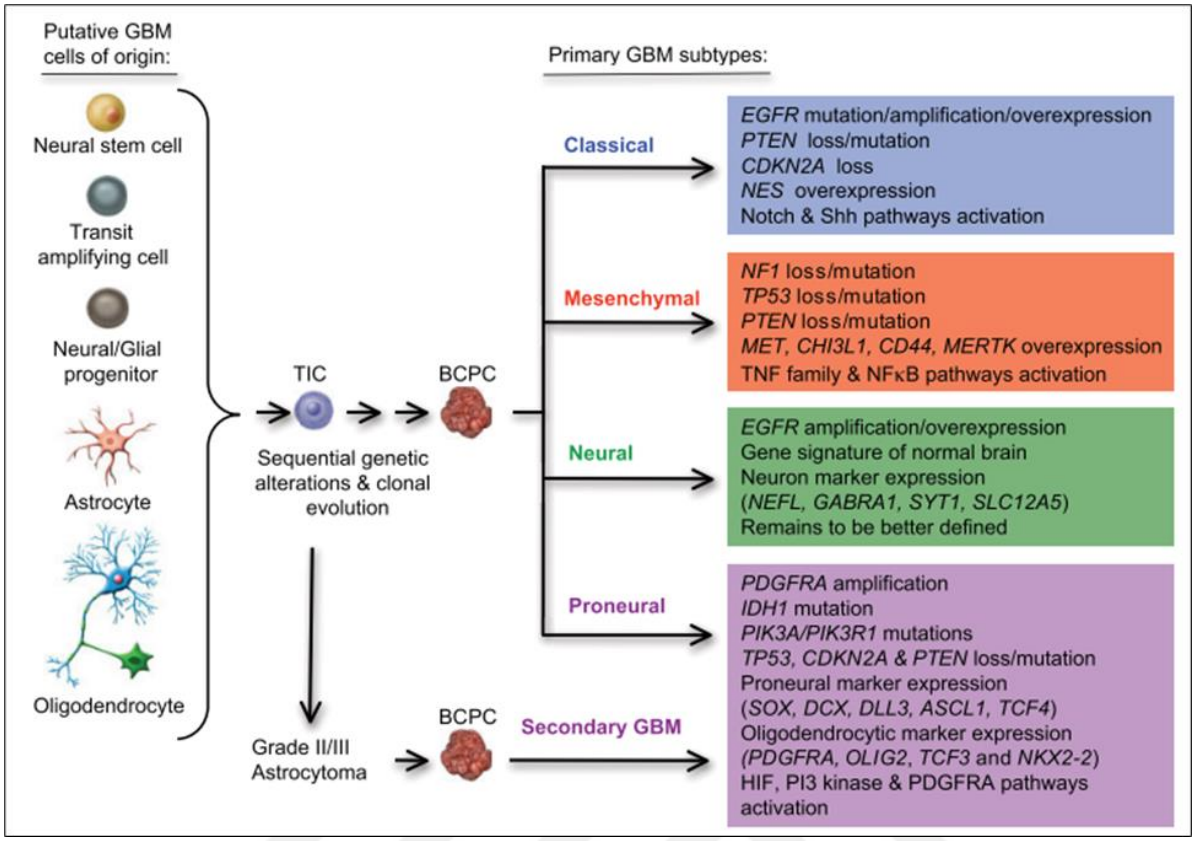

Figure 2.3. Successive genetic alterations detected in the pathogenesis of various glioblastoma subtypes (TIC: Tumor-Initiating Cells, BCBP: Brain Cancer–Propagating Cells) (van Meir et al., 2010).

The classical subtype is characterized by the alterations of chromosomes (chr) 7 and 10 and the epidermal growth factor receptor (EGFR). The chr 10 deletion and EGFR amplification have been observed in 100% and 97% of the GBM classical subtype cases respectively. The mesenchymal subtype is characterized by the deletions at 17q11.2 that include the gene NF1 (neurofibromin 1) and mutation in tumor protein p53 (TP53) and PTEN. In addition to that, in this subtype, the genes in the tumor necrosis factor (TNF) superfamily and NF-kB pathway are greatly expressed and the mesenchymal markers; CHI3L1 and MET are associated. The proneural subtype is featured by the amplification of PDGFRA (platelet-derived growth factor receptor alpha) and mutations in isocitrate dehydrogenase 1 (IDH1) and p53. IDH1 mutation has been observed in 90% of GBM-proneural subtypes. The neural subtype is associated with the expression of neuronal markers including neurofilament light (NEFL), gamma-aminobutyric acid type A receptor alpha-1 subunit (GABRA1), SYT1 and SLC12A5 (K+/Cl–

co-transporter 2). Also, oligodendrocytic and astrocytic differentiation is associated with this subtype. Recently the World Health Organization (WHO) renovated the classification of GBM by considering the molecular characteristics together with histopathology. The classification of subtypes consists of genetic knowledge and histopathological label respectively. According to the latest WHO criteria, GBMs could be classified as IDH1 wild-type and IDH1 mutant (table 2.2) (Cenciarini et al., 2019; Ghosh et al., 2018).

Table 2.2. GBM subtypes and genetic markers (Ghosh et al., 2018).

Sub-class	Genetic markers	Median survival (months)
Classical	CDKN2A, EGFR, NES, PTEN, Notch and SHH pathway	12.2
Mesenchymal	NF1, PTEN, TP53, TNF, NF-kB pathway	11.8
Proneural	PDGFRA, IDH1, PIK3A/PIK3R1, CDKN2A, PTEN, SOX, DCX, DLL3, ASL1, TCF4	11.3
Neural	EGFR, NEFL, GABRAI, SYT1, SLC12A5	13.1
Glioblastoma, IDH1 wild type	TERT, TP53, EGFR, PTEN	9.9
Glioblastoma, IDH1 mutant	TERT, TP53, ATRX	15

GBM IDH1 wild type constitutes about 90 percent of GBMs and is mostly primary glioblastoma. This type of tumor could be seen in patients of various ages (10-69 years) but is most prevalent in 55 years or elder patients. GBM IDH1 wild type is featured by the extensive necrosis, methylation of TERT promoter, and mutations on TP53 and PTEN. GBM IDH1 mutant is a kind of secondary GBM that develops from a preexisting astrocytoma and is more common in younger patients (44 years). This GBM subtype is associated with limited tumor necrosis, altered cell metabolism, and mutations at ATRX, TP53, and TERT promoter (table 2.2) (Ghosh et al., 2018; Hsu et al., 2021).

2.1.3 Tumor microenvironment of GBM and immune escape

The GBM tumor microenvironment (TME) which serves the aggressiveness, heterogeneity, and drug resistance of GBM, consists of various noncancerous cell types in combination with the cancer cells and glioma stem cells (GSCs) (table 2.3). Noncancerous cells can be classified into two categories as immune cells and non-immune cells. Immune cells include myeloid and lymphoid cells (figure 2.4), and non-immune cells include neurons, astrocytes, endothelial cells, etc. The entire cells are located in the extracellular matrix which is made primarily of fibrous proteins and glycoproteins and provides support to cells (Burster et al., 2021; Codrici, Popescu, Tanase, & Enciu, 2022; Lah Turnšek et al., 2021).

Table 2.3. The cell types presented in the GBM tumor microenvironment (Burster et al., 2021; Codrici et al., 2022; Lah Turnšek et al., 2021).

Tumor Microenvironment of GBM			
Immune Cells		Non-immune Cells	Tumor Cells and Glioma Stem Cells
➢ Myeloid Cells	➢ Lymphoid Cells-T cells	• Neurons and Astrocytes	
• Tumor-Associated Macrophages (TAMs)	• CD8+ Cytotoxic T Cells	• Endothelial Cells	
• Bone Marrow-derived Macrophages (BMDMs)	• CD4+ Helper T (Th) Cells	• Pericytes	
• Dendritic Cells (DCs)	• Regulatory T Cells (Tregs)		
• Neutrophils/Tumor-associated Neutrophils (TANs)			
• Myeloid-Derived Suppressor Cells (Mdscs)			

Myeloid cells constitute the major part (30-50 %) of GBM TME. Myeloid-derived suppressor cells (MDSCs) and tumor-associated macrophages (TAMs) from myeloid cells of GBM TME play a critical role in tumor survival, proliferation, and invasion. The MDSCs enhance the survival of tumors by suppressing the natural killer (NK) cell, T cell, CD4+- and CD8+

function. The TAMs have several immunosuppressive features and secrete the substances that actively support tumor growth and invasion. Clinical research has shown that high-grade gliomas have more glioma-associated microglia/macrophages (GAMs) than low-grade gliomas and also, and the decline of GAMs has been shown to considerably slow tumor proliferation in several animal models (Burster et al., 2021; Yeo et al., 2021).

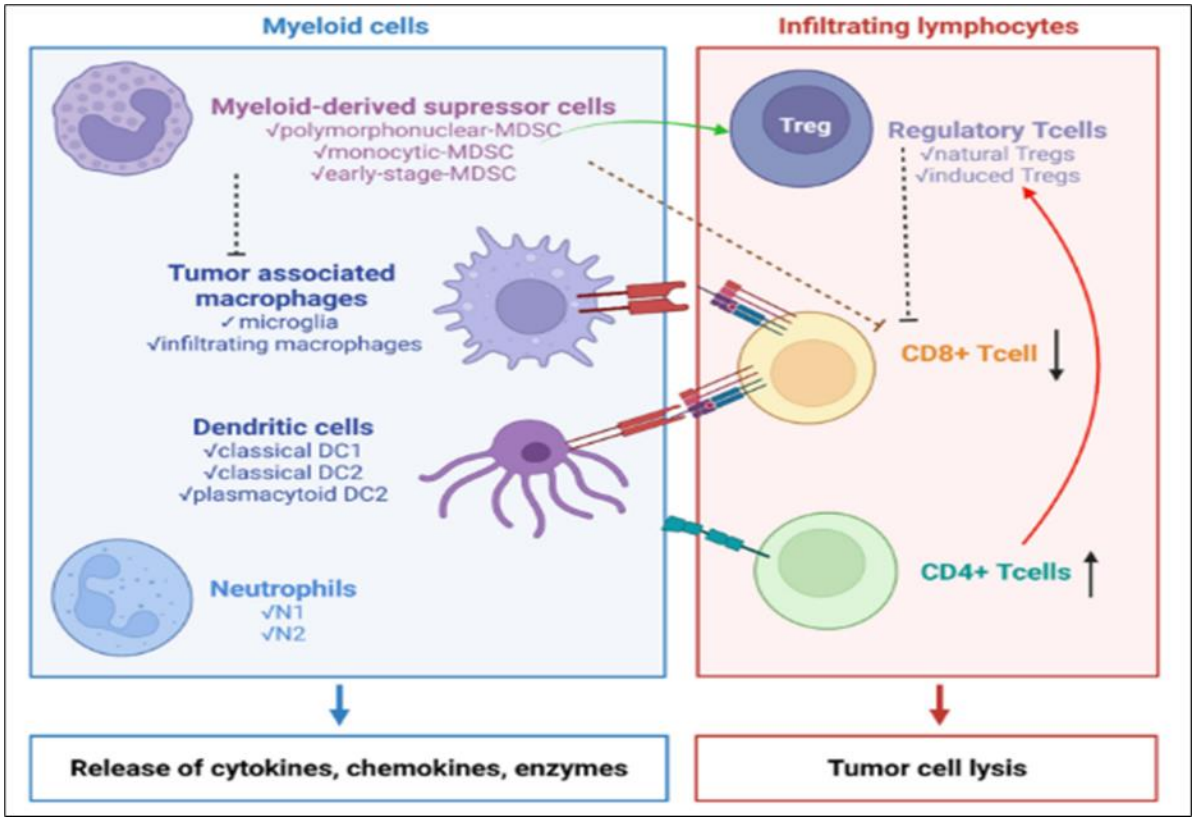

Figure 2.4. The immune cells participated GBM tumor microenvironment (Codrici et al., 2022).

In addition to TAMs which are the massive part of the immune cell group, significant numbers of lymphocytes are also found in glioblastomas. These are mostly T cells (often referred to as tumor-infiltrating lymphocytes (TILs)) however natural killer (NK) cells and rather rare B cells, have also been seen in human glioblastomas. T cells are crucial effector cells with the ability to identify and possibly eradicate cancer cells. However, in an environment with a high level of immunosuppression, TILs can be unfunctional as they lose the ability to fighting with cancer cells (Anghileri et al., 2021; Yeo et al., 2021).

Table 2.4. The immune system factors included in TME of GBM (DeCordova et al., 2020).

Immune system component	Source	Effect on GBM microenvironment
Cytokine		
IL-10	TAM	Enhances Immunosuppression, promotes tumorigenesis, decreases expression of MHC class II on monocytes, promotes Trogs, inhibits expression of TNF-a and IFN-y. suppresses anti-tumor effect of immune cells
TGF-β	TAM and GSC (TGFB2)	Suppresses anti-tumor immune response, promotes tumorigenesis, blocks NK cells activity, Inhibits T-cells, promotes Tregs, downregulates IL-2, Inhibits NKG2D on CD8+ T-cells, upregulates CD133+
IL-6	TAM	Suppresses immune effector cells
CSF-1	TAM	Enhances immunosuppression
Complement system		
FH	GBM cells	Enhances immunosuppression, inactivates C3b, inhibits activation of the complement alternative pathway
C1-IA	GBM cells	Enhances immunosuppression, prevents activation of the complement classical pathway
CD59	GBM cells	Enhances immunosuppression, inhibits the formation of MAC, prevents activation of the complement pathway
CFHR5	GBM cells	Inhibits complement-mediated lysis and decay acceleration of C3 convertase
TAM		
TAM	Microglia and macrophage/ monocyte	Polarises toward M2 phenotype, enhances immunosuppression, promotes tumor invasion, secretes anti-tumor cytokines, expresses FasL which act

Even though the TME of GBM includes immune cells in a great number and variety, glioblastoma exhibits immunosuppressive properties. The tumor-associated macrophages (TAMs), the microglia, and the tumor cells serve the immunosuppressive effect by excreting the various immunosuppressive agents such as chemokines, cytokines, and growth factors (table 2.4). In addition to that, including of some immunosuppressive inflammatory cells to the tumor microenvironment and the activity of several immunosuppressive cell surface factors have a part in the immunosuppressive effect of GBM (table 2.4) (Codrici et al., 2022; Khaddour et al., 2020).

Another important factor preventing the GBM from immune system recognition is the presence of GBM stem cells (GSCs). Also, GSCs play a crucial role in the genesis and development of tumors as well as resistance to standard treatments and tumor recurrence by employing altered signaling pathways (Burster et al., 2021; Sharifzad et al., 2019). GSCs or glioma initiating cells (GICs) are found in newly formed tumors and are known for their capacity to produce tumors in vivo as well as their capacity to self-renew, stemness markers expression, and differentiate into many cell types. Although it is yet unknown whether GSCs develop from NSCs or from other CNS cell types with mutational loads that support the self-renewal phenotype, it was reported that the formation of GSCs may be in two manners (figure 2.5). In the first manner, brain cancer propagating cells (BCPC) that formed by the mutations on neural stem cells (NCS), develop into GSCs when combined with the development of oncogenic mutations. In the second manner, the cells like astrocytes or oligodendrocytes which formed by the differentiation of transformed neural/glial progenitors, develop into GSCs as a result of oncogenic mutations (Behnan et al., 2019; Lah Turnšek et al., 2021).

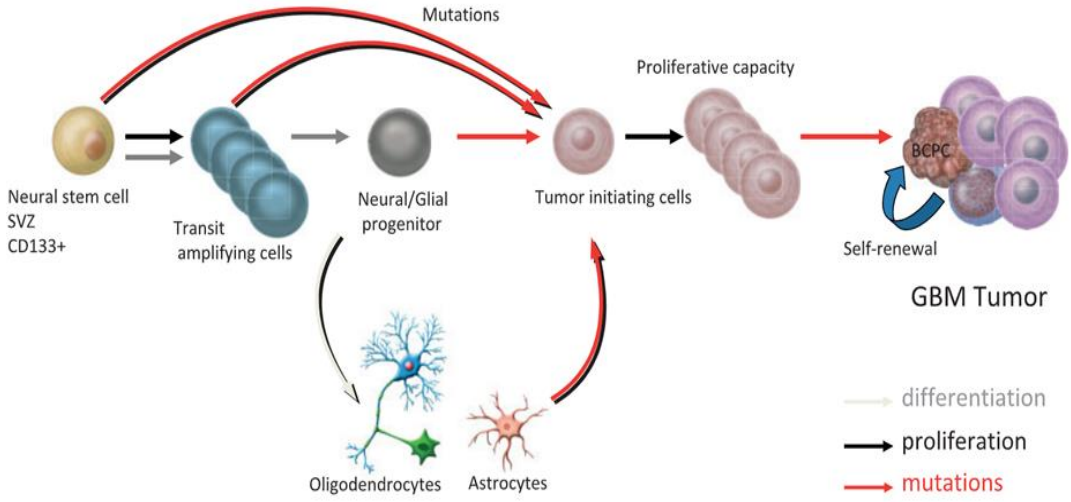

Figure 2.5. Potential Lineage Associations for Formation and ontogeny of Brain Cancer-Propagating Cells (BCPCs), and production of Glioblastoma (GBM) Tumors. GBM tumor arises as a result of the mutations in normal neural stem cells that lead to the formation of tumor–initiating cells (TICs / glioma initiating cells (GICs)) that can self-renew, multiply, and produce brain cancer propagating cells (BCPCs) (van Meir et al., 2010).

Studies points to GSCs as the primary causes of chemoresistance and GBM recurrence. They are protected from treatments that target dividing cells by their poor proliferative activity. Also, the improved DNA repair and multidrug resistance mechanisms of GSCs increase the tumor recurrence and subsistence following radiotherapy and chemotherapy. With an average survival time of only 15 months following surgery and chemo-radio therapy, GBMs that developed from GSCs are the most aggressive brain tumors (Hersh, Gaitsch, Alomari, Lubelski, & Tyler, 2022; Lah Turnšek et al., 2021).

2.1.4 Angiogenesis, invasion, and apoptosis in GBM

Glioblastoma (GBM), a very aggressive brain tumor, is distinguished by impaired blood vessels and invasion along the outer vessel walls and is therefore resistant to treatment. (Caspani et al., 2014).

Angiogenesis is defined as the formation of new capillaries from the blood vessels that already exist. Glioblastoma is distinguished by the formation of new capillaries from preexisting blood vessels that contain hyperpermeable vessels with an increased diameter.

The solid tumor vasculature promotes tumor growth and provides enough oxygen and nutrients. Vascular endothelial cells (ECs) proliferate, migrate, and differentiate as part of the intricate process known as angiogenesis when they are stimulated by certain signals. There are several genes and angiogenic factors such as VEGF, interleukin 6 (IL-6), IL-8, and transforming growth factor (TGF), that promote glioma angiogenesis (Ahir, Engelhard, & Lakka, 2020; Burster et al., 2021).

GBM tumor cells have the remarkable capacity to migrate via healthy blood arteries, and thereby invade the healthy areas (Sharifzad et al., 2019). Diffuse invasion, which allows tumors to evade complete surgical resection and chemo- and radiation treatment, is the main barrier to a cure. Also, GBM tumor cells migration raises recurrences by causing the development of secondary tumors. Despite the unique ability of invasion, only 0.4–2% of GBM develop extracranial metastases. On the contrary other solid tumors, such mammary ductal carcinoma, small-cell lung carcinoma, colorectal, and prostate cancer, usually spread outside of the original organ. The migration paths of GBM tumor cells can be generally categorized into four routes as the invasion cells frequently follow pre-existing road maps in the brain. These routes are the white-matter tracks, perivascular space, leptomeningeal space, and the brain parenchyma (figure 2.6.) (Cuddapah, Robel, Watkins, & Sontheimer, 2014; Seker-Polat et al., 2022). The vasculature and white-matter tracts are the main structural parts of the brain hence GBM cells mostly prefer these regions to invade. The perivascular space is a highly attractive route for tumor cells due to the blood vessels surrounding it. Invasive GBM tumor cells invade the perivascular space so as to reach into blood vessels that supply nutrition and oxygen. Tumor cells use the myelinated axons that make up white-matter tracts to migrate to far-flung regions of the brain (Seker-Polat et al., 2022).

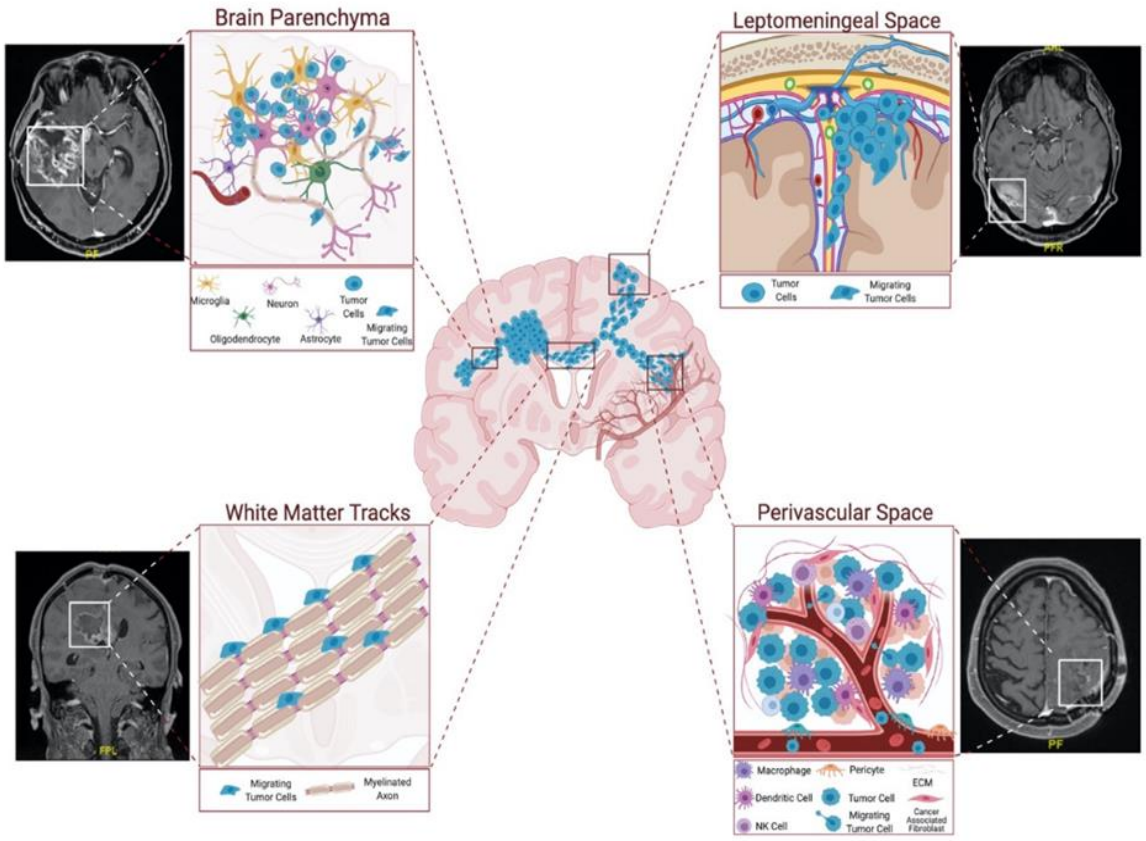

Figure 2.6. The migration routes of GBM tumor cells (Seker-Polat et al., 2022).

Apoptosis is a kind of controlled cell death which the cells are eliminated without toxic byproducts being released into the surroundings. In complex organisms, apoptosis is crucial for maintaining healthy biological processes by destroying damaged cells, and dysregulation of apoptosis can be resulted with the cancer and the other pathophysiological conditions. When avoiding apoptosis or developing resistance takes place, anti-apoptotic proteins attach to pro-apoptotic family members and eliminate their activity. It has been suggested that down-regulation of pro-apoptotic proteins and up-regulation of anti-apoptotic proteins lead to therapeutic resistance in GBM. Additionally, it was reported that, the various member of the TNF receptor pathway and three genes from the Inhibitor of apoptosis (IAP) family are responsible from the apoptosis resistance of GBM (figure 2.7) (Burster et al., 2021; Trejo-Solís et al., 2018).

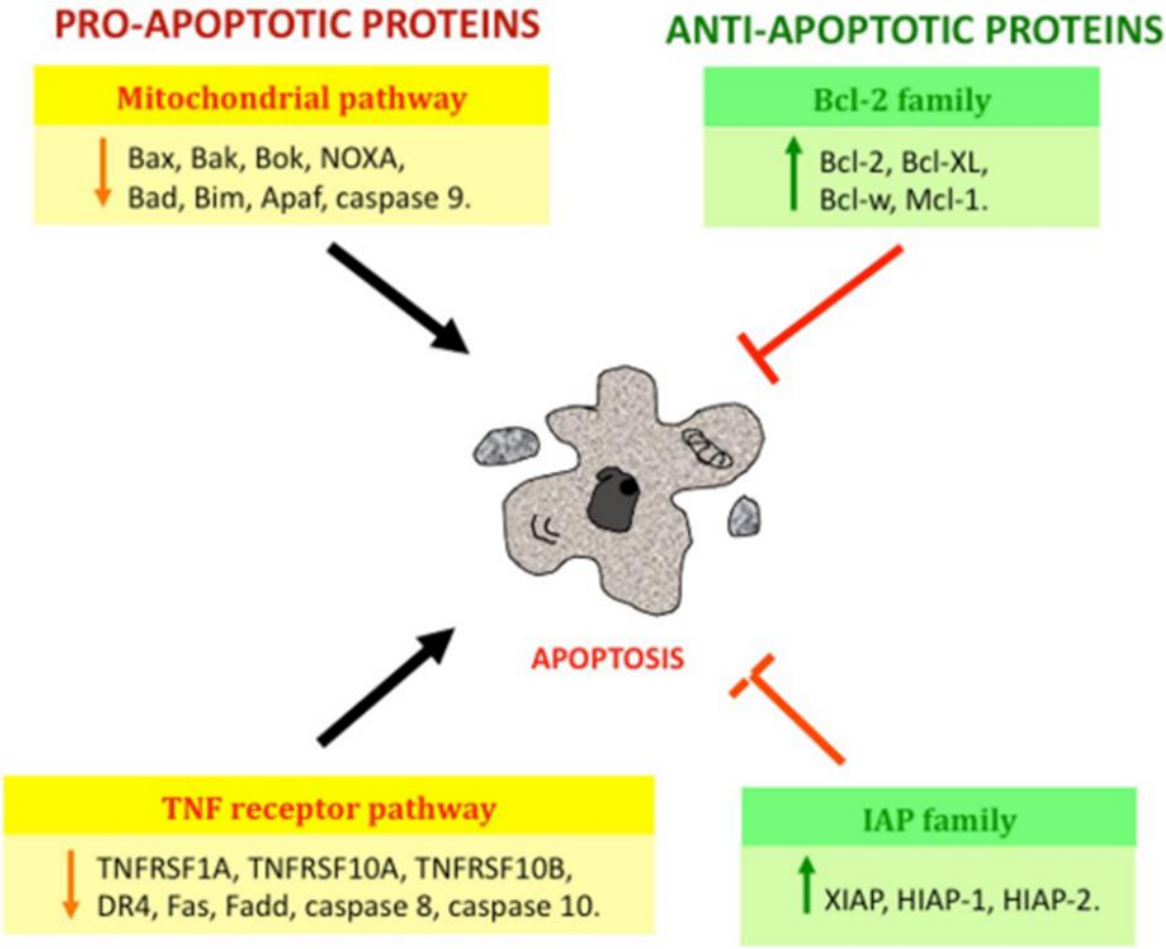

Figure 2.7. The condition of proteins involved in the apoptotic process in GBM. It has been noted that there is an overexpression of anti-apoptotic proteins including Bcl-2, Bcl-xL, Bcl-w, Mcl-1, XIAP, HIAP-1, and HIAP-2, in addition to a downregulation of pro-apoptotic proteins like Bax, Bak, Bok, NOXA, Bad, Bim, Apaf, and caspase-9 and the TNF receptor pathway. (TNFRSF1A, TNFRSF10A, TNFRSF10B, DR4, Fas, Fadd, and caspase-8 and -9). (Black arrows (→): activation, red lines (⊥): inhibition, orange arrows (↓): down regulation, green arrows (↑): upregulation) (Trejo-Solís et al., 2018).

2.2. Tissue Engineering and Scaffolds

Tissue engineering is a multidisciplinary area that utilizes both life and engineering sciences including mechanical engineering, chemical engineering, genetics, material science, biology, and medicine. In 1988 a scientist, Professor Robert Nerem, defined a term " tissue engineering" as using of engineering and life science techniques to create biological alternatives to repair, maintain, or enhance tissue function, and to gain a fundamental

knowledge of structure-function correlations in normal and damaged mammalian tissue (Ng, Zang, Yang, Liu, & Yang, 2012; O'Brien, 2011). Recently, tissue engineering has emerged as a promising method for fixing damaged tissues and overcoming the difficulties posed by traditional organ donation methods. The increasing need for organ transplants in clinical practice has made tissue engineering a significant option (Eltom, Zhong, & Muhammad, 2019). There are three main factors that constitute tissue engineering and named as triad of tissue engineering: cells, growth factors and tissue scaffold (Chan & Leong, 2008).

The majority of all normal cells in human tissues except blood cells are dependent on an extracellular matrix (ECM) (Chan & Leong, 2008). ECM serves as physical support to cells and therefore it gives structure and mechanical properties including elasticity and rigidity depending on the tissue function. Besides, ECM provides a physical milieu for cells to attach, proliferate, migrate, and respond to biochemicals. Briefly the ECM has crucial biochemical and biomechanical missions for the maintaining of differentiation, morphogenesis, homeostasis, elasticity, and integrity (Frantz, Stewart, & Weaver, 2010; Habanjar, Diab-Assaf, Caldefie-Chezet, & Delort, 2021; Poornima et al., 2022).

The tissue scaffold is a three-dimensional (3D) construct established from biological and biomaterials that provides a support for cells and enables cell/ tissue proliferation by mimicking the extracellular matrix (ECM).It has significant missions such as constituting a proper adhesion surface for cells, aiding in interacting with surrounding tissue to react to physiological and biological alterations, transporting the nutrients and wastes and contributing to regeneration of the actual extracellular matrix while degrading gradually itself. In order to perform these missions an ideal scaffold should have several biological and structural properties such as biocompatibility, biodegradability, porosity, and mechanical properties (table 2.5) (Mohanty et al., 2015; Sousa, Mendes, & B??rtolo, 2013; Zhu & Chen, 2013).

Table 2.5. The features of an ideal tissue scaffold (Turnbull et al., 2018).

Scaffold Characteristics	Desirable Features
Biocompatiblity	Non-toxic breakdown products Non-inflammatory scaffold components, avoiding immune rejection
Biodegradability	Controlled scaffold degradation which can complement tissue ingrowth whilst maintaining sufficient support Degradable by host enzymatic or biological processes Allows invading host cells to produce their own extracellular matrix
Bioactivity	Scaffold materials that can interact with and bind to host tissue Osteoconductive and osteoinductive properties Inclusion of biological cues and growth factors to stimulate cell ingrowth, attachment and differentiation
Scaffold Architecture	Interconnected pores allowing diffusion and cell migration Microporosity to present a large surface area for cell-scaffold interactions Macroporosity to allow cell migration and invasion of vasculature Pore size tailored to target tissue and cells Sufficient porosity to facilitate cell ingrowth without weakening mechanical properties Inbuilt vascular channels to enhance angiogenesis in vivo
Mechanical Properties	Compressive, elastic and fatigue strength comparable to host tissue allowing cell mechanoregulation to occur and structural integrity to remain in vivo caffold material that can be readily manipulated in the clinical environment to treat individual patient bone defects

The tissue scaffold must first and foremost be biocompatible for cells to attach, function properly, migrate onto its surface, and start proliferating before the new matrix is established. Besides, biocompatibility is very important in order to prevent immune responses. In the host body, the scaffold must only generate a minimal immune response to avoid triggering a strong

inflammatory response that might hinder healing or result in the body rejecting the scaffold (Chan & Leong, 2008; O'Brien, 2011).

Besides biocompatibility, bioactivity is a crucial criterion for cell attachment, function, migration, and proliferation. This bioactivity includes the interacting with the cellular components to assist and regulate their actions, acting like the cell adhesive ligands to improve cell attachment, operating as a delivery system or reservoir for external growth-stimulating signals to hasten regeneration (Chan & Leong, 2008).

Recently, tissue scaffolds have been utilized as a supporting material for cell cultures and to promote cell proliferation in the healing of damaged tissues. While the healed tissue forms, the biodegradable scaffold degrades gradually in order to allow the cells to replace with the scaffold. This degradation also must be compatible with the cellular components and cells (Eltom et al., 2019; O'Brien, 2011).

The architectural and mechanical properties of a scaffold are another crucial factor for cell proliferation and function normally. The tissue scaffold should supply void volume for the generation and remodeling of new tissue and for vascularization with the intention of assisting the integration of the host tissue after implantation. For the effective metabolite, nutrient and waste transportation, and ideal scaffold should be in interconnected pore structure and high porosity. In addition to interconnected pores and porosity, the scaffold should have proper pore size that facilitates high mass transfer of oxygen across the scaffold and enhances cell migration and water absorption (Chan & Leong, 2008; Eltom et al., 2019). The mechanical properties of scaffold should be consistent with the porous architecture. The mechanical stability of damaged tissue is provided by the scaffold, and therefore the mechanical properties of the scaffold must be compatible with the host tissue. Also, it must be sturdy enough to permit surgical manipulation during implantation (Chan & Leong, 2008; O'Brien, 2011).

2.2.1 Chemical composition and production techniques of scaffolds

Typically, scaffolds are made from natural and synthetic biomaterials (figure 2.8). Natural biomaterials have high biocompatibility, osteoconductivity and low immunogenicity. They

consist of protein origin biomaterials such as collagen, fibrin, gelatin, and polysaccharides such as alginate, agarose, chitosan (Ng et al., 2012).

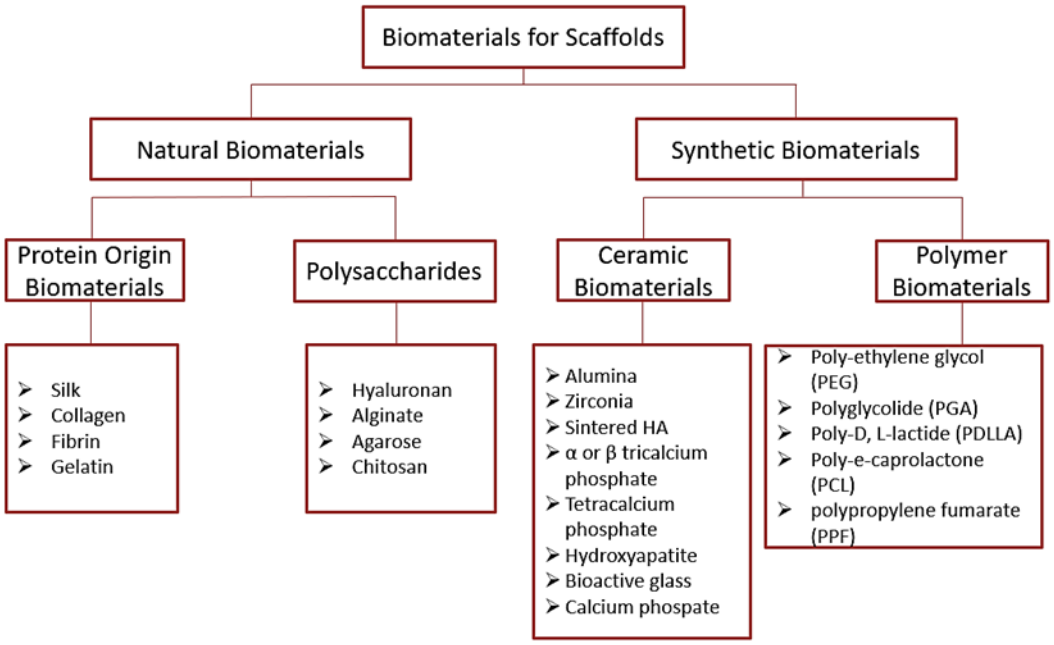

Figure 2.8. Some of the biomaterials used in scaffold production(Ng et al., 2012; O'Brien, 2011; Y. Park, Huh, & Kang, 2021) .

Synthetic biomaterials can be categorized into two groups: ceramic biomaterials including alumina, zirconia, hydroxyapatite, and polymer biomaterials including polypropylene fumarate (PPF), polycaprolactone (PCL), polylactic acid (PLA) (figure 2.8). Synthetic biomaterials have some advantages such as controlled degradation rate, improved cell attachment and production in larger quantities at lower cost. Both natural and synthetic biomaterials have some advantages and disadvantages that should be considered when deciding on the material of scaffold to be produced (table 2.6) (Eltom et al., 2019; Ng et al., 2012). Also in some cases, synthetic and natural materials can be used together to increase adhesion, hydrophilicity, and biocompatibility (Sousa et al., 2013).

Table 2.6. The advantages and disadvantages of natural and synthetic biomaterials used in production of scaffolds (Ng et al., 2012).

Types of scaffold materials	Comments	Examples
Natural materials	*Advantages* Low toxicity Low chronic inflammatory response Biological recognition and biodegradable *Disadvantages* Complexities associated with purification, immunogenicity and pathogen transmission Poor mechanical strength Difficult manipulation Easy denaturation Not available in large quantities Batch-to-batch variations	Alginates Chitosan Collagen Fibrin Fibronectin Glycosaminoglycan Laminin Poly(hydroxyalkanoates) Polysaccharides Silk
Synthetic materials	*Advantages* Large-scale and reproducible production Controllable design with desired mechanical properties, geometries and degradation time *Disadvantages* Lack of cell-recognition signals	Polycaprolactone Poly(ethylene glycol) Poly(ethylene terephthalate) Poly(lactic acid) Poly(lactic-co-glycolic acid) Polypropylene fumarate) Polyurethane

In literature, there are several techniques that have been developed to produce tissue scaffolds. These techniques can be grouped into two headlines: conventional techniques and advanced techniques. Conventional techniques include gas foaming, solvent casting and practical leaching, thermal-induced phase separation, freeze drying and electrospinning are described as processes that use to produce scaffolds with an uninterrupted, continuous pore structure (table 2.7) (Hutmacher, Woodfield, & Dalton, 2014; Zhu & Chen, 2013).

Table 2.7. Conventional techniques that used for tissue scaffold production (Eltom et al., 2019).

Technique	Advantages	Disadvantages
Freeze-drying	1. Use in a variety of purposes 2. Capability of obviating high temperatures 3. The pore size is manageable to be controlled by changing the freezing method	1. High energy consumption 2. Long-term timescale 3. The use of cytotoxic solvents 4. The generation of small 5. Irregular size pores (usually in the range of 15 to 35 μm)
Solvent casting and practical leaching	1. Fits thin membranes of thin wall three-dimensional specimens 2. High porosity (50-90%) 3. Lost cost technique	1. Time consuming since thin membranes are only used 2. The widespread use of very toxic solvents
Gas foaming	1. Porosity up to 85%	1. If the fabrication process did not change, the product obtained might have a closed pore structure or a solid polymeric skin
Electrospinning	1. Essential technique for developing nanofibrous scaffolds for the TE 2. Homogeneous mixture made of fibers with high tensile strength	1. Used solvents can be toxic 2. Problematic to obtain 3D structures as well as sufficient size of pores needed for biomedical applications 3. Process depends on many variables
Thermal-induced phase separation	1. Construction of the thermoplastic crystalline polymer scaffold 2. Low temperature can be utilized for the integration of bioactive molecules 3. The porosity of fibers is more than 98% a higher surface-to-volume ratio than those constructed	1. Only used for thermoplastic

Rapid prototyping techniques include stereolithography, selective laser sintering, solvent-based extrusion free-forming, bioprinting and fused deposition modeling and are described as the production of 3D structures with the layer-by-layer deposition approach (table 2.8) (Mohanty et al., 2015; Zhu & Chen, 2013).

Table 2.8. Rapid prototyping techniques that used for tissue scaffold production (Eltom et al., 2019).

Fabrication technique	Advantages	Disadvantages
Stereolithography (SLA)	1. Enables to overcome the challenges related to wastage in subtractive fabrication methods 2. High resolution 3. Uniformity in pores interconnectivity	1. Has limitations in the process of photopolymerization 2. Requiring massive amounts of monomers and postpolymerization treatment to improve monomer conversion
Selective laser sintering (SLS)	1. Using ultrahigh-molecular-weight polyethylene 2. Provides user excellent control over the microstructures of the produced scaffold by adapting SLS process parameters 3. Utilized to obtain the preferred properties of the created scaffold	1. Steps after processing the spin of the phase are required to remove injected powder 2. High operating temperature
Solvent-based extrusion freeforming (SEF)	1. It can be utilized to make ceramic, metal, and metal/ceramic composite part 2. It can directly or indirectly function in printing the actual part or a mould 3. It is a new fabrication method for tissue engineering that can be utilized for precise control of scaffold structure at micron level 4. Success involves the ability to strictly follow the structure of the natural tissue and the mechanical characteristics of the scaffold	1. Temperature extrusion. Their design includes a change to the factors affecting extrusion pressure, including nozzle length-to-diameter ratio, a paste formulation, and the extrusion velocity
Bioprinting	1. Low costs 2. Higher accuracy and greater shape complexity 3. The high speed of printing with the capability of supporting parallel high cell viability (80/90%)	Depends on existence of cells
Fused deposition modeling (FDM)	1. Useful in the scaffold design under the different aspects of scaffold fabrication. 2. Low-temperature deposition	Has limitations in its application to biodegradable polymers

2.2.1.1 Cryogelation

There is another method namely cryogelation that may be counted among conventional techniques but also stands out among these techniques, as it presents the controlled pore size, equal pore distribution, and improved mechanical integrity. This method allows the production of highly interconnected 3D macroporous scaffolds which are ideal to use in tissue engineering. Also contrary to other conventional methods it is possible to produce scaffolds in a variety of sizes and forms, such as sheets, discs, or monoliths with varied dimensions through cryogelation. Also contrary to conventional methods it is possible to produce scaffolds in a variety of sizes and forms, such as sheets, discs, or monoliths with varied dimensions through cryogelation (Memic et al., 2019; Sharma, Bhat, Vishnoi, Nayak, & Kumar, 2013). The term cryogelation comes from the Greek word 'krios' which means frost or ice and this term refers to a process that produce hydrogels called as cryogels at sub-zero temperatures (Razavi, Qiao, & Thakor, 2019). In cryogelation process (figure 2.9) a polymer and/or monomer -aqueous solvent mixture with the crosslinkers is cooled at subzero temperatures for gelation or polymerization. During the cooling time the ice crystals that perform as a porogen and provide the macroporous structure are formed. These ice crystals are enlarged and interconnected to each other in progress of the time. After gelation or polymerization is completed, cryogels are incubated at room temperature to thaw the ice crystals. The thawing ice crystals leave behind wide voids with extremely dense polymeric wall that giving cryogels interconnected super-macroporous structure (Bencherif, Braschler, & Renaud, 2013; Sharma et al., 2013). Contrary to other conventional porous hydrogels, as a tissue scaffold, cryogels provide an unhampered diffusion for almost all sized solutes and facilitates the infiltration, migration, and proliferation of cells. Besides, cryogels have unique elasticity and shape memory as a result of their interconnected macropores and extremely dense polymer walls (Memic et al., 2019; Rogers & Bencherif, 2019).

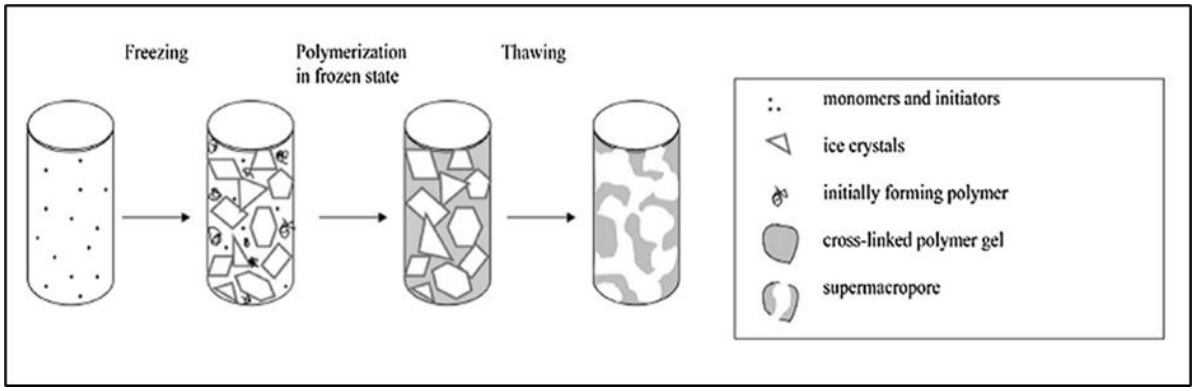

Figure 2.9. The schematic representation of cryogelation process (Plleva, Galaev, & Mattiasson, 2007).

The unique properties of cryogels enable the gives excellent results as a tissue scaffold to establish the 3D cell cultures in tissue engineering. Besides its great potentials in tissue engineering, cryogels has a wide application area including bioseparations, biosensors, drug delivery, monoclonal antibody production and bioreactors owing to their unique features. Cryogels can be produced from various organic and inorganic polymers for different applications (table 2.9(Memic et al., 2019; Rogers & Bencherif, 2019; Saylan & Denizli, 2019).

Table 2.9. Various applications for cryogels, produced from various polymers or monomers (Plleva et al., 2007).

Monomer/polymer Precursors	Process used
Acrylamide	Chromatography of particulate- containing fluids; scaffolds for cell culture
Dimethylacrylamide	Chromatography of particulate- containing fluids; scaffolds for cell culture
Polyvinyl alcohol	As chromatography monolithic medium or non-degradable scaffold for cell culture; immobilization of cells through mechanical entrapment; chemical immobilization of enzymes
Hydroxyethyl methacrylate	As scaffold for cell culture
Dextran methacrylate	As scaffold for cell culture
Hydroxyethyl methacrylate-LLactate- Dextran	As degradable scaffold for cell culture
Agarose	As scaffold for cell culture
Polyethylene glycol	As scaffold for cell culture
N-isopropyl acrylamide	As scaffold for cell culture

2.2.1.2 pHEMA

Poly (2-hydroxyethyl methacrylate) (pHEMA) is a non-toxic synthetic polymer that synthesized via the cross-linking of toxic HEMA monomers (figure 2.10). Otto Wichterle and Drahoslav Lim first researched and invented pHEMA in 1960 while developing contemporary soft hydrogel contact lenses. Since then, various studies have been conducted that revealed the biological and mechanical properties of pHEMA as a biomaterial (Zare et al., 2021). These biological and mechanical properties give pHEMA great potential for biomedical applications such as contact and intraocular lenses (Zasońska et al., 2021), artificial corneas (Peng et al., 2022), controlled drug release systems (Demirci, Sahiner, Yilmaz, Karadag, & Sahiner, 2020), and tissue engineering (Tabatabaee et al., 2022). pHEMA is a neutral hydrophilic, nondegradable, optically transparent, swelling, and inert biomaterial that possesses biocompatibility and mechanical properties resembling living tissues. Also, it is easy synthesized and its most of physical properties can be easily manipulated by cross-

linking or co-polymerization techniques (García-Couce et al., 2021; Tabatabaee et al., 2022; Zasońska et al., 2021).

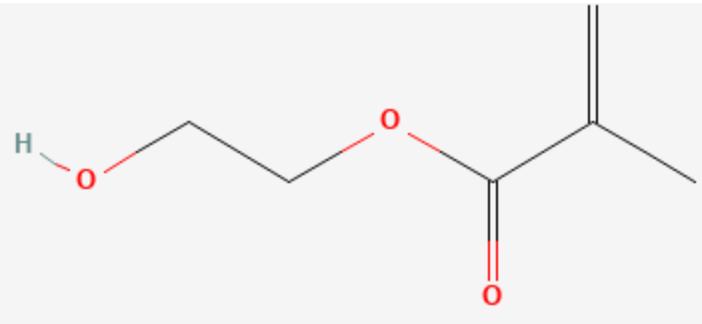

Figure 2.10. The chemical structure of HEMA ("National Center for Biotechnology Information," 2022).

Despite all these positive properties, pHEMA has a weakness about cell adhesion. Although this weakness can be an impediment for tissue engineering in some applications, it can be easily resolved with the combination of some natural polymers (Peng et al., 2022; Tabatabaee et al., 2022). In this study, gelatin, a natural polymer, was used together with pHEMA for scaffold construction to increase cell adhesion.

2.2.1.3 Gelatin

Gelatin is a natural polymer acquired from collagen which is the major structural component of ECM. It is possible to obtain gelatin by thermal denaturalization or alkaline and acidic hydrolysis of collagen and some properties of gelatin, such as melting point, viscosity, and gelling temperature, may vary depending on the method obtained (Fan et al., 2019; Frantz et al., 2010; C. Wang et al., 2021). Gelatin is widely preferred as a biomaterial because it is biocompatible, biodegradable, non-immunogenic, low cost and easy to produce. In addition, another important feature of gelatin is that it provides excellent cell adhesion, enhanced cell proliferation and migration due to containing arginyl–glycyl–aspartic acid (RGD) sequence. The RGD sequence, which is necessary for healthy interactions of cells with the ECM, improves cell adhesion through integrin interactions. A disadvantage of gelatin is its low mechanical stability, but the mechanical properties of the scaffold can be improved by combining gelatin with another biomaterial (Fan et al., 2019; Kim et al., 2017; Mehrotra et al., 2020; Tabatabaee et al., 2022; C. Y. Wang et al., 2020).

2.2.2 3D cell cultures and tumor models

A better understanding of mechanisms underlying the cell and tissue function, formation and pathology has been mostly possible by cell culture systems. The first cell culture was carried out in 1907 by a scientist named Harrison while studying the origin and formation of nerve fibers. Since then, cell culture methods have undergone continuous improvement and have served many studies. At the beginning of cell culture studies cells were mostly cultured as adherent to surface called as two-dimensional monolayer cell culture model. However, over time, the 2D cell culture method fell short for an in-depth understanding of cell biology and tumor research. Herein the researchers have tended to three-dimensional (3D) cell culture approaches that are closer to in vivo conditions than the 2D model. 3D cell culture model enables to improving studies on drug metabolism, protein synthesis, stimuli responses and cell behaviors and have great contribute to many studies such as cancer, stem cell and drug discovery (Caicedo-Carvajal, Liu, Remache, Goy, & Suh, 2011; Chaicharoenaudomrung et al., 2019; Jensen & Teng, 2020). In fact, the 2D cell culture model has some advantages such as easy to perform, low-cost requirement and show great performances on some functional tests. But unfortunately, 2D cell culture model has lots of disadvantages that made 3D cell culture model superior to 2D (table 2.10). The first of these disadvantages is lack of cell-cell and cell-extracellular environment interactions, as in the natural structures of tissue or tumor (figure 2.11). The cell-cell and cell-extracellular environment interactions are in charge of various cellular mechanisms such as cell proliferation, viability, differentiation, gene and protein expression, drug metabolism and stimuli response. In 2D cell cultures, the lack of interactions also causes the loosing of cell polarity which alters how those cells react to different events including apoptosis (Kapałczyńska et al., 2018; H.-J. Park & Helfman, 2019).

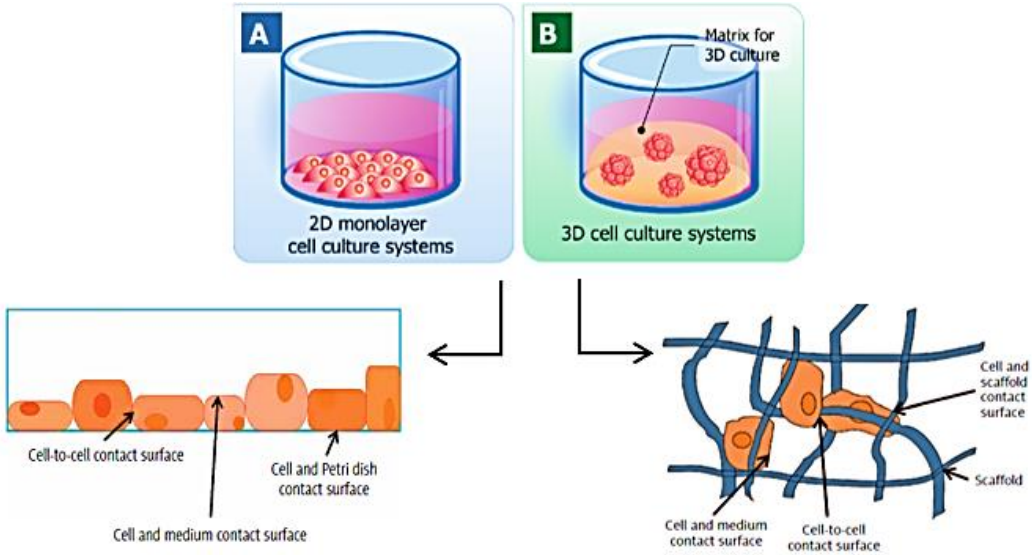

Figure 2.11. In 2D cell culture systems, cells adhere to the surface of a plastic or glass petri dish and therefore cell-cell and cell-environment interactions is restricted, while the 3D cell culture system provides rich interactions (Chaicharoenaudomrung et al., 2019; Kapałczyńska et al., 2018).

In 2D culture the natural cell morphology cannot preserved. Since cells can just grow and extend in two dimensions, they have a flat and stretched shape. The alteration in morphology can impact the cell function, cell signaling, secretion and the arrangement of the components within the cell. Furthermore, the gene expression, protein splicing, and expression and cell biochemistry alter in 2D cultured cells(Jensen & Teng, 2020; Kapałczyńska et al., 2018).

Table 2.10. The important characteristics of 2D and 3D cell cultures (Jensen & Teng, 2020).

Important characteristics	2D cell culture	3D cell culture
Cell shape	Cells shape is flat and elongated since the cells can only grow and expand two dimensionally Cells grow into a monolayer on the plate	Natural cell shape is preserved and cell growth Cells grow into 3D aggregates/spheroids Spheroids contain multiple layers
Cell exposure to medium	All cells in the culture receive the same amount of nutrients and growth factors from the medium in the plate This causes more cells to be in the same stage of the cell cycle	Nutrients does not have to be equally divided amongst all cells but can be if needed The core cells often remain inactive since they receive less oxygen and growth factors from the medium This process resembles the core cells in tumor cells, making it possible to mimic the behavior and structure of a tumor cell in vivo
Cell junction	Cell junctions are less common and less accurately represent real junctions	Cell junctions are common and allow for cell-to-cell communication Cells communicate through exchange ions, small molecules, and electrical currents
Cell differentiation	Cell differentiation is poor	Cells are well differentiated
Drug sensitivity	Cells often have little resistance to drugs making it appear as though drugs administered to the cells were a successful treatment Drugs are not well metabolized	Cells often have more resistance to drug treatment Drug metabolism is much better Gives a more accurate representation of the drug's effects

Table 2.10. The important characteristics of 2D and 3D cell cultures (Jensen & Teng, 2020) (continuation).

Important characteristics	2D cell culture	3D cell culture
Cell proliferation	Cells proliferate at an unnaturally rapid pace	Proliferation rates are realistic and can be high or low depending on technique and types of cells being studied.
Expression levels	Gene and protein expression levels are often vastly different compared to in vivo models	Gene and protein expression levels resemble levels found from cells in vivo
Cost	For large-scale studies, it is much cheaper than using 3D culture	Are typically more expensive than 2D cell culture techniques and require more time 3D cell culturing reduces the differences between in vitro and in vivo drug screening, decreasing the likelihood of needing to use animal models
Apoptosis	Drugs can easily induce apoptosis in cells	Higher rates of resistance for drug-induced apoptosis
Response to stimuli	Inaccurate representation of response to mechanical stimuli of cells Cells cannot experience gravity since they are unable to expand into the third dimension	Accurate representation of response tommechanical stimuli of cells Cells can experience gravity giving a more accurate representation of a cell in vivo
Usage and analysis	Highly replicable and easily interpretable Better for long-term cultures	Can be difficult to replicate experiments Can be difficult to interpret data

Another important problem of 2D cell culture is that cells can access to components of medium such as nutrients, signal molecules, metabolites and oxygen unlimitedly by contrast with the in vivo cells. A natural concentration gradient exists for these components in vivo tissue. Drug responses of cells and several cell function such as migration, signaling and

motility are influenced by these gradients. For this reason, the estimation of drug efficacy and toxicity cannot be successful in 2D models. However, 3D model offers a better implementation that able to overcome of all these problems (Chaicharoenaudomrung et al., 2019; Kapałczyńska et al., 2018; Langhans, 2018).

Soft agar solution was used to create one of the earliest three-dimensional cultures developed by Hamburg and Salmon in the 1970s. Since then, numerous 3D cell culture model has been applied and enable to enlighten lots of studies. According to applying method, 3D cell cultures basically divided into 3 models; scaffold-based, scaffold free and hybrid (figure 2.12) (Cortesi & Giordano, 2022; Kapałczyńska et al., 2018).

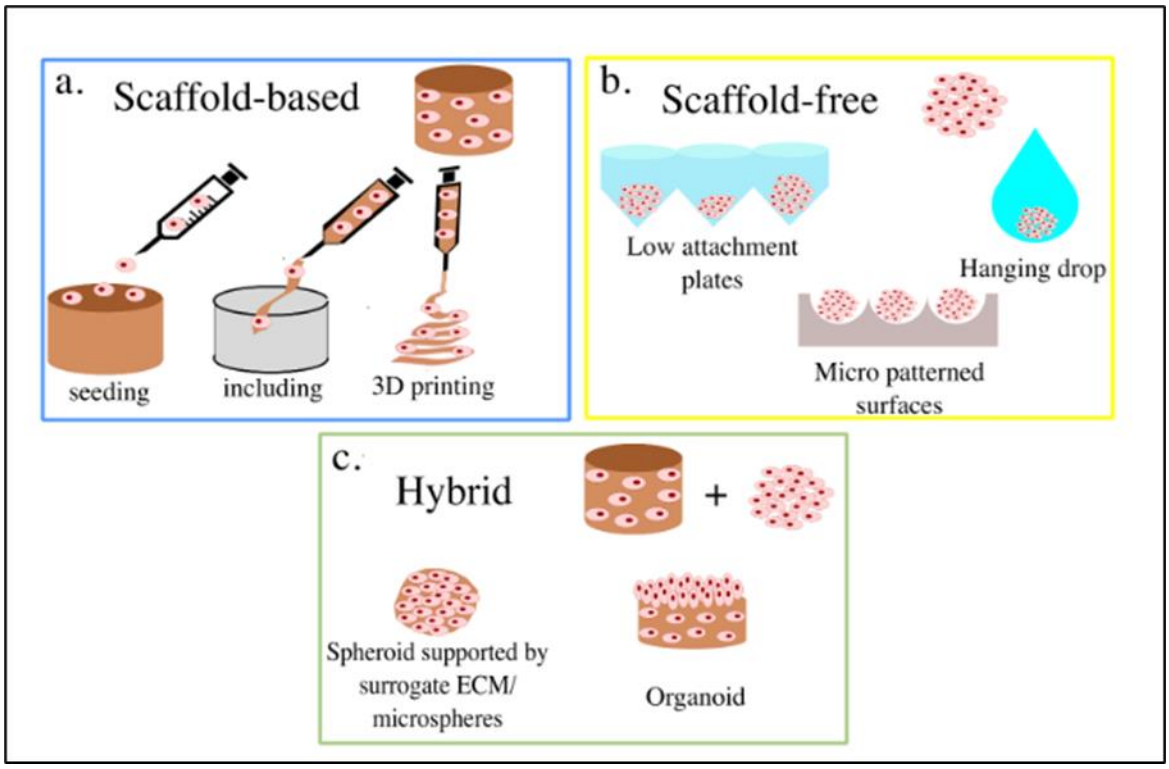

Figure 2.12. A general overview of 3D cell culture models; (A) scaffold-based model which depends on an extrinsic supporting material, (B) scaffold-free model that cells are grown self-assembly as spheroids or clusters, and (C) hybrid model (Cortesi & Giordano, 2022).

The scaffold-based model has some advantages over the other 3D cell culture models such as enable to construction with a wide range of materials to achieve the desired properties, allowing for the creation of co-cultures, being customizable and medium cost (Cortesi & Giordano, 2022).

3D cell culture methods are intended to close the gap between in vivo and in vitro tumor models. In the ideal tumor model, a repeatable in vivo-like tumor micro-environment including an extracellular matrix (ECM) is required for tumor cells to proliferate, develop three-dimensional structures, and simulate their invasive activity. The 3D cell culture systems promise to maintain the in vivo phenotype of cancer cells by structurally mimicking the tumor microenvironment (Kievit et al., 2010; L. Ma et al., 2018). Besides the cell-cell and cell-ECM interactions which are able to be provided in 3D models, play important role in cell signaling that influences the drug responses of the tumor. Hence, 3D tumor models have shown promising use in cancer drug screening and cancer biology research (Caicedo-Carvajal et al., 2011; Estrada et al., 2016).

Until today many researchers have strived to develop an ideal 3D tumor model for GBM with various scaffolds and they published several studies on this subject (table 2.11)

Table 2.11. Certain studies about 3D GBM cell culture

Scaffold Material	Cell Line	Projected and Results	Reference
GelMA (gelatin methacrylate) hydrogel	U-251MG Glioblastoma cell line and Patient derived Glioma cells	Researchers was aimed to investigate the treatment-resistant glioblastoma cells and they reported that glioma cells grown in 3D-GelMA hydrogel exhibit mesenchymal-like properties with increased cytokine production and partially recap the immune cell-infiltration.	(Shah et al., 2021)
Poly (ethylene-glycol)-based hydrogel	Patient derived Glioma cells	Researchers was planned to demonstrate the effect of hydrogel stiffness on GBM cells, and their studies showed that decreasing hydrogel stiffness enhanced the GBM cell proliferation and increasing hydrogel stiffness further enhanced drug resistance.	(Wang et al., 2021)
Polylactic acid (PLA)	U87 Glioblastoma cell line	Researchers was intended to analyze the gene expressions of GBM tumor cells cultured under 2D and 3D and their study revealed that the hypoxia related genes which contributes the drug resistance mechanisms were upregulated in 3D cell culture condition compared to 2D conditions.	(L. Ma et al., 2018)
Polystyrene	E2, R10, and G7 Glioblastoma cell line	Researchers was aimed to compare the therapeutic agent's responses of 2D and 3D cultured GBM cells with the clinical trials and they reported that therapeutic agents responses of 3D cultured GBM cells are identical with the clinical trials.	(Gomez-Roman, Stevenson, Gilmour, Hamilton, & Chalmers, 2017)

Table 2.11. Certain studies about 3D GBM cell culture (continuation).

Scaffold Material	Cell Line	Projected and Results	Reference
Collagen	U-251 Glioblastoma cell line	The researchers were aimed to investigate the anti-glioma drug efficacies and different drug resistance mechanisms on 3D platform, and they revealed that glioma cells cultured on their 3D scaffolds showed a greater degree of dedifferentiation and quiescence than cells in 2D culture. 3D cultured cells also exhibited enhanced resistance to chemotherapeutic alkylating agents and upregulation of O6-methylguanine DNA methyltransferase (MGMT). In addition to that their tumor cells in 3D culture showed chemotherapy resistance patterns similar to those observed in glioma patients.	(Lv et al., 2016)
Electrospun polystyrene scaffolds coated with laminin	U-251 Glioblastoma cell line	Researchers was aimed to compare gene and protein expression in 2D, and 3D systems and their results demonstrated the influence of 3D (versus 2D) context on integrin expression and how it profoundly affects ECM signaling.	(N. K. L. Ma et al., 2016)

In this study, a scaffold-based 3D cell culture model was applied to create a 3D GBM cancer cell culture system.

3. METHODOLOGY

In this study, it was aimed to develop a 3D cell culture system for GBM. All methods applied for this purpose are given in figure 3.1.

Figure 3.1. The methods applied in this study.

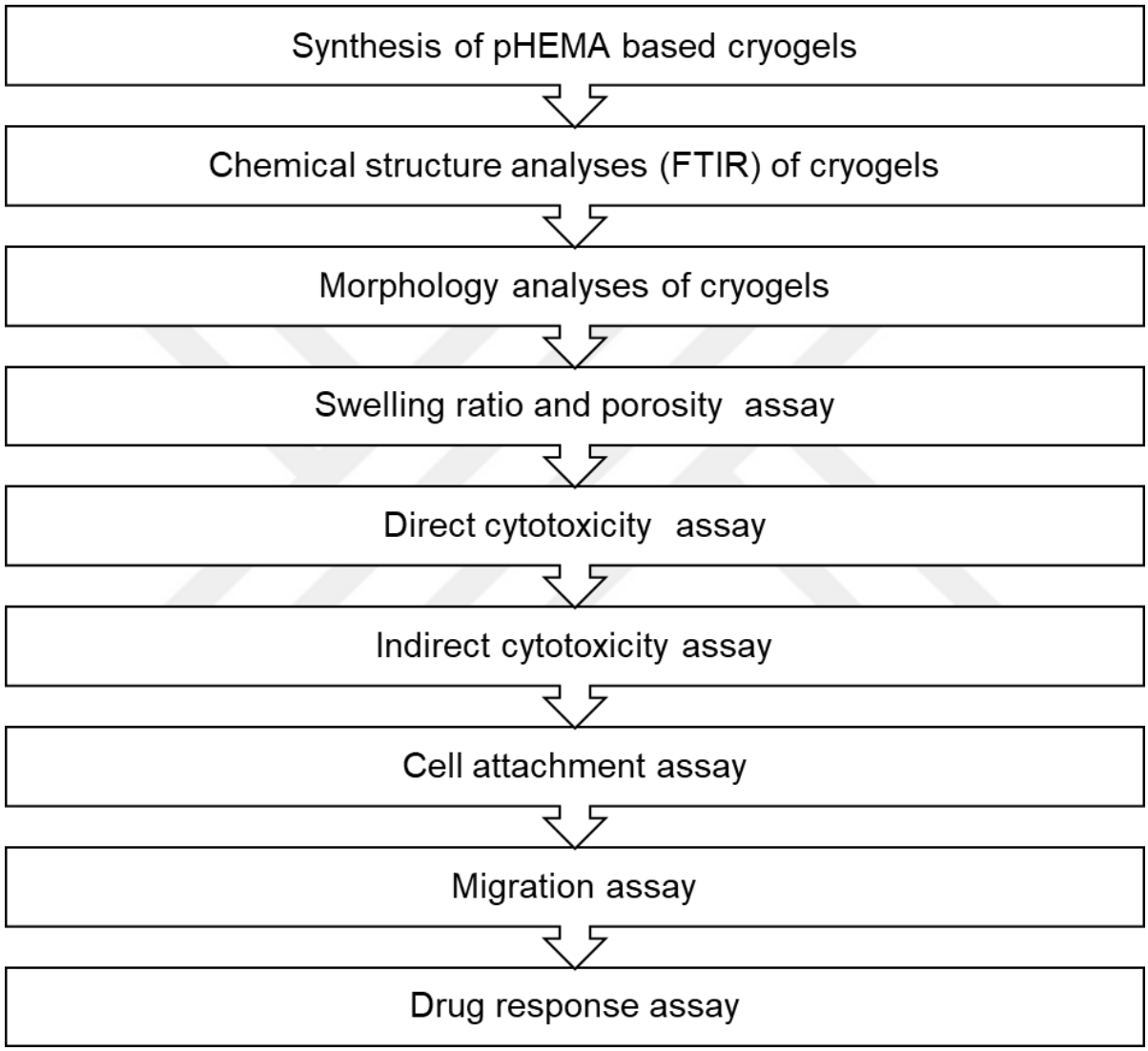

3.1. Synthesis And Characterization of pHEMA-Gelatin Cryogels

pHEMA-gelatin cryogels were used as the scaffold to create the 3D cell culture. pHEMA was crosslinked with MBAA (N, N′-methylenebis (acrylamide)), and gelatin was crosslinked with glutaraldehyde. Cryogels were synthesized at 3 different temperatures (-12 ^{o}C, -16 ^{o}C, and -20

^{o}C) and with 3 different amounts of gelatin (0,2g (1% (w/w)), 0,3g (1,5% (w/w)), 0,4g (2%(w/w))) (see Table 3.1) by following the protocol below.

1. Solution A was prepared by dissolving gelatin (Sigma, USA) in 3 mL of ultra-pure water.
2. Solution B was prepared by mixing 1,3 mL HEMA (10% (v/v)) (Sigma, USA) and 2 mL ultra-pure water.
3. Solution C was prepared by dissolving 0,275 g MBAA (Sigma, USA) in 10 mL ultra-pure water.
4. Solutions A, B, and C were mixed.
5. For 0,2 g gelatin 20 µL, for 0,3 g gelatin 30 µL, and for 0,4 g gelatin 40 µL glutaraldehyde (25%, v/v) was added to the mixture.
6. 130 µL APS (100mg/mL) (Sigma, USA) and 25 µL TEMED (Sigma, USA) were added.
7. Finally, the mixture was poured into 2 mL syringes and left in a cryostat for cryogelation at different temperatures (-12 oC, -16 oC, -20 oC).
8. When the cryogelation process was finished, the cryogels were washed with ultrapure water.

Table 3.1. The temperatures and the gelatin quantities of cryogels.

Temperature (^{o}C)	**-12**			**-16**			**-20**		
Gelatin (g)	0,2	0,3	0,4	0,2	0,3	0,4	0,2	0,3	0,4
Code	122	123	124	162	163	164	202	203	204

Afterward, characterization and in-vitro cell studies were performed. Chemical structure analyses, morphology analyses, polymerization yield calculation, swelling, and porosity assays were performed within the characterization studies.

3.1.1. Chemical structure analyses

The pHEMA-gelatin-based cryogels were dried by a freeze-dryer and the chemical structures of cryogels were investigated by Fourier transform infrared (FTIR) spectroscopy (Jasco, FT/IR-6700).

3.1.2. Morphology analyses

The morphology of cryogels was analyzed by scanning electron microscopy (SEM). To prepare cryogels for SEM analyses cryogels were cut into 1 mm thick (D=8mm) and dried by freeze-dryer. Then cryogels were coated with gold-palladium and examined using a scanning electron microscope (FEI, Quanta 650 Field Emission SEM). The pore sizes of the cryogels were measured from the SEM images by using ImageJ software.

3.1.3. Swelling ratio and porosity assay

Cryogels were cut into 1 mm thick (D=8mm) as a half circle and dried by freeze-dryer for 20 minutes. The dry weight of cryogels (m_d) was recorded. Cryogels were immersed in ultrapure water and weighed (m_w) every minute until the weights were fixed. Before weighing the swollen cryogels excess water was taken away from the cryogels with filter paper. The swelling ratio and swelling degree of cryogels were calculated with equation 3.1 and 3.2 respectively.

$$Swelling\ ratio(\%) = \left[\frac{m_w - m_d}{m_d}\right] x100 \quad (3.1)$$

$$Swelling\ degree\left(g_{water}/g_{cryogel}\right) = \left[\frac{m_w - m_d}{m_d}\right] \quad (3.2)$$

To investigate the macroporosity (%), cryogels were cut into 1 mm thick (D=8 mm) as a half circle and dried by freeze-dryer for 20 minutes. The dry weight of cryogels (m_d) were recorded. Cryogels were swelled up with ultra-pure water. The swollen weight of cryogels (m_w) was recorded. Then swollen cryogels were squeezed and weighed (m_s). The macroporosity rate of cryogels was calculated with equation 3.3.

$$Macroporosity(\%) = \left[\frac{m_w - m_s}{m_w}\right] x100 \quad (3.3)$$

3.1.4. Polymerization yield

Cryogels were dried by freeze-dryer and weighed (m_d). The total monomer mass (m_t) was determined and the polymerization yield of cryogels was calculated with equation 3.4.

$$Yield(\%) = \left[\frac{m_d}{m_t}\right] x100 \quad (3.4)$$

3.2. In Vitro Cell Studies

3.2.1. Cells and culture conditions

The cell studies were conducted with mouse embryonic fibroblast (MEF, (CF-1) (ATCC® SCRC-1040™)) and glioblastoma (U-87 MG, (ATCC® HTB-14™)) (GBM) cell lines. Cells were cultured with Dulbecco's Modified Eagle's medium (DMEM, Hyclone) enriched with 10% fetal bovine serum (FBS, South America) and 55 μM β-mercaptoethanol (Merck) (used for MEF cells only). Cells were incubated in a humidified incubator at 37 ^{o}C and 5% CO_2.

3.2.2. Sterilization of Scaffolds

Scaffolds were sterilized with 70% ethanol (Merck). They were cut into 1 mm thick (D=8 mm) as a half circle and were kept in 70% ethanol for 2 hours in sterile Petri dishes. After that, scaffolds were washed with sterile ultra-pure water twice and kept in ultra-pure water for 2 hours. Then, scaffolds were placed into a 24-well plate and kept in DMEM for 2 hours after washing with culture medium (DMEM) twice. Before cell seeding, DMEM was removed, and scaffolds were left for 1 hour to dry.

3.2.3. Cytotoxicity Assay

The cytotoxicity of the scaffolds was investigated by both direct and indirect assay. For the direct cytotoxicity assay, the $1x10^5$ /well U-87 MG and MEF cells were directly seeded onto scaffolds and incubated for 1, 3, and 5 days. For the indirect cytotoxicity assay, scaffolds were incubated in 20 mL culture medium for 5 days at 37 ^{o}C and then given to MEF cells seeded into 24 well plates ($1x10^4$ cell/ well) for 1,3, and 5 days. Cytotoxicity was investigated through neutral red (NR) (3-Amino-7-dimethylamino-2-methylphenazine hydrochloride) cell viability assay. Neutral red is a cationic, water soluble and non-toxic dye that is taken up by the healthy cells and then trapped in their lysosomes. The neutral red cell viability assay is based on the spectrophotometric measuring of the trapped dye in the lysosomes of viable cells (Langbeen, Jorssen, Granata, & Fransen, 2014; Miller, Bankier, Al-Shaeri, & Hartl, 2015). The followed NR assay protocol is as below.

1. The medium was aspirated.
2. Cells were washed with PBS (Merck).

3. 1 mL NR solution (33%) (Sigma) was added.
4. Samples were incubated for 2 hours.
5. NR solution was aspirated.
6. 1 mL NR solubilization solution (1% Acetic Acid (Merck), 49% ultra-pure H_2O, 50% Ethanol (Merck)) was added.
7. Samples were left on the agitator for 1 hour.
8. The absorbance values of each sample were measured at 540 nm using a microplate reader.
9. For each group, a negative control group was formed with an empty scaffold, and the absorbance of the negative control group was subtracted from the absorbance of the corresponding group.

3.2.4. Cell attachment analysis

Observation of cell attachment on the scaffold was performed by scanning electron microscope (SEM) analysis. U-87 MG cells were seeded onto scaffolds and incubated. After 24 hours, culture medium was aspirated, and samples were washed twice with sterile ultra-pure water. Then cells were fixed for 1 hour in a dark place using 2,5% (v/v) glutaraldehyde at 4^{o}C. After fixation, the samples were washed twice with ultra-pure water and kept at different ethanol concentrations (30%, 50%, 70%, and 100%) for 3 minutes each. Afterward, samples were dried by freeze-dryer and examined with SEM (FEI, Quanta 650 Field Emission SEM) by coating with gold-palladium.

3.2.5. Migration assay

The pHEMA-gelatin-based cryogel scaffold (164) was cut into 1mm thick (D=18 mm), sterilized, and placed into 24 well plates. A sterile plastic ring (D=5 mm) was placed in the center of each well (figure 3.2). 25 x 10^4 GBM cells were suspended in 10 μL culture medium and seeded onto each well as a densed drop. Cultures were left for 2 hours in an incubator for cells to attach to scaffolds. At the end of 2 hours, the cells were washed twice with PBS to remove non-attached cells and then culture medium was added. After 24 hours, migration of GBM cells on scaffolds was examined by DAPI (4',6-diamidino-2-phenylindole, dihydrochloride) staining. The protocol for DAPI staining is as follows.

1. Culture medium was aspirated.
2. Cells were washed with PBS (Merck) twice.
3. 1 mL paraformaldehyde (4%) was added to each well and waited for 20 minutes.
4. Cells were washed with PBS twice.
5. 1 mL 0,1% Triton X-100 (Sigma) was added to each well and waited for 10 minutes.
6. Cells were washed with PBS twice.
7. DAPI was diluted in PBS (1/1000, v/v)
8. 1 mL DAPI solution was added to each well and waited for 30 minutes.
9. Cells were washed with BSA (Sigma) - PBS solution (%1 w/v) twice.
10. Cells were examined under a fluorescence attachment microscope.

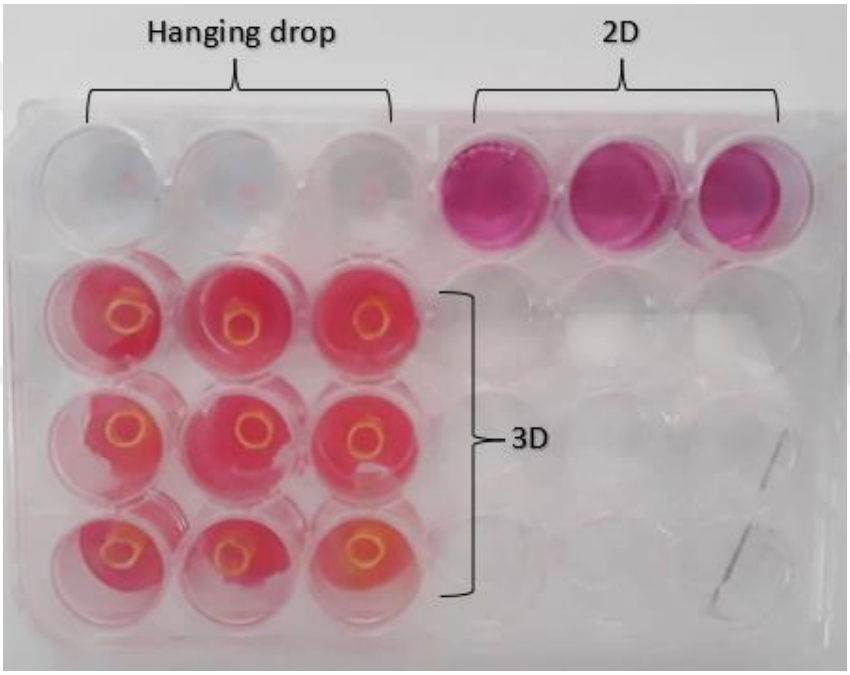

Figure 3.2. GBM cells were cultured on cryogel scaffold coded as 164 for migration assay. For accurate assessment of migration, a sterile plastic ring was placed on the scaffold and a dense cell suspension was given to the center of the ring.

3.2.6. Drug response assay

Drug response assay was performed with the chemotherapeutic drugs temozolomide and etoposide. First of all, the 50% inhibitor concentration (IC50) values of chemotherapeutic drugs were determined for 2D cultured GBM cells. Cells were cultured in 24 well plates and except the control group, cultures were exposed to various doses of etoposide (5, 10, 20, 40,

60 μM) and temozolomide (500, 750, 1000, 1250, 1500, 1750, 2000 μM) for 3 days. The IC50 values were estimated by neutral red assay.

The drug responses of GBM cells were investigated by culturing the cells in 2D, hanging drop, and scaffold-based 3D. Cultures were conducted in 24 well plates. $1x10^5$ GBM cells were cultured two-dimensionally. For hanging drop and 3D culture, $1x10^5$ cells were suspended in a 25 μL culture medium. The volume of the culture medium was kept equal to the volume of the pHEMA-gelatin cryogel scaffold (h=1 mm, D=8mm, half circle). The cell suspension was dropped on the surface of the well plate for hanging drop culture and on the surface of the scaffold for the 3D culture. Hanging drop and 3D cultures were kept in an incubator for 1 hour for cell attachment and then culture medium was given. The next day of the culture, temozolomide and etoposide were given to the cultures. The schematic representation of the culture plates is found in figure 3.3. The GBM cells were exposed to the drugs for 1, 3, and 5 days and then drug responses were evaluated by neutral red cell viability assay and DAPI staining.

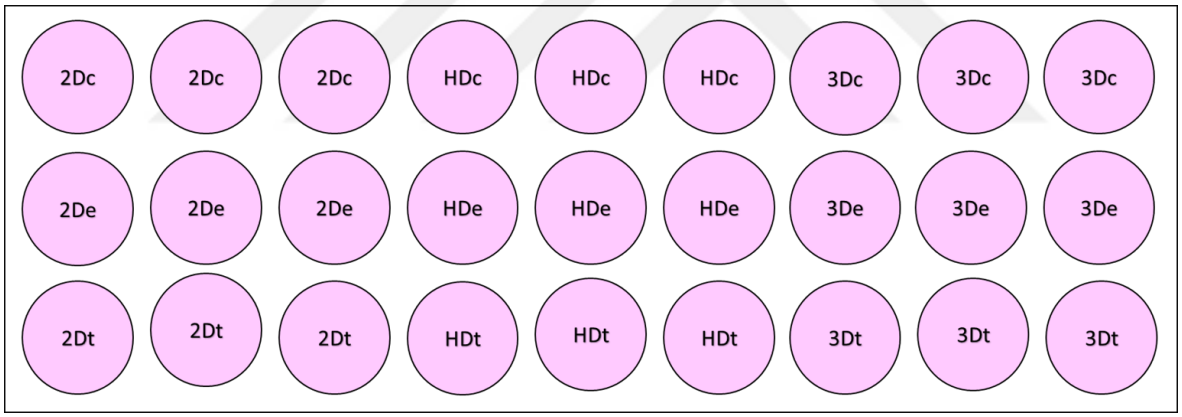

Figure 3.3. The schematic representation of 24 well plates. (2Dc= control group of 2D cell culture, HDc= control group of hanging drop cell culture, 3Dc= control group of scaffold-based 3D cell culture, 2De= etoposide given 2D cell culture, 2Dt= temozolomide given 2D cell culture, HDe= etoposide given hanging drop cell culture, HDt= temozolomide given hanging drop cell culture, 3De= etoposide given scaffold-based 3D cell culture, 3Dt= temozolomide given scaffold-based 3D cell culture.)

3.3. Statistical Analyses

All in vitro cell studies were carried out in triplicate. The statistical analyses were made using Microsoft Excel 2021. The one-way analysis (ANOVA) of variance was used to compare the data. In addition to that, the significance of the data in comparison to the controls was evaluated using the two-tailed un-paired t-test. The level of significance was established as $p<0,001$.

4. ANALYSIS AND DISCUSSION

4.1. Synthesis and Characterization of pHEMA-Gelatin Cryogels

PHEMA-gelatin based cryogels were synthesized at 12 ^{o}C, -16 ^{o}C, and -20 ^{o}C. After the cryogelation process, the ice crystals in the cryogel melted and left behind a macroporous structure. The synthesized cryogels had a sponge-like structure. Images of cryogels after washing with ultra-pure water are in figure 4.1. As the amount of gelatin in the cryogels increases, it is seen that it becomes darker yellow.

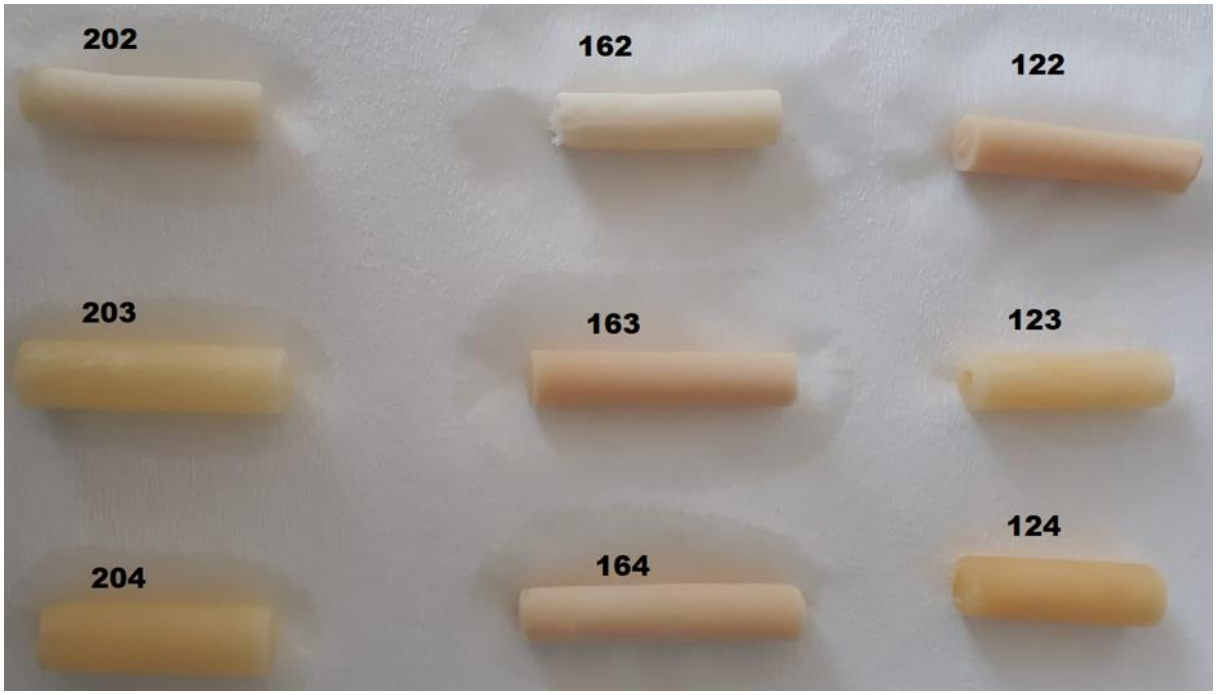

Figure 4.1. The optical photographs of synthesized pHEMA-gelatin-based cryogels.

4.1.1. Chemical structure analyses

The chemical structures of pHEMA-gelatin-based cryogels were revealed by FTIR spectroscopy. The structure analyses were made for the cryogel samples coded as 162, 163 and 164 and the FTIR results were presented in figure 4.2.

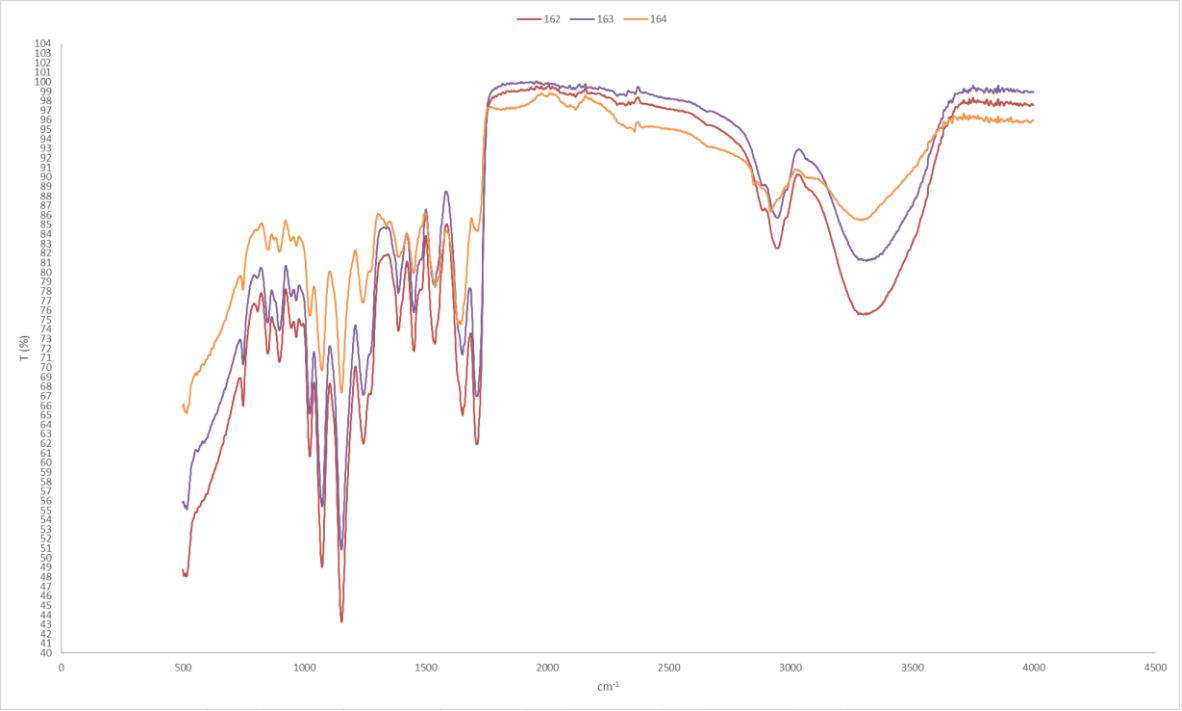

Figure 4.2. The FTIR spectra of cryogels coded as 162, 163 and 164.

The characteristic peaks of pHEMA were observed in all FTIR spectra (figure 4.2). Peaks at about 3300 cm indicated O-H and N-H bonds (Filipović et al., 2022), peaks at about 1710 cm indicated C=O bonds (Liu et al., 2020), and peaks at about 1450 cm indicated C-O-H bonds (Demirci et al., 2020). In addition to that, the peaks at between 1640 and 1240 cm finding in all FTIR spectrums pointed the characteristic "amid groups" of gelatin (Babić Radić et al., 2022). The peaks at around 1640 cm indicated the C-O bonds (amid I) (Filipović et al., 2022), the peaks at around 1530 cm indicated the N-H bonds (amid II) (Çetin, Kahraman, & Gümüsderelioglu, 2011) and the peaks at around 1240 cm indicated the C-N bonds (amid III) (C. Y. Wang et al., 2020). As a summary, FTIR spectra clearly revealed the presence of pHEMA and successful incorporation of gelatin into the structure.

4.1.2. Morphology Analyses

Morphological examinations of cryogels were made by SEM. The SEM images of cryogels are found in figure 4.3.

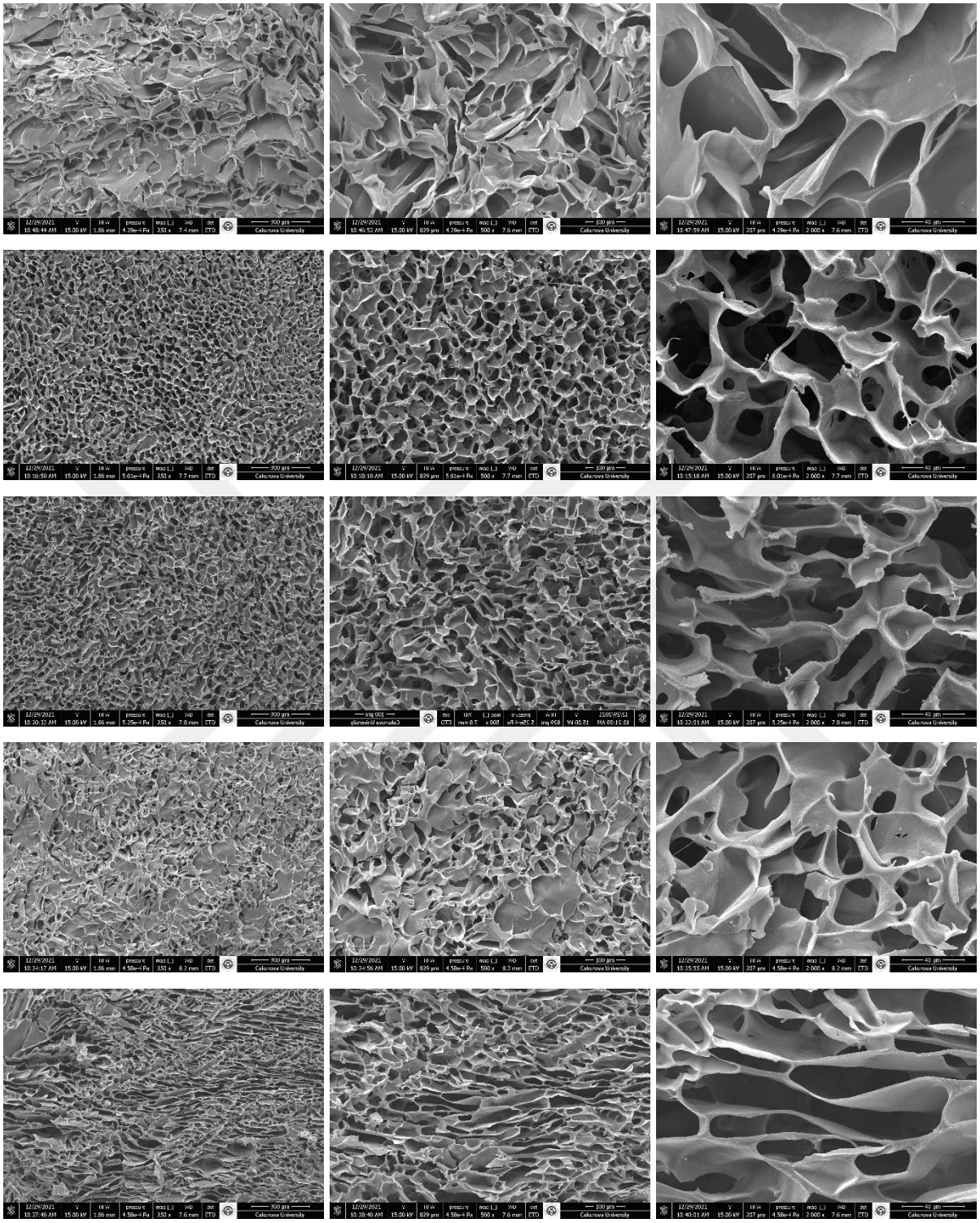

Figure 4.3. The SEM images of pHEMA-gelatin based cryogels. (first line - 204, second line -162, third line -163, fourth line -164, fifth line – 124).

According to SEM images, it was observed that all the synthesized cryogels had highly porous microstructure. While the lower cryogelation temperature resulted in a lower open pore number, increasing gelatin concentration caused a lower open pore number. The results are supported by the literature (Bakhshpour, Idil, Perçin, & Denizli, 2019; Bakhshpour, Yavuz, & Denizli, 2018; Çetin et al., 2011; Savina, Zoughaib, & Yergeshov, 2021).

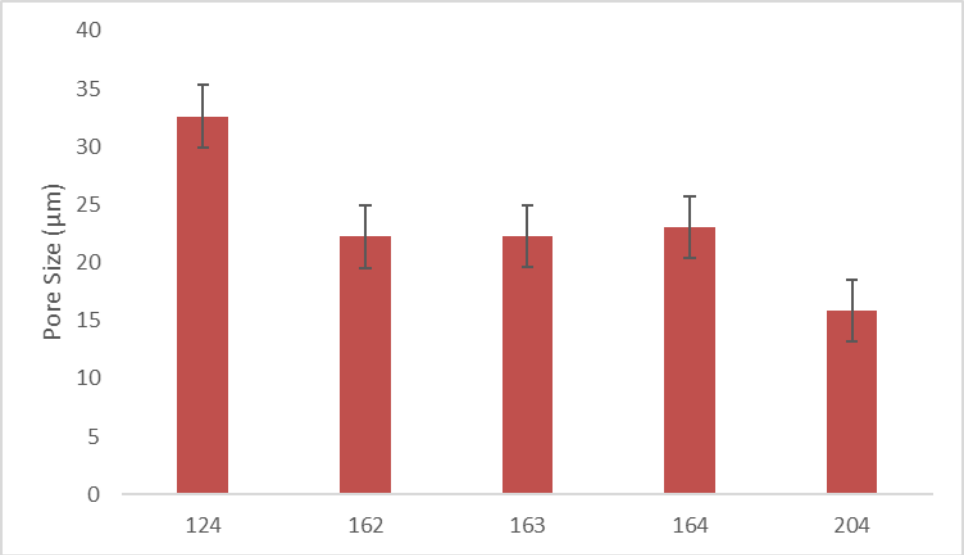

Figure 4.4. The pore sizes of cryogels determined by the ImageJ software

The maximum and minimum pore sizes were observed at cryogel synthesized at -12 and -20 respectively (figure 4.4.). It has been reported in the literature that the pore size is reduced by lowering the cryogelation temperature. The formation of pores in the cryogelation process is facilitated by solvent crystals that act as templates. At lower temperatures, more solvent will freeze, resulting in less space between the solvent crystals ((Bakhshpour et al., 2019, 2018; Savina et al., 2021). It was also observed that increasing gelatin concentration caused an increase in pore size.

Cryogels are known as sponge-like macroporous hydrogels and have highly interconnected pores that facilitate cell adhesion, proliferation and migration (Bencherif et al., 2013; Rogers & Bencherif, 2019). The pHEMA-gelatin-based cryogels synthesized in this study fit this description and were found to have a highly interconnected microporous structure.

4.1.3. Swelling ratio and porosity assay

All the synthesized pHEMA-gelatin-based cryogels were kept in ultrapure water and weighed every minute until their weight was constant to find out the swelling ratio. The cryogels were weighed when swollen, and then the swollen cryogels were squeezed to examine the macroporosity. There was a significant difference in shape between dry, swollen and squeezed cryogels. (Figure 4.5).

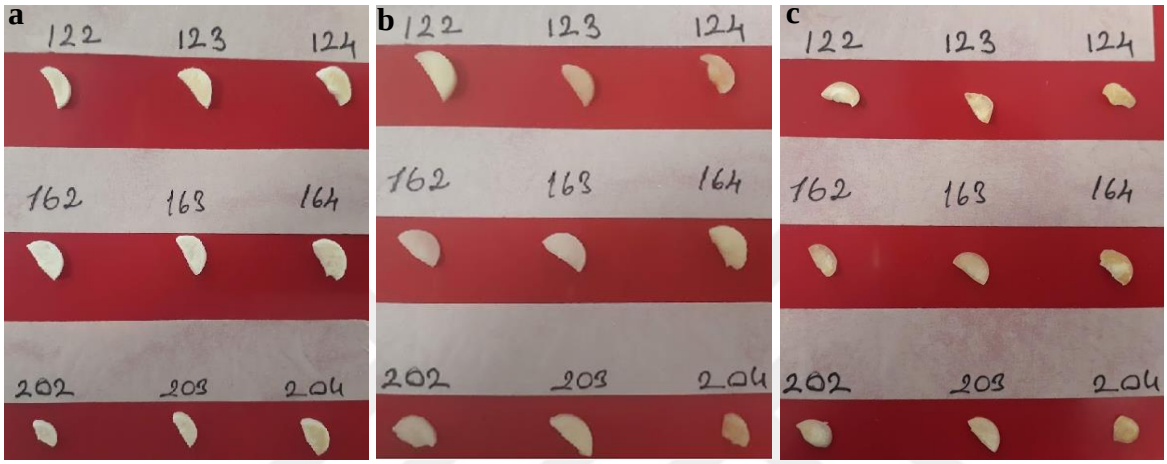

Figure 4.5. The optical photographs of synthesized pHEMA-gelatin-based cryogels. (a- dry cryogels, b- swollen cryogels, c- squeezed cryogels).

The swelling ratio of each cryogel was calculated for every minute and graphed in figure 4.6. Considering this graph, it is seen that all cryogels swell completely within 7-8 minutes. The rapid swelling is a characteristic behavior of highly porous and hydrophilic hydrogel materials (Filipović et al., 2022). This characteristic behavior was seen on all the samples.

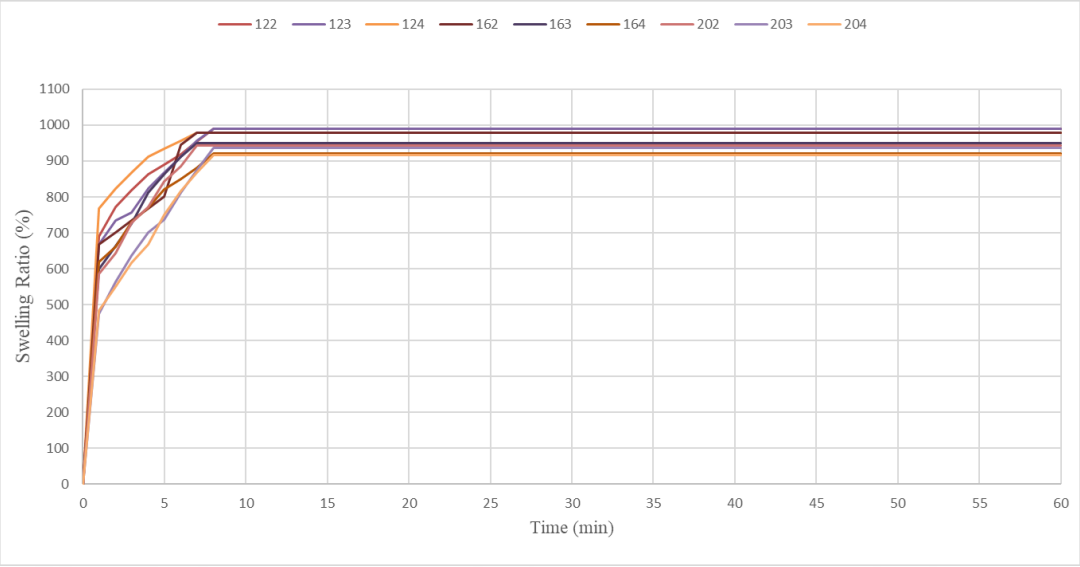

Figure 4.6. The swelling ratio of pHEMA-gelatin-based cryogels.

In the final stage, it was determined that the swelling rate of all cryogels was over 900%. The swelling ratio of cryogels coded as 122, 123, 124, 162, 163, 164, 202, 203, and 204 was 990,91%, 988,89%, 977,78%, 977,78%, 950%, 920%, 942,86%, 937,5%, and 916,67% respectively (table 4.1).

pHEMA is a hydrophilic and swelling polymer (Zasońska et al., 2021). Gelatin is also hydrophilic and has a high-water absorption capacity (Chen et al., 2018). In literature, it is seen that the swelling rate of pHEMA based cryogels is between 800%-1000%, and pHEMA-gelatin-based cryogels and hydrogels are around 500% (Demirci et al., 2020; Filipović et al., 2022; Işık Perçin, Aracagök, İdil, Denizli, & Mattiasson, 2021; Tabatabaee et al., 2022). All the cryogels synthesized in this study had a high swelling ratio; however, the increasing gelatin concentration resulted in a decreasing swelling ratio. This decrease was also seen in macroporosity. The macroporosity of cryogels coded as 122, 123, 124, 162, 163, 164, 202, 203, and 204 was 89,17%, 88,78%, 87,63%, 88,66%, 88,1%, 87,25%, 87,67%, 86,75%, and 84,31% respectively. It was reported that the cross linker and the cross-linking degree of the cryogels have massive impact on swelling and porosity characteristics (Memic et al., 2019; Yang et al., 2018). The crosslinking of gelatin makes the structure more compact and causes the reduction in swelling (Çetin et al., 2011). In this study glutaraldehyde was used as a cross linker for gelatin. Glutaraldehyde, which is the most preferred cross linker for collagen-based scaffolds, reacts with the amin groups of gelatins (Olde Damink et al., 1995). The decreases

in macroporosity with increasing gelatin concentration may be due to cross-linking mechanism. This circumstance is also supported by literature. In one study, Çetin et al. (2011) reported that increasing gelatin concentration resulted in a significant change in morphology and a decrease in the number of pores (Çetin et al., 2011). However, the macroporosity of all cryogels in this study was between 79% and 82%. These values are higher than macroporosity of some HEMA based cryogels (Demirci et al., 2020; Işık Perçin et al., 2021) and some HEMA-gelatin based cryogels (Babić Radić et al., 2022; Filipović et al., 2022) reported in the literature.

Table 4.1. Calculated swelling ratio, swelling degree, macroporosity and polymerization yield values of cryogels.

Cryogel	**122**	**123**	**124**	**162**	**163**	**164**	**202**	**203**	**204**
Swelling ratio (%)	990,91	988,89	977,78	977,78	950	920	942,86	937,5	916,67
Swelling degree (gwater/gcryogel)	9,91	9,89	9,78	9,78	9,5	9,2	9,43	9,38	9,17
Macroporosity (%)	89,17	88,78	87,63	88,66	88,1	87,25	87,67	86,75	84,31
Polymerization yield (%)	93	93	93	94	93	94	94	93	94

In Table 4.1, it is seen that the swelling and porosity values of cryogels synthesized at 3 different temperatures (for example 122, 162, and 202) with the same gelatin ratio decrease as the temperature decreases. This was also observed in the pore sizes of cryogels. Likewise, at lower temperatures, the more solvent freezes, leaving less space behind. Thus, macroporous structures with smaller pore diameters and thick polymer walls are formed (Bakhshpour et al., 2019, 2018; Savina et al., 2021).

Swelling and macroporosity properties are very important for a cryogel used as tissue scaffold. Because these properties are directly related to the ability of the scaffold to mimic the ECM. Thus, transport of nutrition, biochemicals and wastes, cell attachment, ingrowth, and migration are significantly affected by these properties of the cryogel (Chang & Wang, 2011; Guo, Yang, Zhou, Chen, & Li, 2017; Memic et al., 2019). As seen in Table 4.1, the

pHEMA-gelatin-based cryogels synthesized in this study had excellent swelling capacity and macroporosity. Therefore, it is predicted that the pHEMA-gelatin-based cryogels synthesized in this study will be successful in use as tissue scaffolds due to these excellent properties.

4.1.4. Polymerization yield

The total monomer mass used for gelation was calculated and the polymerization yield was calculated with equation 3.4. The polymerization yields of cryogels were chancing from 93% to 94% (see table 4.1). Therefore, it was thought that all the cryogels in this study could be synthesized successfully with high yield.

4.2. In Vitro Cell Studies

4.2.1. Cytotoxicity Assay

The cytotoxicity of the scaffolds was investigated through direct and indirect cytotoxicity assay.

4.2.1.1. Direct cytotoxicity

The neutral red assay results of 1,3 and 5 days of cultured MEF and GBM cells are figured out in figure 4.7 and figure 4.8 respectively. The cytotoxicity of the pHEMA-gelatin based cryogel scaffolds was evaluated by comparing it with the viability of the 2D seeded cells.

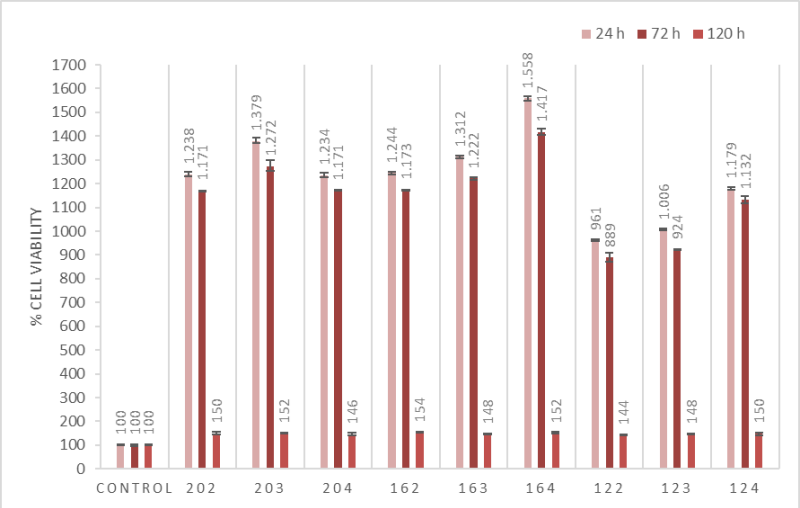

Figure 4.7. The viabilities (%) of MEF cells seeded as 2D (control) and seeded onto pHEMA-gelatin based cryogel scaffolds (202, 203, 204, 122,123, 124, 162, 163, 164) according to neutral red assay results ($p<0,001$).

According to neutral red assay results, the viability of MEF cells for all the synthesized pHEMA-gelatin based cryogel scaffolds (coded as 202, 203, 204, 122,123, 124, 162, 163, and 164) was higher than the control group. Cell viability ranged from 961% to 1558% for 24 hours cultured cells, 889% to 1417% for 72 hours cultured cells and 144% to 152% for 120 hours cultured cells. These results indicated that all scaffolds did not possess a cytotoxic effect for noncancerous MEF cells. Also, considering that MEF cells reached more than 961% viability in 24 hours, it was clearly suggested that pHEMA-gelatin based cryogel scaffolds not only were not cytotoxic but also, presented an excessive area to attachment and proliferation of MEF cells. Additionally, according to the cell viability assay even though MEF cell viability was higher than the control group for each scaffold in all culture periods, there was a decrease in viability for 1 to 3- and 5-day cultures at each scaffolds group. It was considered that these decreases were the over-proliferation of MEF cells and not related to scaffolds.

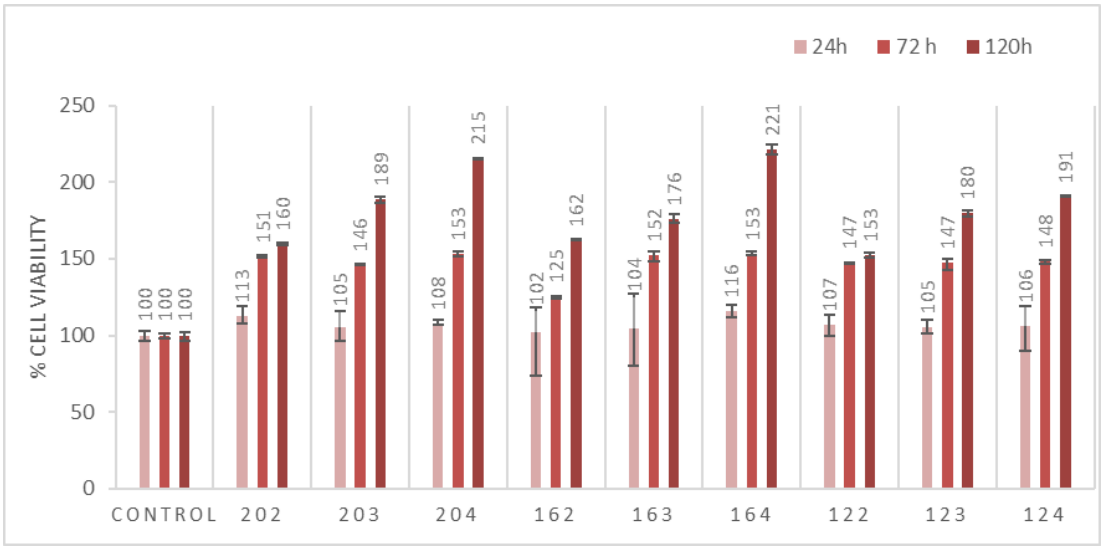

Figure 4.8. The viabilities (%) of GBM cells seeded as 2D (control) and seeded onto pHEMA-gelatin based cryogel scaffolds (202, 203, 204, 122,123, 124, 162, 163, 164) according to neutral red assay results ($p<0,001$).

The cell viability assay results revealed that all the synthesized pHEMA-gelatin-based scaffolds (202, 203, 204, 122,123, 124, 162, 163, 164) had no cytotoxic effect on GBM cells as well as it was on MEF cells. The viability of GBM cells seeded onto scaffolds was higher than the viability of the control group for each scaffold and all incubation periods. Cell viability ranged from 102% to 116% for 24 hours cultured cells, 125% to 153% for 72 hours cultured cells, and 153% to 221% for 120 hours cultured cells. Moreover, proliferation of GBM cells continued in all scaffolds as the culture time increased. Thus, these results showed that all the scaffolds were suitable for GBM cell attachment and proliferation besides their properties of not being cytotoxic for cells. Of all the pHEMA-gelatin-based cryogel scaffolds, the cryogel encoded 164 offered the highest cell viability for both MEF and GBM cells. Cell viability of GBM cells cultured on 164-code cryogel was 116%, 153%, and 221% for the 1-, 3-, and 5-day incubation periods, respectively. For the rest of the study, 164 coded cryogel produced with 0.4g gelatin at -16 ºC was chosen as the GBM cancer cell scaffold.

4.2.1.2. Indirect cytotoxicity

The indirect cytotoxicity of the pHEMA-gelatin -based cryogel coded as 164 was evaluated using the non-cancerous MEF cells by using neutral red assay. The assay results were graphed out in figure 4.9.

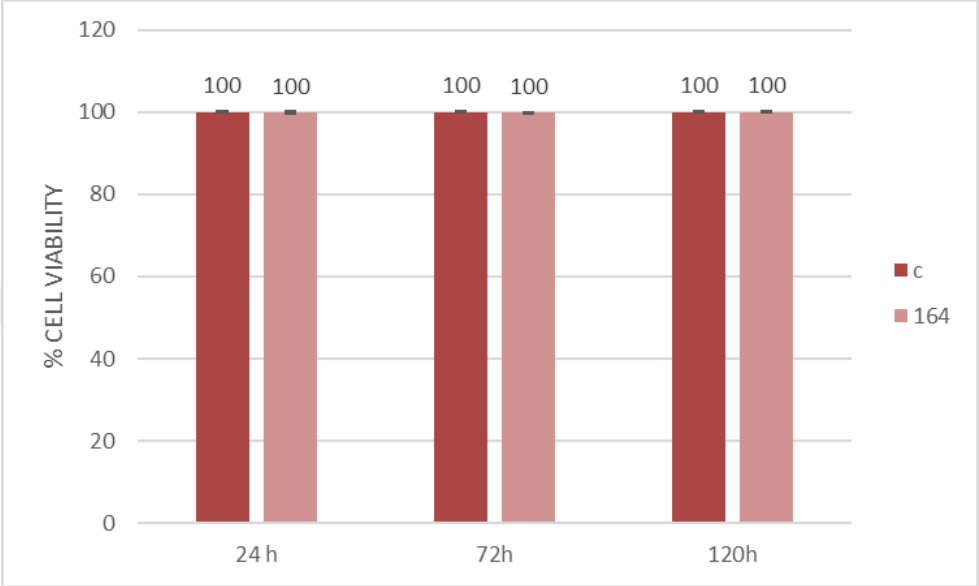

Figure 4.9. The indirect cytotoxicity assay results of pHEMA-gelatin based cryogel scaffold coded as 164 on MEF cells ($p<0,001$).

The neutral red assay results clearly indicated that this synthesized pHEMA-gelatin based cryogel scaffold had no indirect cytotoxic effect on MEF cells. pHEMA is already known as a biocompatible, nonbiodegradable, and inert material (Zasońska et al., 2021). Also, gelatin is known as biocompatible and biodegradable. However, even if gelatin degraded in a culture medium, showing a cytotoxic effect would be unexpected as it is a natural biopolymer and part of the extracellular matrix (Fan et al., 2019). Indirect cytotoxicity assay results supported that the cryogels included no residues that could be toxic to cells.

4.2.2. Cell attachment

Cell attachment was examined by SEM analyses of cells cultured on cryogels for one day (figure 4.10, figure 4.11) and by DAPI staining of cells cultured on cryogels for days 1 and 3 (figure 4.12).

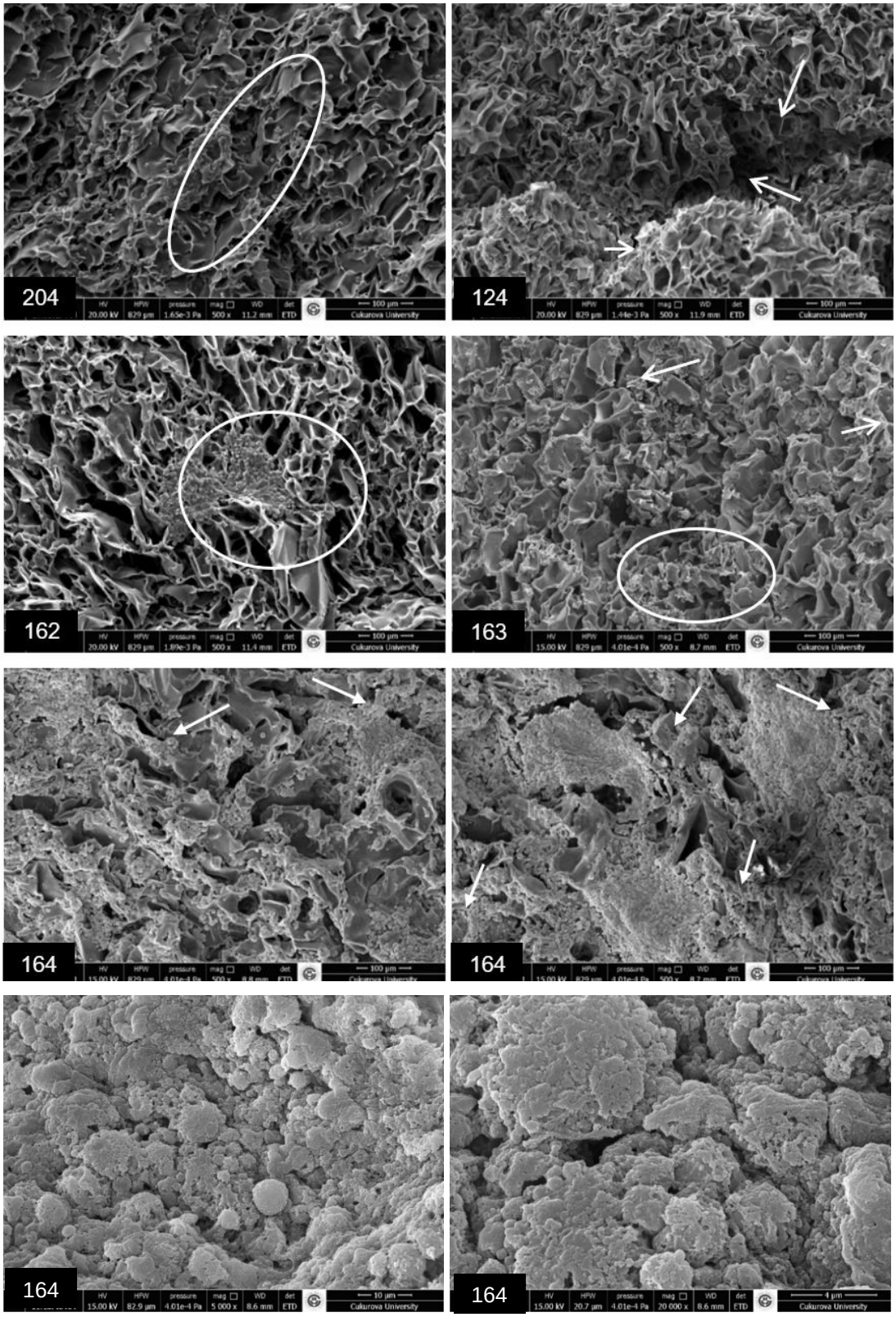

Figure 4.10. The SEM images of one day cultured GBM cells on pHEMA-gelatin based cryogels. Cells were pointed with arrows and circles.

It was observed that GBM cells could attach to all the synthesized pHEMA-gelatin-based cryogels. In figure 4.10 cells attached to cryogels were pointed with arrows and circles. While the cells were crowded in the first seeded areas, it was observed that the cells tended to migrate to another area, adhered to the pores of cryogels, and invaded into the scaffold despite it was the early stages of culture.

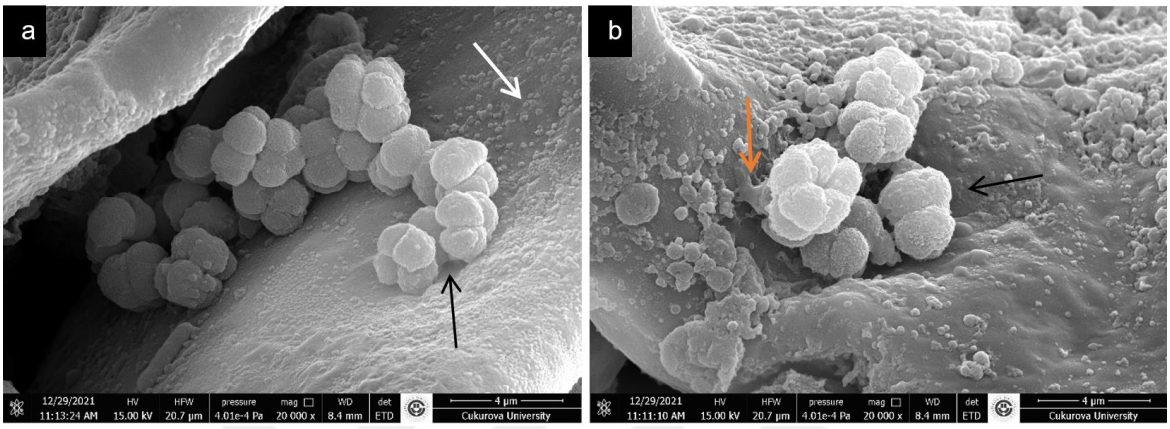

Figure 4.11. The SEM images of GBM cells cultured on cryogel coded as 164. The black arrows points to the GBM cells, the white arrow points to the extracellular elements and the orange arrow points to the lamellipodia.

When figure 4.11-b was examined, the formation of lamellipodia which is a characteristic part of motile cells, was observed. Lamellipodia is a structure that consists of actin filaments, attached to the surface, and enables the motility of the cell (Innocenti, 2018). Motility is very important for tumor invasion. The observation of lamellipodia supports that the GBM cells cultured on pHEMA-gelatin- based cryogel was successfully attached to the surface and migrated. Also, it was thought that the observation of lamellipodia means that the GBM cells tended to create their own extracellular matrix since the movement of lamellipodia is regulated by the extracellular matrix proteins (Ballestrem, Wehrle-Haller, Hinz, & Imhof, 2000). In figure 4.11-a there are some particles pointed with a white arrow. Considered together with lamellipodia formation, these particles have been considered as extracellular matrix elements that GBM cells produced to create their extracellular matrix. Therefore, the non-cytotoxic and highly microporous pHEMA-gelatin-based-cryogel synthesized in this study seems suitable for the constructing of a 3D GBM tumor model.

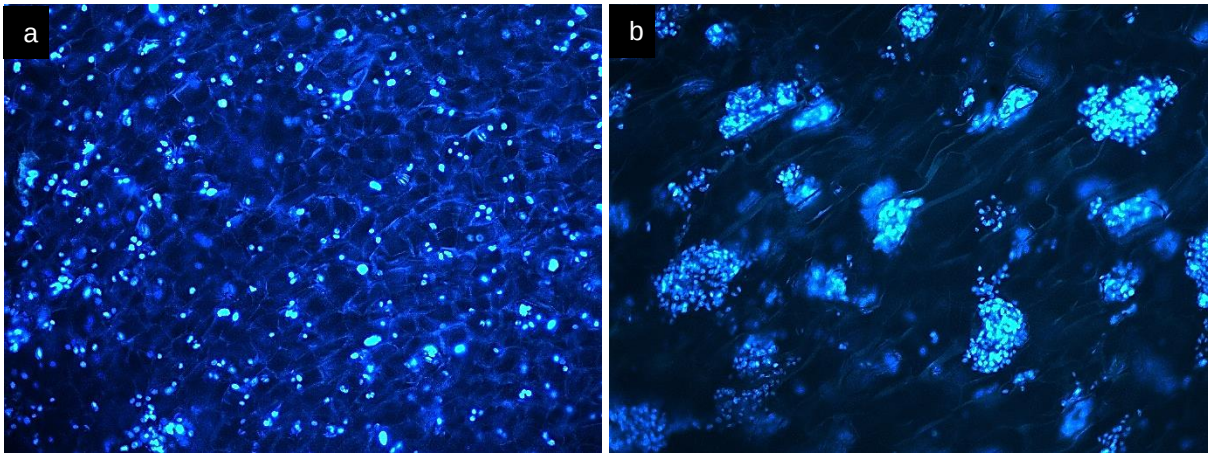

Figure 4.12. The DAPI staining images of GBM cells cultured on cryogel coded as 164. a- One day cultured GBM cells, b- 3 days cultured GBM cells.

The cell attachment was also observed by DAPI staining (figure 4.12). GBM cells appeared adhered to the cryogel surface in the fluorescence microscopy image of both 1- and 3-day cultures. The GBM cells tended to form clusters and appeared to have a distinct and coordinated intercellular mechanism of communication. It is possible to see the formation of a fusion of two cells or a merge of more cells (Bryukhovetskiy et al., 2018; Manome et al., 2010). When looking at both SEM and DAPI staining images GBM cells seemed to form clusters. Especially the tending of GBM to forming clusters was seen as more obvious in 3-day cultured cells (figure 12-b).

4.2.3. Migration assay

The migration of GBM cells on pHEMA-gelatin-based cryogel scaffold (coded as 164) was investigated by DAPI staining. The microscope images of the stained cells are shown in figure 4.13.

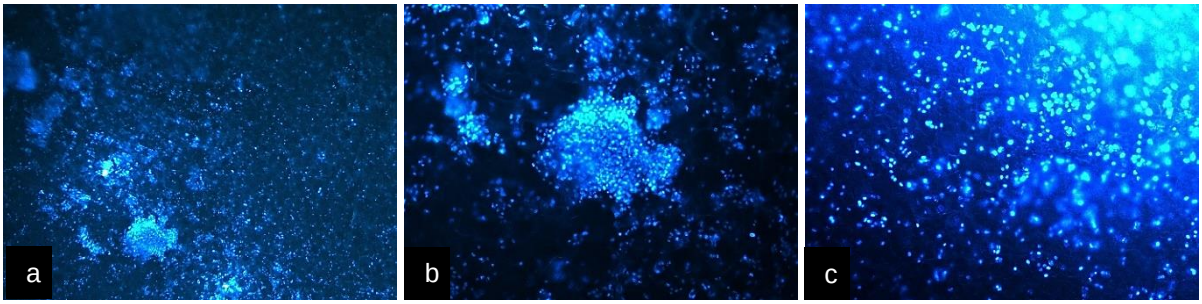

Figure 4.13. The DAPI satining images of one day cultured cells for migration assay. (a-4X, b-10X, c-20X)

As seen in figure 4.13 the GBM cells which were seeded on the center of the scaffold adhered, preserved the viability, and migrated to surface of the scaffold. Moreover, GBM tumor cells not only migrated on the surface of the cryogel but also migrated into the pores of the cryogel scaffold. It was thought that the highly porous structure of pHEMA-gelatin-based cryogel presented a suitable microenvironment that facilitates the adhesion, proliferation, and migration of GBM tumor cells.

4.2.4. Drug response assay

The chemosensitivity of GBM cells cultured on pHEMA-gelatin based cryogel scaffold (coded as 164) was evaluated by investigating the responses of GBM cells against chemotherapeutic drugs temozolomide and etoposide. The IC_{50} values of chemotherapeutic drugs temozolomide and etoposide on GBM cells for 72 hours were determined by performing neutral red cell viability assay. The cell viability results of cultures for each drug were graphed out in figure 4.14.

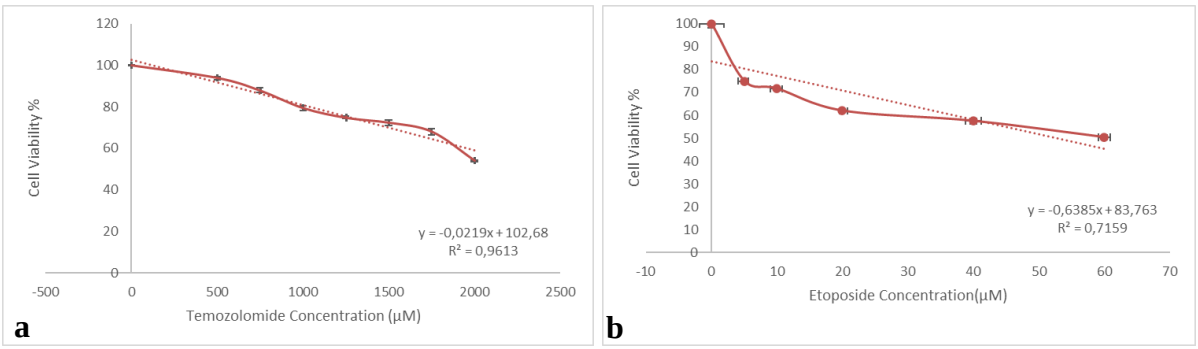

Figure 4.14. The neutral red cell viability assay results of (a) temozolomide and (b) etoposide given cells ($p<0,001$).

The IC_{50} values of each drug on GBM cells for 72 hours were calculated according to cell viabilities. The IC_{50} of temozolomide was determined as 2405 µM and the IC_{50} of etoposide was determined as 60 µM.

The IC_{50} values of the drugs were given to cells cultured as 2D, hanging drop, and 3D and drug responses were observed by neutral red assay. The neutral red assay results for each culture group were graphed out in figure 4.15.

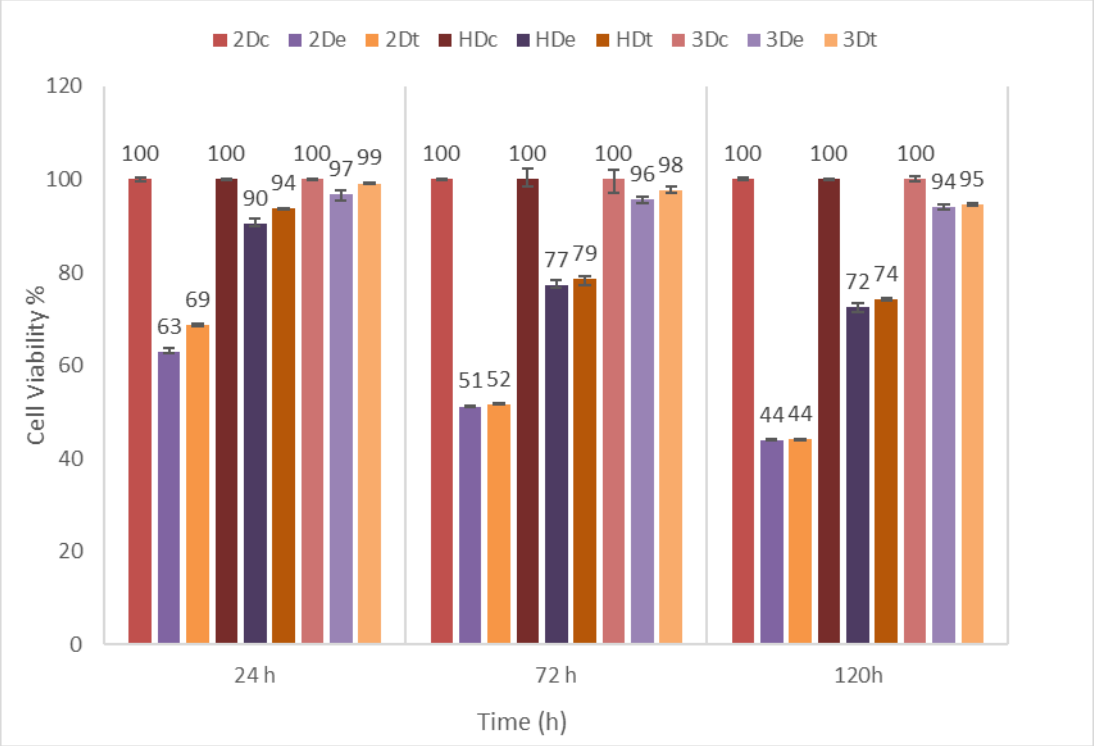

Figure 4.15. The neutral red cell viability assay results of temozolomide and etoposide given cells (2Dc= control group of 2D cell culture, HDc= control group of hanging drop cell culture, 3Dc= control group of 3D cell culture, 2De= etoposide given 2D cell culture, 2Dt= temozolomide given 2D cell culture, HDe= etoposide given hanging drop cell culture, HDt= temozolomide given hanging drop cell culture, 3De= etoposide given 3D cell culture, 3Dt= temozolomide given 3D cell culture) ($p<0,001$).

According to neutral red assay, the chemotherapeutic drugs significantly reduced the viability of 2D cultured GBM cells for all 3 incubation periods (1, 3 and 5 days). Etoposide reduced viability to 63%, 51%, and 44%, while temozolomide reduced viability to 69%, 52%, and 44% in 24-hour, 72-hour, and 120-hour cultures, respectively. In hanging drop cultures cell

viabilities were higher than 2D cultures. Etoposide reduced viability to 90%, 77%, and 72%, while temozolomide reduced viability to 94%, 79%, and 74% in 24-hour, 72-hour, and 120-hour cultures, respectively. However, the highest viability was observed in 3D cultures. The chemotherapeutic drugs etoposide and temozolomide did not appear to be as effective in 3D cultured cells as they were in 2D. Etoposide reduced viability to 97%, 96%, and 94%, while temozolomide reduced viability to 99%, 98%, and 95% in 24-hour, 72-hour, and 120-hour cultures, respectively in 3D cultures. In 72 hours, cultures, both drugs inhibited nearly half of the viability of 2D cultured cells. Whereas in 3D cultures etoposide and temozolomide could inhibit the viability of cells only 4% and 2% respectively. These results were also confirmed with DAPI staining (figure 4.16). A greater reduction in DAPI-stained nuclei was observed in 2D and hanging drop cultures than in 3D.

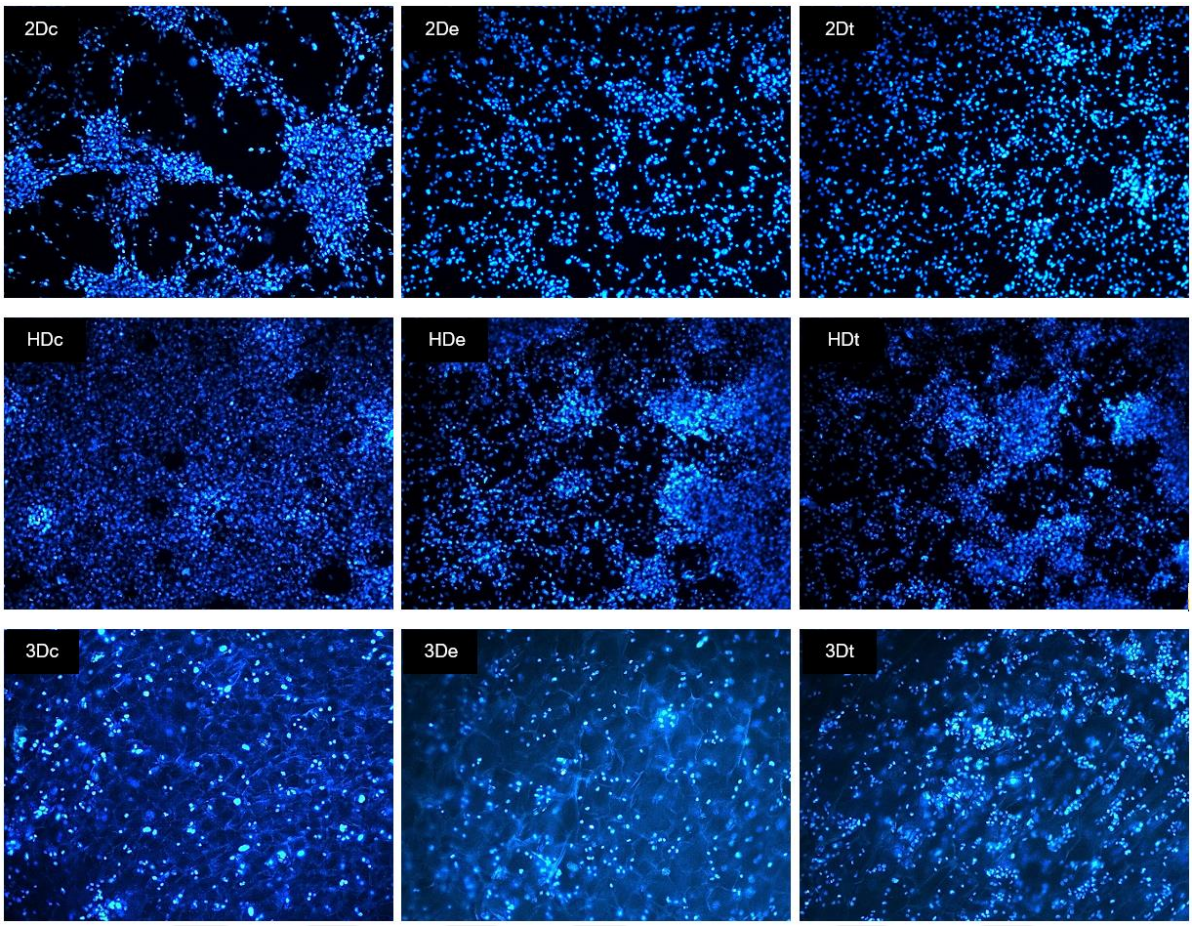

Figure 4.16. The DAPI staining images of one day cultured GBM cells with etoposide and temozolomide (10X) (2Dc= control group of 2D cell culture, HDc= control group of hanging drop cell culture, 3Dc= control group of 3D cell culture, 2De= etoposide given 2D cell culture, 2Dt= temozolomide given 2D cell culture, HDe= etoposide given hanging drop cell culture, HDt= temozolomide given hanging drop cell culture 3De= etoposide given 3D cell culture, 3Dt= temozolomide given 3D cell culture).

The results revealed that GBM cells presented more resistance when cultured in 3D than in 2D. There are several studies in the literature that support these results and show that 3D cultured GBM cells are more resistant to chemotherapeutic drugs than 2D culture (Dai, Ma, Lan, & Xu, 2016; Lv et al., 2016; Musah-Eroje & Watson, 2019; Shah et al., 2021; C. Y. Wang et al., 2020). Hence, the drug resistance results confirmed that creating a 3D GBM cell culture with the pHEMA-gelatin-based cryogel scaffold was successful.

According to researchers, solid tumors respond to chemotherapeutics with rapid adaptation (Lovitt et al., 2014). Also, GBM is known as a highly aggressive tumor that shows resistance to treatments with chemotherapeutics (Bolcaen et al., 2021; Burster et al., 2021). There are various parameters that influence the efficacy of anti-cancer therapies in vivo. The use of 3D cell culture models allows for the creation of these parameters in vitro (Habanjar et al., 2021; Lovitt et al., 2014). Therefore, the findings supported by the literature suggest that 3D cultures will be more effective than 2D in drug studies for GBM. In addition, considering all these issues, it is thought that the 3D GBM cell culture created with the pHEMA-gelatin-based cryogel scaffold could be suitable for use as a drug testing platform.

5. CONCLUSION

This study was aimed to establish a novel 3D glioblastoma model with pHEMA-gelatin-based cryogel scaffold. pHEMA-gelatin-based cryogels were successfully synthesized at 3 different cryogelation temperatures (-12 ^{o}C, -16 ^{o}C, and -20 ^{o}C) and with 3 different gelatin concentrations (0.2g, 0.3g, 0.4g). Considering the characterization analyses and cytotoxicity assays, all of the synthesized cryogels were suitable to use as a scaffold in terms of the porosity, swelling characteristic and being not cytotoxic. The cryogel used for drug response analysis was synthesized at -16 °C with a concentration of 0.4 g gelatin (164) which gives the best cell viability results. This pHEMA-gelatin based cryogel that had 91%polymerization yield and highly porous structure with 80,39% macroporosity and 920% swelling, presented a suitable microenvironment that facilitates the adhesion, proliferation, and migration of GBM cells. This microenvironment encouraged cells to behave as they would in vivo, and weaker drug responses were observed in contrast to 2D cultured cells. In a conclusion, all findings in this study indicated that this pHEMA-gelatin-based cryogel has the potential as a scaffold to be used to construct a GBM tumor model. In future studies, it would be appropriate to investigate the potential of the synthesized cryogel as a scaffold for the GBM tumor model by examining the effects on the expression of oncogene, tumor suppressor and metastatic genes by molecular biology techniques like real-time PCR and western blot.

REFERANCES

Ahir, B. K., Engelhard, H. H., & Lakka, S. S. (2020). Tumor development and angiogenesis in adult brain tumor: Glioblastoma. In Molecular Neurobiology (Vol. 57, Issue 5, pp. 2461–2478). Springer. https://doi.org/10.1007/s12035-020-01892-8

Anghileri, E., Patanè, M., di Ianni, N., Sambruni, I., Maffezzini, M., Milani, M., Maddaloni, L., Pollo, B., Eoli, M., & Pellegatta, S. (2021). Deciphering the labyrinthine system of the immune microenvironment in recurrent glioblastoma: Recent original advances and lessons from clinical immunotherapeutic approaches. Cancers, 13(24). https://doi.org/10.3390/cancers13246156

Babić Radić, M. M., Filipović, V. v., Vuković, J. S., Vukomanović, M., Rubert, M., Hofmann, S., Müller, R., & Tomić, S. L. (2022). Bioactive interpenetrating hydrogel networks based on 2-hydroxyethyl methacrylate and gelatin intertwined with alginate and dopped with apatite as scaffolding biomaterials. Polymers, 14(15). https://doi.org/10.3390/polym14153112

Bailly, C., Vidal, A., Bonnemaire, C., Kraeber-Bodéré, F., Chérel, M., Pallardy, A., Rousseau, C., Garcion, E., Lacoeuille, F., Hindré, F., Valable, S., Bernaudin, M., Bodet-Milin, C., & Bourgeois, M. (2019). Potential for nuclear medicine therapy for glioblastoma treatment. Frontiers in Pharmacology, 10(July), 1–9. https://doi.org/10.3389/fphar.2019.00772

Bakhshpour, M., Idil, N., Perçin, I., & Denizli, A. (2019). Biomedical applications of polymeric cryogels. Applied Sciences, 9(3), 553. https://doi.org/10.3390/app9030553

Bakhshpour, M., Yavuz, H., & Denizli, A. (2018). Controlled release of mitomycin C from PHEMAH–Cu (II) cryogel membranes. Artificial Cells, Nanomedicine and Biotechnology, 46(sup1), 946–954. https://doi.org/10.1080/21691401.2018.1439840

Ballestrem, C., Wehrle-Haller, B., Hinz, B., & Imhof, B. A. (2000). Actin-dependent lamellipodia formation and microtubule-dependent tail retraction control-directed cell migration. Molecular Biology of the Cell, 11(9), 2999–3012. https://doi.org/10.1091/mbc.11.9.2999

Behl, T., Sharma, A., Sharma, L., Sehgal, A., Singh, S., Sharma, N., Zengin, G., Bungau, S., Toma, M. M., Gitea, D., Babes, E. E., Pusta, C. T. J., & Bumbu, A. G. (2021). Current perspective on the natural compounds and drug delivery techniques in glioblastoma multiforme. Cancers, 13(11), 1–30. https://doi.org/10.3390/cancers13112765

Behnan, J., Finocchiaro, G., & Hanna, G. (2019). The landscape of the mesenchymal signature in brain tumours. Brain, 142(4), 847–866. https://doi.org/10.1093/brain/awz044

Bencherif, S. A., Braschler, T. M., & Renaud, P. (2013). Advances in the design of macroporous polymer scaffolds for potential applications in dentistry. Journal of Periodontal & Implant Science, 43(6), 251. https://doi.org/10.5051/jpis.2013.43.6.251

Bjorland, L. S., Fluge, O., Gilje, B., Mahesparan, R., & Farbu, E. (2021). Treatment approach and survival from glioblastoma: Results from a population-based retrospective cohort study from Western Norway. BMJ Open, 11(3), 1–9. https://doi.org/10.1136/bmjopen-2020-043208

Bolcaen, J., Kleynhans, J., Nair, S., Verhoeven, J., Goethals, I., Sathekge, M., Vandevoorde, C., & Ebenhan, T. (2021). A perspective on the radiopharmaceutical requirements for imaging and therapy of glioblastoma. Theranostics, 11(16), 7911–7947. https://doi.org/10.7150/THNO.56639

Bryukhovetskiy, I., Ponomarenko, A., Lyakhova, I., Zaitsev, S., Zayats, Y., Korneyko, M., Eliseikina, M., Mischenko, P., Shevchenko, V., Shanker Sharma, H., Sharma, A., & Khotimchenko, Y. (2018). Personalized regulation of glioblastoma cancer stem cells based on biomedical technologies: From theory to experiment (Review). International Journal of Molecular Medicine. https://doi.org/10.3892/ijmm.2018.3668

Burster, T., Traut, R., Yermekkyzy, Z., Mayer, K., Westhoff, M. A., Bischof, J., & Knippschild, U. (2021). Critical view of novel treatment strategies for glioblastoma: Failure and success of resistance mechanisms by glioblastoma cells. Frontiers in Cell and Developmental Biology, 9(August), 1–16. https://doi.org/10.3389/fcell.2021.695325

Caicedo-Carvajal, C. E., Liu, Q., Remache, Y., Goy, A., & Suh, K. S. (2011). Cancer tissue engineering: A novel 3D polystyrene scaffold for in vitro isolation and amplification of lymphoma cancer cells from heterogeneous Cell mixtures. Journal of Tissue Engineering, 2(1), 1–10. https://doi.org/10.4061/2011/362326

Caspani, E. M., Crossley, P. H., Redondo-Garcia, C., & Martinez, S. (2014). Glioblastoma: A pathogenic crosstalk between tumor cells and pericytes. PLoS ONE, 9(7), e101402. https://doi.org/10.1371/journal.pone.0101402

Cenciarini, M., Valentino, M., Belia, S., Sforna, L., Rosa, P., Ronchetti, S., D'Adamo, M. C., & Pessia, M. (2019). Dexamethasone in glioblastoma multiforme therapy: Mechanisms and controversies. Frontiers in Molecular Neuroscience, 12(March), 1–13. https://doi.org/10.3389/fnmol.2019.00065

Çetin, D., Kahraman, A. S., & Gümüsderelioglu, M. (2011). Novel scaffolds based on poly (2-hydroxyethyl methacrylate) superporous hydrogels for bone tissue engineering. Journal of Biomaterials Science, Polymer Edition, 22(9), 1157–1178. https://doi.org/10.1163/092050610X501704

Chaicharoenaudomrung, N., Kunhorm, P., & Noisa, P. (2019). Three-dimensional cell culture systems as an in vitro platform for cancer and stem cell modeling. World Journal of Stem Cells, 11(12), 1065–1083. https://doi.org/10.4252/wjsc.v11.i12.1065

Chan, B. P., & Leong, K. W. (2008). Scaffolding in tissue engineering: general approaches and tissue-specific considerations. European Spine Journal, 17(S4), 467–479. https://doi.org/10.1007/s00586-008-0745-3

Chang, H.-I., & Wang, Y. (2011). Cell responses to surface and architecture of tissue engineering scaffolds. Regenerative Medicine and Tissue Engineering - Cells and Biomaterials. https://doi.org/10.5772/21983

Chen, Y., Lu, W., Guo, Y., Zhu, Y., Lu, H., & Wu, Y. (2018). Superhydrophobic coatings on gelatin-based films: fabrication, characterization, and cytotoxicity studies. RSC Advances, 8(42), 23712–23719. https://doi.org/10.1039/C8RA04066D

Codrici, E., Popescu, I., Tanase, C., & Enciu, A.-M. (2022). Friends with benefits: Chemokines , glioblastoma-associated microglia / macrophages , and tumor microenvironment. International Journal of Molecular Sciences, 23, 2509. https://doi.org/10.3390/ijms23052509

Cortesi, M., & Giordano, E. (2022). Non-destructive monitoring of 3D cell cultures: new technologies and applications. PeerJ, 10. https://doi.org/10.7717/peerj.13338

Cuddapah, V. A., Robel, S., Watkins, S., & Sontheimer, H. (2014). A neurocentric perspective on glioma invasion. In Nature Reviews Neuroscience (Vol. 15, Issue 7, pp. 455–465). Nature Publishing Group. https://doi.org/10.1038/nrn3765

Dai, X., Ma, C., Lan, Q., & Xu, T. (2016). 3D bioprinted glioma stem cells for brain tumor model and applications of drug susceptibility. Biofabrication, 8(4). https://doi.org/10.1088/1758-5090/8/4/045005

DeCordova, S., Shastri, A., Tsolaki, A. G., Yasmin, H., Klein, L., Singh, S. K., & Kishore, U. (2020). Molecular heterogeneity and immunosuppressive microenvironment in glioblastoma. Frontiers in Immunology, 11(July), 1–18. https://doi.org/10.3389/fimmu.2020.01402

Demirci, S., Sahiner, M., Yilmaz, S., Karadag, E., & Sahiner, N. (2020). Enhanced enzymatic activity and stability by in situ entrapment of α-Glucosidase within super porous p(HEMA) cryogels during synthesis. Biotechnology Reports, 28. https://doi.org/10.1016/j.btre.2020.e00534

di Cintio, F., Dal Bo, M., Baboci, L., de Mattia, E., Polano, M., & Toffoli, G. (2020). The molecular and microenvironmental landscape of glioblastomas: Implications for the novel

treatment choices. Frontiers in Neuroscience, 14(November), 1–25. https://doi.org/10.3389/fnins.2020.603647

di Filippo, L. D., Duarte, J. L., Luiz, M. T., de Araújo, J. T. C., & Chorilli, M. (2021). Drug delivery nanosystems in glioblastoma multiforme treatment: Current state of the art. Current Neuropharmacology, 19(6), 787–812. https://doi.org/10.2174/1570159X18666200831160627

Elkamhawy, A., Viswanath, A. N. I., Pae, A. N., Kim, H. Y., Heo, J., Park, W., Lee, C., Yang, H., Kim, K. H., Nam, D., Seol, H. J., Cho, H., & Roh, E. J. (2015). Discovery of potent and selective cytotoxic activity of new quinazoline-ureas against TMZ-resistant glioblastoma multiforme (GBM). European Journal of Medicinal Chemistry, 103, 210–222. https://doi.org/10.1016/j.ejmech.2015.08.001

Eltom, A., Zhong, G., & Muhammad, A. (2019). Scaffold techniques and designs in tissue engineering functions and purposes: A Review. Advances in Materials Science and Engineering, 2019. https://doi.org/10.1155/2019/3429527

Estrada, M. F., Rebelo, S. P., Davies, E. J., Pinto, M. T., Pereira, H., Santo, V. E., Smalley, M. J., Barry, S. T., Gualda, E. J., Alves, P. M., Anderson, E., & Brito, C. (2016). Modelling the tumour microenvironment in long-term microencapsulated 3D co-cultures recapitulates phenotypic features of disease progression. Biomaterials, 78, 50–61. https://doi.org/10.1016/j.biomaterials.2015.11.030

Fan, D., Staufer, U., & Accardo, A. (2019). Engineered 3d polymer and hydrogel microenvironments for cell culture applications. Bioengineering, 6(4). https://doi.org/10.3390/bioengineering6040113

Filipović, V. v., Babić Radić, M. M., Vuković, J. S., Vukomanović, M., Rubert, M., Hofmann, S., Müller, R., & Tomić, S. L. (2022). Biodegradable hydrogel scaffolds based on 2-hydroxyethyl methacrylate, gelatin, poly(β-amino esters), and hydroxyapatite. Polymers, 14(1). https://doi.org/10.3390/polym14010018

Frantz, C., Stewart, K. M., & Weaver, V. M. (2010). The extracellular matrix at a glance. Journal of Cell Science, 123(123), 4195–4200. https://doi.org/10.1242/jcs.023820

García-Couce, J., Vernhes, M., Bada, N., Agüero, L., Valdés, O., Alvarez-Barreto, J., Fuentes, G., Almirall, A., Cruz, L. J., & Jervis, P. J. (2021). Synthesis and evaluation of AlgNa-g-Poly(QCL-co-HEMA) hydrogels as platform for chondrocyte proliferation and controlled release of betamethasone. Int. J. Mol. Sci, 22, 5730. https://doi.org/10.3390/ijms

Ghosh, D., Nandi, S., & Bhattacharjee, S. (2018). Combination therapy to checkmate Glioblastoma: clinical challenges and advances. Clinical and Translational Medicine, 7(1). https://doi.org/10.1186/s40169-018-0211-8

Gomez-Roman, N., Stevenson, K., Gilmour, L., Hamilton, G., & Chalmers, A. J. (2017). A novel 3D human glioblastoma cell culture system for modeling drug and radiation responses. Neuro-Oncology, 19(2), 229–241. https://doi.org/10.1093/neuonc/now164

Guo, Z., Yang, C., Zhou, Z., Chen, S., & Li, F. (2017). Characterization of biodegradable poly(lactic acid) porous scaffolds prepared using selective enzymatic degradation for tissue engineering. RSC Advances, 7(54), 34063–34070. https://doi.org/10.1039/c7ra03574h

Habanjar, O., Diab-Assaf, M., Caldefie-Chezet, F., & Delort, L. (2021). 3D cell culture systems: Tumor application, advantages, and disadvantages. International Journal of Molecular Sciences, 22(22), 12200. https://doi.org/10.3390/ijms222212200

Hanif, F., Muzaffar, K., Perveen, K., Malhi, S. M., & Simjee, S. U. (2017). Glioblastoma multiforme: A review of its epidemiology and pathogenesis through clinical presentation and treatment. Asian Pacific Journal of Cancer Prevention, 18, 3–9. https://doi.org/10.22034/APJCP.2017.18.1.3

Hersh, A. M., Gaitsch, H., Alomari, S., Lubelski, D., & Tyler, B. M. (2022). Molecular pathways and genomic landscape of glioblastoma stem cells: Opportunities for targeted therapy. Cancers, 14(15), 3743. https://doi.org/10.3390/cancers14153743

Hsu, J. F., Chu, S. M., Liao, C. C., Wang, C. J., Wang, Y. S., Lai, M. Y., Wang, H. C., Huang, H. R., & Tsai, M. H. (2021). Nanotechnology and nanocarrier-based drug delivery as the potential therapeutic strategy for glioblastoma multiforme: An update. Cancers, 13(2), 1–22. https://doi.org/10.3390/cancers13020195

Hutmacher, D. W., Woodfield, T. B. F., & Dalton, P. D. (2014). Scaffold design and fabrication. In Tissue Engineering (pp. 311–346). Elsevier. https://doi.org/10.1016/B978-0-12-420145-3.00010-9

Innocenti, M. (2018). New insights into the formation and the function of lamellipodia and ruffles in mesenchymal cell migration. Cell Adhesion & Migration, 1–16. https://doi.org/10.1080/19336918.2018.1448352

Jensen, C., & Teng, Y. (2020). Is it time to start transitioning from 2d to 3d cell culture? Frontiers in Molecular Biosciences, 7. https://doi.org/10.3389/fmolb.2020.00033

Kao, H. H., Kuo, C. Y., Chen, K. S., & Chen, J. P. (2019). Preparation of gelatin and gelatin/hyaluronic acid cryogel scaffolds for the 3D culture of mesothelial cells and mesothelium tissue regeneration. International Journal of Molecular Sciences, 20(18). https://doi.org/10.3390/ijms20184527

Kapałczyńska, M., Kolenda, T., Przybyła, W., Zajączkowska, M., Teresiak, A., Filas, V., Ibbs, M., Bliźniak, R., Łuczewski, Ł., & Lamperska, K. (2018). 2D and 3D cell cultures – a

comparison of different types of cancer cell cultures. Archives of Medical Science, 14(4), 910–919. https://doi.org/10.5114/aoms.2016.63743

Khaddour, K., Johanns, T. M., & Ansstas, G. (2020). The landscape of novel therapeutics and challenges in glioblastoma multiforme: Contemporary state and future directions. Pharmaceuticals, 13(11), 1–26. https://doi.org/10.3390/ph13110389

Kievit, F. M., Florczyk, S. J., Leung, M. C., Veiseh, O., Park, J. O., Disis, M. L., & Zhang, M. (2010). Chitosan-alginate 3D scaffolds as a mimic of the glioma tumor microenvironment. Biomaterials, 31(22), 5903–5910. https://doi.org/10.1016/j.biomaterials.2010.03.062

Kim, A. Y., Kim, Y., Lee, H., Yoon, Y., Kim, W.-H., & Kweon, O.-K. (2017). Effect of gelatin on osteogenic cell sheet formation using canine adipose-derived mesenchymal stem cells. Cell Transplantation, 26, 115–123. https://doi.org/10.3727/096368916X693338

Klasen, A., Kessari, R., Mercier, L., Valade, C., Grill, J., Desmaris, R., & Paci, A. (2014). Stability of etoposide solutions in disposable infusion devices for day hospital cancer practices. Drugs in R&D, 14(1), 13–23. https://doi.org/10.1007/s40268-014-0037-9

Korbecki, J., Gutowska, I., Kojder, I., Jezewski, D., Goschorska, M., Lukomska, A., Lubkowska, A., Chlubek, D., & Baranowska-Bosiacka, I. (2018). New extracellular factors in glioblastoma multiforme development: Neurotensin, growth differentiation factor-15, sphingosine-1-phosphate, and cytomegalovirus infection. Oncotarget, 9(6), 7219–7270. https://doi.org/10.18632/oncotarget.24102

Kuo, Y., & Chen, Y. (2015). Targeting delivery of etoposide to inhibit the growth of human glioblastoma multiforme using lactoferrin- and folic acid-grafted poly(lactide-co-glycolide) nanoparticles. International Journal of Pharmaceutics, 479(1), 138–149. https://doi.org/10.1016/j.ijpharm.2014.12.070

Lah Turnšek, T., Jiao, X., Novak, M., Jammula, S., Cicero, G., Ashton, A. W., Joyce, D., & Pestell, R. G. (2021). An update on glioblastoma biology, genetics, and current therapies: Novel inhibitors of the G protein-coupled receptor CCR5. International Journal of Molecular Sciences, 22(9). https://doi.org/10.3390/ijms22094464

Langbeen, A., Jorssen, E. P. A., Granata, N., & Fransen, E. (2014). Effects of neutral red assisted viability assessment on the cryotolerance of isolated bovine preantral follicles. 1727–1736. https://doi.org/10.1007/s10815-014-0340-y

Langhans, S. A. (2018). Three-dimensional in vitro cell culture models in drug discovery and drug repositioning. Frontiers in Pharmacology, 9(JAN), 1–14. https://doi.org/10.3389/fphar.2018.00006

Lenin, S., Ponthier, E., Scheer, K. G., Yeo, E. C. F., Tea, M. N., Ebert, L. M., Mansilla, M. O., Poonnoose, S., Baumgartner, U., Day, B. W., Ormsby, R. J., Pitson, S. M., & Gomez, G. A. (2021). A drug screening pipeline using 2d and 3d patient-derived in vitro models for pre-clinical analysis of therapy response in glioblastoma. International Journal of Molecular Sciences, 22(9). https://doi.org/10.3390/ijms22094322

Li, N., Zhang, P., Kiang, K. M. Y., Cheng, Y. S., & Leung, G. K. K. (2018). Caffeine sensitizes U87-MG human glioblastoma cells to temozolomide through mitotic catastrophe by impeding G2 arrest. BioMed Research International, 2018. https://doi.org/10.1155/2018/5364973

Liu, T., Zhang, W., Wang, J., Zhang, Y., Wang, H., Sun, F., & Cai, L. (2020). Improved dimensional stability and mold resistance of bamboo via in situ growth of poly (hydroxyethyl methacrylate-N-isopropyl acrylamide). Polymers, 12(7). https://doi.org/10.3390/polym12071584

Logun, M. T., Bisel, N. S., Tanasse, E. A., Zhao, W., Gunasekera, B., Mao, L., & Karumbaiah, L. (2016). Glioma cell invasion is significantly enhanced in composite hydrogel matrices composed of chondroitin 4- and 4,6-sulfated glycosaminoglycans. J. Mater. Chem. B, 4(36), 6052–6064. https://doi.org/10.1039/C6TB01083K

Lovitt, C. J., Shelper, T. B., & Avery, V. M. (2014). Advanced cell culture techniques for cancer drug discovery. Biology, 3(2), 345–367. https://doi.org/10.3390/biology3020345

Lv, D., Yu, S., Ping, Y., Wu, H., Zhao, X., Zhang, H., Cui, Y., Chen, B., Zhang, X., Dai, J., Bian, X., & Yao, X. (2016). A three-dimensional collagen scaffold cell culture system for screening anti-glioma therapeutics. Oncotarget, 7(35). https://doi.org/10.18632/oncotarget.10885

Ma, L., Zhang, B., Zhou, C., Li, Y., Li, B., Yu, M., Luo, Y., Gao, L., Zhang, D., Xue, Q., Qiu, Q., Lin, B., Zou, J., & Yang, H. (2018). The comparison genomics analysis with glioblastoma multiforme (GBM) cells under 3D and 2D cell culture conditions. Colloids and Surfaces B: Biointerfaces, 172, 665–673. https://doi.org/10.1016/j.colsurfb.2018.09.034

Ma, N. K. L., Lim, J. K., Leong, M. F., Sandanaraj, E., Ang, B. T., Tang, C., & Wan, A. C. A. (2016). Collaboration of 3D context and extracellular matrix in the development of glioma stemness in a 3D model. Biomaterials, 78, 62–73. https://doi.org/10.1016/j.biomaterials.2015.11.031

Manome, Y., Mizuno, S., Akiyama, N., Fujioka, K., Saito, H., Hataba, Y., Kobayashi, T., & Watanabe, M. (2010). Three-dimensional cell culture of glioma and morphological comparison of four different human cell lines. Anticancer Research, 30(2), 383–389.

Mehrotra, D., Dwivedi, R., Nandana, D., & Singh, R. K. (2020). From injectable to 3D printed hydrogels in maxillofacial tissue engineering: A review. In Journal of Oral Biology and Craniofacial Research (Vol. 10, Issue 4, pp. 680–689). Elsevier B.V. https://doi.org/10.1016/j.jobcr.2020.09.006

Memic, A., Colombani, T., Eggermont, L. J., Rezaeeyazdi, M., Steingold, J., Rogers, Z. J., Navare, K. J., Mohammed, H. S., & Bencherif, S. A. (2019). Latest advances in cryogel technology for biomedical applications. Advanced Therapeutics, 2(4), 1800114. https://doi.org/10.1002/adtp.201800114

Miller, M. A., Bankier, C., Al-Shaeri, M. A. M., & Hartl, M. G. J. (2015). Neutral red cytotoxicity assays for assessing in vivo carbon nanotube ecotoxicity in mussels — Comparing microscope and microplate methods. Marine Pollution Bulletin, 101(2), 903–907. https://doi.org/10.1016/j.marpolbul.2015.10.072

Mohanty, S., Larsen, L. B., Trifol, J., Szabo, P., Burri, H. V. R., Canali, C., Dufva, M., Emnéus, J., & Wolff, A. (2015). Fabrication of scalable and structured tissue engineering scaffolds using water dissolvable sacrificial 3D printed moulds. Materials Science and Engineering: C, 55(2015), 569–578. https://doi.org/10.1016/j.msec.2015.06.002

Musah-Eroje, A., & Watson, S. (2019). A novel 3D in vitro model of glioblastoma reveals resistance to temozolomide which was potentiated by hypoxia. Journal of Neuro-Oncology, 142(2), 231–240. https://doi.org/10.1007/s11060-019-03107-0

National Center for Biotechnology Information. (2022). PubChem compound summary for CID 13360, 2-Hydroxyethyl Methacrylate. Retrieved November 27, 2022, from Https://Pubchem.Ncbi.Nlm.Nih.Gov/Compound/2-Hydroxyethyl-Methacrylate.

Ng, R., Zang, R., Yang, K. K., Liu, N., & Yang, S. T. (2012). Three-dimensional fibrous scaffolds with microstructures and nanotextures for tissue engineering. RSC Advances, 2(27), 10110–10124. https://doi.org/10.1039/c2ra21085a

O'Brien, F. J. (2011). Biomaterials & scaffolds for tissue engineering. Materials Today, 14(3), 88–95. https://doi.org/10.1016/S1369-7021(11)70058-X

Ohgaki, H., & Kleihues, P. (2005). Epidemiology and etiology of gliomas. Acta Neuropathologica, 109(1), 93–108. https://doi.org/10.1007/s00401-005-0991-y

Olde Damink, L. H. H., Dijkstra, P. J., van Luyn, M. J. A., van Wachem, P. B., Nieuwenhuis, P., & Feijen, J. (1995). Glutaraldehyde as a crosslinking agent for collagen-based biomaterials. Journal of Materials Science: Materials in Medicine, 6(8), 460–472. https://doi.org/10.1007/BF00123371

Park, H.-J., & Helfman, D. M. (2019). Up-regulated fibronectin in 3D culture facilitates spreading of triple negative breast cancer cells on 2D through integrin β-5 and Src. Scientific Reports, 9(1), 19950. https://doi.org/10.1038/s41598-019-56276-3

Park, Y., Huh, K. M., & Kang, S. W. (2021). Applications of biomaterials in 3d cell culture and contributions of 3d cell culture to drug development and basic biomedical research. In International Journal of Molecular Sciences (Vol. 22, Issue 5, pp. 1–21). MDPI AG. https://doi.org/10.3390/ijms22052491

Peng, W., Lu, X., Wu, J., Wang, Y., Zhu, X., Ouyang, H., Li, L., Wu, J., Liu, Y., & Bao, J. (2022). Autoclaving pHEMA-based hydrogels immersed in deionized water has no effect on physicochemical properties and cell behaviors. ACS Omega. https://doi.org/10.1021/acsomega.2c03096

Perçin, I., Aracagök, Y. D., İdil, N., Denizli, A., & Mattiasson, B. (2021). 1353 Laccase bound to cryogel functionalized with phenylalanine for the decolorization of textile dyes. TURKISH JOURNAL OF CHEMISTRY, 45(5), 1353–1365. https://doi.org/10.3906/kim-2106-16

Plleva, F. M., Galaev, I. Y., & Mattiasson, B. (2007). Macroporous gels prepared at subzero temperatures as novel materials for chromatography of particulate-containing fluids and cell culture applications. Journal of Separation Science, 30(11), 1657–1671. https://doi.org/10.1002/jssc.200700127

Poornima, K., Francis, A. P., Hoda, M., Eladl, M. A., Subramanian, S., Veeraraghavan, V. P., El-Sherbiny, M., Asseri, S. M., Hussamuldin, A. B. A., Surapaneni, K. M., Mony, U., & Rajagopalan, R. (2022). Implications of three-dimensional cell culture in cancer therapeutic research. Frontiers in Oncology, 12. https://doi.org/10.3389/fonc.2022.891673

Qiu, J., Shi, Z., & Jiang, J. (2017). Cyclooxygenase-2 in glioblastoma multiforme. Drug Discovery Today, 22(1), 148–156. https://doi.org/10.1016/j.drudis.2016.09.017

Razavi, M., Qiao, Y., & Thakor, A. S. (2019). Three-dimensional cryogels for biomedical applications. In Journal of Biomedical Materials Research - Part A (Vol. 107, Issue 12, pp. 2736–2755). John Wiley and Sons Inc. https://doi.org/10.1002/jbm.a.36777

Rogers, Z. J., & Bencherif, S. A. (2019). Cryogelation and cryogels. In Gels (Vol. 5, Issue 4). MDPI Multidisciplinary Digital Publishing Institute. https://doi.org/10.3390/gels5040046

Savina, I. N., Zoughaib, M., & Yergeshov, A. A. (2021). Design and assessment of biodegradable macroporous cryogels as advanced tissue engineering and drug carrying materials. Gels, 7(3), 79. https://doi.org/10.3390/gels7030079

Saylan, & Denizli. (2019). Supermacroporous composite cryogels in biomedical applications. Gels, 5(2), 20. https://doi.org/10.3390/gels5020020

Seker-Polat, F., Degirmenci, N. P., Solaroglu, I., & Bagci-Onder, T. (2022). Tumor cell infiltration into the brain in glioblastoma: From mechanisms to clinical perspectives. Cancers, 14(2). https://doi.org/10.3390/cancers14020443

Shah, N., Hallur, P. M., Ganesh, R. A., Sonpatki, P., Naik, D., Chandrachari, K. P., Puchalski, R. B., & Chaubey, A. (2021). Gelatin methacrylate hydrogels culture model for glioblastoma cells enriches for mesenchymal-like state and models interactions with immune cells. Scientific Reports, 11(1), 17727. https://doi.org/10.1038/s41598-021-97059-z

Shapiro, W. R. (1998). Biology and treatment of malignant glioma. Oncology (Williston Park, N.Y.), 12(2), 233–240; discussion 240, 246. http://www.ncbi.nlm.nih.gov/pubmed/9507524

Sharifzad, F., Ghavami, S., Verdi, J., Mardpour, S., Mollapour, M., Azizi, Z., Taghikhani, A., Łos, M. J., & Fakharian, E. (2019). Glioblastoma cancer stem cell biology: Potential theranostic targets. Drug Resistance Updates, 42(February 2018), 35–45. https://doi.org/10.1016/j.drup.2018.03.003

Sharma, A., Bhat, S., Vishnoi, T., Nayak, V., & Kumar, A. (2013). Three-dimensional supermacroporous carrageenan-gelatin cryogel matrix for tissue engineering applications. BioMed Research International, 2013. https://doi.org/10.1155/2013/478279

Silantyev, Falzone, Libra, Gurina, Kardashova, Nikolouzakis, Nosyrev, Sutton, Panayioti, & Tsatsakis. (2019). Current and future trends on diagnosis and prognosis of glioblastoma: From Molecular biology to proteomics. Cells, 8(8), 863. https://doi.org/10.3390/cells8080863

Sontheimer, H. (2008). A role for glutamate in growth and invasion of primary brain tumors. Journal of Neurochemistry, 105(2), 287–295. https://doi.org/10.1111/j.1471-4159.2008.05301.x

Sousa, I., Mendes, A., & Bártolo, P. J. (2013). PCL scaffolds with collagen bioactivator for applications in tissue engineering. Procedia Engineering, 59, 279–284. https://doi.org/10.1016/j.proeng.2013.05.122

Stupp, R., Mason, W. P., van den Bent, M. J., Weller, M., Fisher, B., Taphoorn, M. J. B., Belanger, K., Brandes, A. A., Marosi, C., Bogdahn, U., Curschmann, J., Janzer, R. C., Ludwin, S. K., Gorlia, T., Allgeier, A., Lacombe, D., Cairncross, J. G., Eisenhauer, E., & Mirimanoff, R. O. (2005). Radiotherapy plus concomitant and adjuvant temozolomide for glioblastoma. New England Journal of Medicine, 352(10), 987–996. https://doi.org/10.1056/NEJMoa043330

Sung, H., Ferlay, J., Siegel, R. L., Laversanne, M., Soerjomataram, I., Jemal, A., & Bray, F. (2021). Global Cancer Statistics 2020: GLOBOCAN estimates of incidence and mortality worldwide for 36 cancers in 185 countries. CA: A Cancer Journal for Clinicians, 71(3), 209–249. https://doi.org/10.3322/caac.21660

Tabatabaee, S., Baheiraei, N., & Salehnia, M. (2022). Fabrication and characterization of PHEMA–gelatin scaffold enriched with graphene oxide for bone tissue engineering. Journal of Orthopaedic Surgery and Research, 17(1), 1–19. https://doi.org/10.1186/s13018-022-03122-4

Taylor, O. G., Brzozowski, J. S., & Skelding, K. A. (2019). Glioblastoma multiforme: An overview of emerging therapeutic targets. Frontiers in Oncology, 9(SEP), 1–11. https://doi.org/10.3389/fonc.2019.00963

Trejo-Solís, C., Serrano-Garcia, N., Escamilla-Ramírez, Á., Castillo-Rodríguez, R. A., Jimenez-Farfan, D., Palencia, G., Calvillo, M., Alvarez-Lemus, M. A., Flores-Nájera, A., Cruz-Salgado, A., & Sotelo, J. (2018). Autophagic and apoptotic pathways as targets for chemotherapy in glioblastoma. International Journal of Molecular Sciences, 19(12). https://doi.org/10.3390/ijms19123773

Turnbull, G., Clarke, J., Picard, F., Riches, P., Jia, L., Han, F., Li, B., & Shu, W. (2018). 3D bioactive composite scaffolds for bone tissue engineering. In Bioactive Materials (Vol. 3, Issue 3, pp. 278–314). KeAi Communications Co. https://doi.org/10.1016/j.bioactmat.2017.10.001

van Meir, E. G., Hadjipanayis, C. G., Norden, A. D., Shu, H. K., Wen, P. Y., & Olson, J. J. (2010). Exciting new advances in neuro-oncology: the avenue to a cure for malignant glioma. CA: A Cancer Journal for Clinicians, 60(3), 166–193. https://doi.org/10.3322/caac.20069

von Neubeck, C., Seidlitz, A., Kitzler, H. H., Beuthien-Baumann, B., & Krause, M. (2015). Glioblastoma multiforme: Emerging treatments and stratification markers beyond new drugs. British Journal of Radiology, 88(1053). https://doi.org/10.1259/bjr.20150354

Wang, C., Sinha, S., Jiang, X., Murphy, L., Fitch, S., Wilson, C., Grant, G., & Yang, F. (2021). Matrix stiffness modulates patient-derived glioblastoma cell fates in three-dimensional hydrogels. Tissue Engineering - Part A, 27(5–6), 390–401. https://doi.org/10.1089/ten.tea.2020.0110

Wang, C. Y., Hong, P. da, Wang, D. H., Cherng, J. H., Chang, S. J., Liu, C. C., Fang, T. J., & Wang, Y. W. (2020). Polymeric gelatin scaffolds affect mesenchymal stem cell differentiation and its diverse applications in tissue engineering. International Journal of Molecular Sciences, 21(22), 1–15. https://doi.org/10.3390/ijms21228632

Xiong, D. D., Xu, W. Q., He, R. Q., Dang, Y. W., Chen, G., & Luo, D. Z. (2019). In silico analysis identified miRNA based therapeutic agents against glioblastoma multiforme. Oncology Reports, 41(4), 2194–2208. https://doi.org/10.3892/or.2019.7022

Yadav, A. A., Chee, G., Wu, X., Patel, D., Yalowich, J. C., & Hasinoff, B. B. (2015). Structure-based design, synthesis, and biological testing of piperazine-linked bis-epipodophyllotoxin etoposide analogs. Bioorganic & Medicinal Chemistry, 23(13), 3542–3551. https://doi.org/10.1016/j.bmc.2015.04.022

Yang, G., Xiao, Z., Long, H., Ma, K., Zhang, J., Ren, X., & Zhang, J. (2018). Assessment of the characteristics and biocompatibility of gelatin sponge scaffolds prepared by various crosslinking methods. Scientific Reports, 8(1), 1616. https://doi.org/10.1038/s41598-018-20006-y

Yeo, E. C. F., Brown, M. P., Gargett, T., & Ebert, L. M. (2021). The role of cytokines and chemokines in shaping the immune microenvironment of glioblastoma: Implications for immunotherapy. Cells, 10(3), 1–25. https://doi.org/10.3390/cells10030607

Yool, A. J., & Ramesh, S. (2020). Molecular targets for combined therapeutic strategies to limit glioblastoma cell migration and invasion. Frontiers in Pharmacology, 11(March). https://doi.org/10.3389/fphar.2020.00358

Zare, M., Bigham, A., Zare, M., Luo, H., Rezvani Ghomi, E., & Ramakrishna, S. (2021). Phema: An overview for biomedical applications. International Journal of Molecular Sciences, 22(12). https://doi.org/10.3390/ijms22126376

Zasońska, B. A., Brož, A., Šlouf, M., Hodan, J., Petrovský, E., Hlídková, H., & Horák, D. (2021). Magnetic superporous poly (2-hydroxyethyl methacrylate) hydrogel scaffolds for bone tissue engineering. Polymers, 13(11), 1871. https://doi.org/10.3390/polym13111871

Zhu, N., & Chen, X. (2013). Biofabrication of tissue scaffolds. In R. Pignatello (Ed.), Advances in Biomaterials Science and Biomedical Applications (pp. 315–328). InTech. https://doi.org/10.5772/56420

APPENDİX

Appendix A- ANOVA analyses for cytotoxicity assays of MEF cells

Appendix B- ANOVA analyses for cytotoxicity assay of GBM cells

Appendix C- t-test analyses for cytotoxicity assay of MEF cells

Appendix D- t-test analyses for cytotoxicity assay of GBM cells

Appendix E- ANOVA analyses for dose optimization (IC_{50} determination) assay

Appendix G- ANOVA analyses for drug response assay

Appendix A- ANOVA analyses for cytotoxicity assays of MEF cells

Table A.1. ANOVA analyses for cytotoxicity assay of one day cultured MEF cells (p<0,001)

SUMMARY

Groups	*Count*	*Sum*	*Average*	*Variance*
Control	3	0,293	0,097667	2,33E-06
202	3	3,626	1,208667	8,63E-05
203	3	4,041	1,347	0,000117
204	3	3,615	1,205	7,6E-05
162	3	3,646	1,215333	3,03E-05
163	3	3,845	1,281667	3,03E-05
164	3	4,566	1,522	9,1E-05
122	3	2,815	0,938333	1,03E-05
123	3	2,947	0,982333	1,23E-05
124	3	3,454	1,151333	1,73E-05

ANOVA

Source of Variation	*SS*	*df*	*MS*	*F*	*P-value*	*F crit*
Between Groups	4,065789	9	0,451754	9544,106	2,55E-34	5,239228
Within Groups	0,000947	20	4,73E-05			
Total	4,066736	29				

Table A.2. ANOVA analyses for cytotoxicity assay of 3 days cultured MEF cells (p<0,001)

SUMMARY

Groups	*Count*	*Sum*	*Average*	*Variance*
Control	3	0,386	0,128667	1,73E-05
202	3	4,519	1,506333	4,33E-06
203	3	4,911	1,637	0,000873
204	3	4,521	1,507	7E-06
162	3	4,529	1,509667	3,33E-07
163	3	4,715	1,571667	5,03E-05
164	3	5,471	1,823667	0,00029
122	3	3,432	1,144	0,000607
123	3	3,566	1,188667	4,33E-06
124	3	4,37	1,456667	0,000405

ANOVA

Source of Variation	*SS*	*df*	*MS*	*F*	*P-value*	*F crit*
Between Groups	6,005622	9	0,667291	2953,488	3,15E-29	5,239228
Within Groups	0,004519	20	0,000226			
Total	6,010140667	29				

Table A.3.- ANOVA analyses for cytotoxicity assay of 5 days cultured MEF cells (p<0,001)

SUMMARY

Groups	*Count*	*Sum*	*Average*	*Variance*
Control	3	5,224	1,741333	0,000265
202	3	7,835	2,611667	0,00084
203	3	7,966	2,655333	9,33E-06
204	3	7,603	2,534333	0,001022
162	3	8,024	2,674667	1,63E-05
163	3	7,752	2,584	1,3E-05
164	3	7,965	2,655	0,000244
122	3	7,506	2,502	0,000121
123	3	7,743	2,581	2,1E-05
124	3	7,822	2,607333	0,00089

ANOVA

Source of Variation	*SS*	*df*	*MS*	*F*	*P-value*	*F crit*
Between Groups	2,072627	9	0,230292	668,8697	8,58E-23	5,239228
Within Groups	0,006886	20	0,000344			
Total	2,079513	29				

Appendix B- ANOVA analyses for cytotoxicity assay of GBM cells

Table B.1. ANOVA analyses for cytotoxicity assay of 1 days cultured GBM cells (p<0,001)

SUMMARY

Groups	*Count*	*Sum*	*Average*	*Variance*
Control	3	0,479	0,159667	2,63E-05
202	3	0,765	0,255	8,4E-05
203	3	0,903	0,301	0,000247
204	3	1,032	0,344	7E-06
162	3	0,777	0,259	0,001591
163	3	0,843	0,281	0,001372
164	3	1,06	0,353333	4,63E-05
122	3	0,731	0,243667	0,000122
123	3	0,863	0,287667	5,83E-05
124	3	0,913	0,304333	0,000576

ANOVA

Source of Variation	*SS*	*df*	*MS*	*F*	*P-value*	*F crit*
Between Groups	0,08226	9	0,00914	22,12721	1,62E-08	5,239228
Within Groups	0,008261	20	0,000413			
Total	0,090521	29				

Table B.2. ANOVA analyses for cytotoxicity assay of 3 days cultured GBM cells (p<0,001)

SUMMARY

Groups	*Count*	*Sum*	*Average*	*Variance*
Control	3	5,594	1,864667	0,001084
202	3	8,474	2,824667	6,93E-05
203	3	8,173	2,724333	0,000108
204	3	8,556	2,852	0,000673
162	3	7,005	2,335	0,000273
163	3	8,517	2,839	0,003724
164	3	8,569	2,856333	0,000625
122	3	8,224	2,741333	0,000105
123	3	8,236	2,745333	0,004864
124	3	8,305	2,768333	0,000622

ANOVA

Source of Variation	*SS*	*df*	*MS*	*F*	*P-value*	*F crit*
Between Groups	2,706836	9	0,30076	247,5523	1,65E-18	5,239228
Within Groups	0,024299	20	0,001215			
Total	2,731135	29				

Table B.3. ANOVA analyses for cytotoxicity assay of 5 days cultured GBM cells (p<0,001)

SUMMARY

Groups	*Count*	*Sum*	*Average*	*Variance*
Control	3	6,436	2,145333	0,004842
202	3	7,26	2,42	0,000417
203	3	6,765	2,255	0,001519
204	3	6,952	2,317333	3,73E-05
162	3	6,595	2,198333	0,000162
163	3	6,713	2,237667	0,003446
164	3	7,434	2,478	0,004764
122	3	6,868	2,289333	0,001546
123	3	6,772	2,257333	0,00199
124	3	6,827	2,275667	3,63E-05

ANOVA

Source of Variation	*SS*	*df*	*MS*	*F*	*P-value*	*F crit*
Between Groups	0,262475	9	0,029164	15,54465	3,36E-07	5,239228
Within Groups	0,037523	20	0,001876			
Total	0,299997	29				

Appendix C- t-test analyses for cytotoxicity assay of MEF cells

Table C.1. t-test analyses for cytotoxicity assay of 1-day cultured MEF cells (p<0,001)

	Control	*202*	*Control*	*203*	*Control*	*204*	*Control*	*162*	*Control*	*163*	*Control*	*164*	*Control*	*122*	*Control*	*123*	*Control*	*124*
Mean	0,097667	1,208667	0,097667	1,347	0,097667	1,205	0,097667	1,215333	0,097667	1,281667	0,097667	1,522	0,097667	0,938333	0,097667	0,982333	0,097667	1,151333
Variance	2,33E-06	8,63E-05	2,33E-06	0,000117	2,33E-06	7,6E-05	2,33E-06	3,03E-05	2,33E-06	3,03E-05	2,33E-06	9,1E-05	2,33E-06	1,03E-05	2,33E-06	1,23E-05	2,33E-06	1,73E-05
Observations	3	3	3	3	3	3	3	3	3	3	3	3	3	3	3	3	3	3
Pearson Correlation	0,551911		0,453921		-0,97622		0,614132		0,693375		0,720577		0,644902		0,40389		-0,05241	
Hypothesized Mean Difference	0		0		0		0		0		0		0		0		0	
df	2		2		2		2		2		2		2		2		2	
t Stat	-225,223		-211,849		-187,771		-409,634		-447,51		-290,07		-578,586		-476,672		-404,725	
P(T<=t) one-tail	9,86E-06		1,11E-05		1,42E-05		2,98E-06		2,5E-06		5,94E-06		1,49E-06		2,2E-06		3,05E-06	
t Critical one-tail	22,32712		22,32712		22,32712		22,32712		22,32712		22,32712		22,32712		22,32712		22,32712	
P(T<=t) two-tail	1,97E-05		2,23E-05		2,84E-05		5,96E-06		4,99E-06		1,19E-05		2,99E-06		4,4E-06		6,1E-06	
t Critical two-tail	31,59905		31,59905		31,59905		31,59905		31,59905		31,59905		31,59905		31,59905		31,59905	

Table C.2. t-test analyses for cytotoxicity assay of 3-days cultured MEF cells (p<0,001)

	Control	*202*	*Control*	*203*	*Control*	*204*	*Control*	*162*	*Control*	*163*	*Control*	*164*	*Control*	*122*	*Control*	*123*	*Control*	*124*
Mean	0,12867	1,50633	0,12867	1,637	0,12867	1,507	0,12867	1,50967	0,12867	1,57167	0,12867	1,82367	0,12867	1,144	0,12867	1,18867	0,12867	1,45667
Variance	1,7E-05	4,3E-06	1,7E-05	0,00087	1,7E-05	7E-06	1,7E-05	3,3E-07	1,7E-05	5E-05	1,7E-05	0,00029	1,7E-05	0,00061	1,7E-05	4,3E-06	1,7E-05	0,00041
Observations	3	3	3	3	3	3	3	3	3	3	3	3	3	3	3	3	3	3
Pearson Correlation	-0,5		-0,878		-0,4539		-0,6934		-0,9028		0,97736		-0,1365		0,84615		-0,7954	
Hypothesized Mean Difference	0		0		0		0		0		0		0		0		0	
df	2		2		2		2		2		2		2		2		2	
t Stat	-433,26		-78,544		-407,43		-521,97		-227,21		-225,83		-68,855		-693,93		-97,549	
P(T<=t) one-tail	2,7E-06		8,1E-05		3E-06		1,8E-06		9,7E-06		9,8E-06		0,00011		1E-06		5,3E-05	
t Critical one-tail	22,3271		22,3271		22,3271		22,3271		22,3271		22,3271		22,3271		22,3271		22,3271	
P(T<=t) two-tail	5,3E-06		0,00016		6E-06		3,7E-06		1,9E-05		2E-05		0,00021		2,1E-06		0,00011	
t Critical two-tail	31,5991		31,5991		31,5991		31,5991		31,5991		31,5991		31,5991		31,5991		31,5991	

Table C.3. t-test analyses for cytotoxicity assay of 5-days cultured MEF cells (p<0,001)

	Control	*202*	*Control*	*203*	*Control*	*204*	*Control*	*162*	*Control*	*163*	*Control*	*164*	*Control*	*122*	*Control*	*123*	*Control*	*124*
Mean	1,74133	2,61167	1,74133	2,65533	1,74133	2,53433	1,74133	2,67467	1,74133	2,584	1,74133	2,655	1,74133	2,502	1,74133	2,581	1,74133	2,60733
Variance	0,00027	0,00084	0,00027	9,3E-06	0,00027	0,00102	0,00027	1,6E-05	0,00027	1,3E-05	0,00027	0,00024	0,00027	0,00012	0,00027	2,1E-05	0,00027	0,00089
Observations	3	3	3	3	3	3	3	3	3	3	3	3	3	3	3	3	3	3
Pearson Correlation	0,99041		-0,978		-0,8403		0,87597		-0,8003		0,99826		0,92086		0,30812		-0,9992	
Hypothesized Mean Difference	0		0		0		0		0		0		0		0		0	
df	2		2		2		2		2		2		2		2		2	
t Stat	-115,5		-82,08		-29,533		-125,35		-75,64		-1370,5		-175,54		-93,812		-32,523	
P(T<=t) one-tail	3,7E-05		7,4E-05		0,00057		3,2E-05		8,7E-05		2,7E-07		1,6E-05		5,7E-05		0,00047	
t Critical one-tail	22,3271		22,3271		22,3271		22,3271		22,3271		22,3271		22,3271		22,3271		22,3271	
P(T<=t) two-tail	7,5E-05		0,00015		0,00114		6,4E-05		0,00017		5,3E-07		3,2E-05		0,00011		0,00094	
t Critical two-tail	31,5991		31,5991		31,5991		31,5991		31,5991		31,5991		31,5991		31,5991		31,5991	

Appendix D- t-test analyses for cytotoxicity assay of GBM cells

Table D.1. t-test analyses for cytotoxicity assay of 1-days cultured GBM cells (p<0,001)

	Control	*202*	*Control*	*203*	*Control*	*204*	*Control*	*162*	*Control*	*163*	*Control*	*164*	*Control*	*122*	*Control*	*123*	*Control*	*124*
Mean	2,14533	2,42	2,14533	2,255	2,14533	2,31733	2,14533	2,19833	2,14533	2,23767	2,14533	2,478	2,14533	2,28933	2,14533	2,25733	2,14533	2,27567
Variance	0,00484	0,00042	0,00484	0,00152	0,00484	3,7E-05	0,00484	0,00016	0,00484	0,00345	0,00484	0,00476	0,00484	0,00155	0,00484	0,00199	0,00484	3,6E-05
Observations	3	3	3	3	3	3	3	3	3	3	3	3	3	3	3	3	3	3
Pearson Correlation	-0,2762		-0,1342		0,21011		0,54853		0,73294		0,8884		-0,6593		-0,2835		0,80145	
Hypothesized Mean Difference	0		0		0		0		0		0		0		0		0	
df	2		2		2		2		2		2		2		2		2	
t Stat	-6,1192		-2,256		-4,345		-1,4457		-3,3344		-17,596		-2,4945		-2,0927		-3,4807	
P(T<=t) one-tail	0,01284		0,07636		0,02455		0,14258		0,03969		0,00161		0,06504		0,08573		0,03678	
t Critical one-tail	22,3271		22,3271		22,3271		22,3271		22,3271		22,3271		22,3271		22,3271		22,3271	
P(T<=t) two-tail	0,02568		0,15272		0,0491		0,28515		0,07938		0,00321		0,13007		0,17145		0,07355	
t Critical two-tail	31,5991		31,5991		31,5991		31,5991		31,5991		31,5991		31,5991		31,5991		31,5991	

Table D.2. t-test analyses for cytotoxicity assay of 3-days cultured GBM cells (p<0,001)

	Control	*202*	*Control*	*203*	*Control*	*204*	*Control*	*162*	*Control*	*163*	*Control*	*164*	*Control*	*122*	*Control*	*123*	*Control*	*124*
Mean	1,86467	2,82467	1,86467	2,72433	1,86467	2,852	1,86467	2,335	1,86467	2,839	1,86467	2,85633	1,86467	2,74133	1,86467	2,74533	1,86467	2,76833
Variance	0,00108	6,9E-05	0,00108	0,00011	0,00108	0,00067	0,00108	0,00027	0,00108	0,00372	0,00108	0,00063	0,00108	0,00011	0,00108	0,00486	0,00108	0,00062
Observations	3	3	3	3	3	3	3	3	3	3	3	3	3	3	3	3	3	3
Pearson Correlation	0,40604		-0,9944		0,79192		-0,2913		-0,7002		-0,9671		-0,3561		-0,7404		0,94972	
Hypothesized Mean Difference	0		0		0		0		0		0		0		0		0	
df	2		2		2		2		2		2		2		2		2	
t Stat	-54,495		-34,393		-85,046		-19,909		-19,33		-29,889		-40,149		-15,775		-129,39	
P(T<=t) one-tail	0,00017		0,00042		6,9E-05		0,00126		0,00133		0,00056		0,00031		0,002		3E-05	
t Critical one-tail	22,3271		22,3271		22,3271		22,3271		22,3271		22,3271		22,3271		22,3271		22,3271	
P(T<=t) two-tail	0,00034		0,00084		0,00014		0,00251		0,00267		0,00112		0,00062		0,00399		6E-05	
t Critical two-tail	31,5991		31,5991		31,5991		31,5991		31,5991		31,5991		31,5991		31,5991		31,5991	

Table D.3. t-test analyses for cytotoxicity assay of 5-days cultured GBM cells (p<0,001)

	Control	*202*	*Control*	*203*	*Control*	*204*	*Control*	*162*	*Control*	*163*	*Control*	*164*	*Control*	*122*	*Control*	*123*	*Control*	*124*
Mean	0,15967	0,255	0,15967	0,301	0,15967	0,344	0,15967	0,259	0,15967	0,281	0,15967	0,35333	0,15967	0,24367	0,15967	0,28767	0,15967	0,30433
Variance	2,6E-05	8,4E-05	2,6E-05	0,00025	2,6E-05	7E-06	2,6E-05	0,00159	2,6E-05	0,00137	2,6E-05	4,6E-05	2,6E-05	0,00012	2,6E-05	5,8E-05	2,6E-05	0,00058
Observations	3	3	3	3	3	3	3	3	3	3	3	3	3	3	3	3	3	3
Pearson Correlation	0,91427		-0,7936		0,84702		0,96978		-0,3367		0,86363		0,19087		-0,1063		0,09064	
Hypothesized Mean Difference	0		0		0		0		0		0		0		0		0	
df	2		2		2		2		2		2		2		2		2	
t Stat	-33,474		-12,219		-99,322		-4,9251		-5,3792		-95,516		-12,91		-22,989		-10,401	
P(T<=t) one-tail	0,00045		0,00332		5,1E-05		0,01942		0,01643		5,5E-05		0,00297		0,00094		0,00456	
t Critical one-tail	22,3271		22,3271		22,3271		22,3271		22,3271		22,3271		22,3271		22,3271		22,3271	
P(T<=t) two-tail	0,00089		0,00663		0,0001		0,03884		0,03287		0,00011		0,00595		0,00189		0,00912	
t Critical two-tail	31,5991		31,5991		31,5991		31,5991		31,5991		31,5991		31,5991		31,5991		31,5991	

Appendix E- ANOVA analyses for dose optimization (IC_{50} determination) assay

Table E.1. ANOVA analyses for dose optimization (IC_{50} determination) assay of TMZ ($p<0,001$).

SUMMARY

Groups	*Count*	*Sum*	*Average*	*Variance*
Control	3	1,743	0,581	0,000001
500 µM	3	1,637	0,545667	3,33E-05
750 µM	3	1,53	0,51	4,9E-05
1000 µM	3	1,383	0,461	4,9E-05
1250 µM	3	1,301	0,433667	1,43E-05
1500 µM	3	1,26	0,42	5,7E-05
1750 µM	3	1,193	0,397667	8,13E-05
2000 µM	3	0,94	0,313333	6,33E-06

ANOVA

Source of Variation	*SS*	*df*	*MS*	*F*	*P-value*	*F crit*
Between Groups	0,156395	7	0,022342	613,5154	3,17E-18	6,460391
Within Groups	0,000583	16	3,64E-05			
Total	0,156978	23				

Table E.2. ANOVA analyses for dose optimization (IC_{50} determination) assay of Etoposide ($p<0,001$).

SUMMARY

Groups	*Count*	*Sum*	*Average*	*Variance*
Control	3	0,965	0,321667	3,63E-05
5 μM	3	0,723	0,241	7E-06
10 μM	3	0,691	0,230333	9,33E-06
20 μM	3	0,598	0,199333	5,33E-06
40 μM	3	0,555	0,185	0,000016
60 μM	3	0,486	0,162	9E-06

ANOVA

Source of Variation	*SS*	*df*	*MS*	*F*	*P-value*	*F crit*
Between Groups	0,047513	5	0,009503	686,9365	2,6E-14	8,892109
Within Groups	0,000166	12	1,38E-05			
Total	0,047679	17				

Appendix F1- t-test analyses for indirect cytotoxicity assay

Table F.1. t-test analyses for indirect cytotoxicity assay of 1-day cultured cells (p<0,001).

	c	*164*
Mean	1,115667	1,114667
Variance	2,33E-06	9,33E-06
Observations	3	3
Pearson Correlation	-0,14286	
Hypothesized Mean Difference	1	
df	2	
t Stat	-479,904	
P(T<=t) one-tail	2,17E-06	
t Critical one-tail	22,32712	
P(T<=t) two-tail	4,34E-06	
t Critical two-tail	31,59905	

Table F.2. t-test analyses for indirect cytotoxicity assay of 3-days cultured cells (p<0,001).

	c	*164*
Mean	1,335333	1,332333
Variance	9,33E-06	1,63E-05
Observations	3	3
Pearson Correlation	-0,45896	
Hypothesized Mean Difference	1	
df	2	
t Stat	-283,893	
P(T<=t) one-tail	6,2E-06	
t Critical one-tail	22,32712	
P(T<=t) two-tail	1,24E-05	
t Critical two-tail	31,59905	

Table F.3. t-test analyses for indirect cytotoxicity assay of 5-days cultured cells (p<0,001).

	c	*164*
Mean	1,474	1,474333
Variance	1,3E-05	9,33E-06
Observations	3	3
Pearson Correlation	0,544705	
Hypothesized Mean Difference	1	
df	2	
t Stat	-538,996	
P(T<=t) one-tail	1,72E-06	
t Critical one-tail	22,32712	
P(T<=t) two-tail	3,44E-06	
t Critical two-tail	31,59905	

Appendix G- ANOVA analyses for drug response assay

Table G.1.ANOVA analyses for drug response assay (1-day cultured cells) (p<0,001).

SUMMARY

Groups	*Count*	*Sum*	*Average*	*Variance*
2Dc	3	6,52	2,173333	0,000116
2De	3	4,106	1,368667	0,000252
2Dt	3	4,477	1,492333	1,23E-05

ANOVA

Source of Variation	*SS*	*df*	*MS*	*F*	*P-value*	*F crit*
Between Groups	1,126543	2	0,563271	4435,208	3,09E-10	27
Within Groups	0,000762	6	0,000127			
Total	1,127305	8				

SUMMARY

Groups	*Count*	*Sum*	*Average*	*Variance*
HDc	3	7,227	2,409	1E-06
HDe	3	6,534	2,178	0,000547
HDt	3	6,773	2,257667	1,73E-05

ANOVA

Source of Variation	*SS*	*df*	*MS*	*F*	*P-value*	*F crit*
Between Groups	0,08261	2	0,041305	219,1881	2,46E-06	27
Within Groups	0,001131	6	0,000188			
Total	0,08374	8				

SUMMARY

Groups	*Count*	*Sum*	*Average*	*Variance*
3Dc	3	7,866	2,622	4E-06
3De	3	7,616	2,538667	0,000905
3Dt	3	7,798	2,599333	2,03E-05

ANOVA

Source of Variation	*SS*	*df*	*MS*	*F*	*P-value*	*F crit*
Between Groups	0,011139	2	0,005569	17,97203	0,002927	27
Within Groups	0,001859	6	0,00031			
Total	0,012998	8				

Table G.2. ANOVA analyses for drug response assay (3-days cultured cells) (p<0,001).

SUMMARY

Groups	*Count*	*Sum*	*Average*	*Variance*
2D Control	3	9,297	3,099	2,8E-05
2D Etoposide	3	4,756	1,585333	1,03E-05
2D TMZ	3	4,796	1,598667	2,23E-05

ANOVA

Source of Variation	*SS*	*df*	*MS*	*F*	*P-value*	*F crit*
Between Groups	4,542365	2	2,271182	112311,2	1,91E-14	27
Within Groups	0,000121	6	2,02E-05			
Total	4,542486	8				

SUMMARY

Groups	*Count*	*Sum*	*Average*	*Variance*
HD Control	3	7,429	2,476333	0,00238
HD Etoposide	3	5,743	1,914333	0,000481
HD TMZ	3	5,837	1,945667	0,000709

ANOVA

Source of Variation	*SS*	*df*	*MS*	*F*	*P-value*	*F crit*
Between Groups	0,598433	2	0,299216	251,372	1,64E-06	27
Within Groups	0,007142	6	0,00119			
Total	0,605575	8				

SUMMARY

Groups	*Count*	*Sum*	*Average*	*Variance*
3D Control	3	8,64	2,88	0,005587
3D Etop	3	8,257	2,752333	0,000352
3D TMZ	3	8,44	2,813333	0,000384

ANOVA

Source of Variation	*SS*	*df*	*MS*	*F*	*P-value*	*F crit*
Between Groups	0,024464	2	0,012232	5,803015	0,039579	27
Within Groups	0,012647	6	0,002108			
Total	0,037112	8				

Table G.3. ANOVA analyses for drug response assay (5-days cultured cells) (p<0,001).

SUMMARY

Groups	*Count*	*Sum*	*Average*	*Variance*
2D Control	3	8,187	2,729	4,9E-05
2D Etoposide	3	3,597	1,199	9E-06
2D TMZ	3	3,607	1,202333	2,33E-06

ANOVA

Source of Variation	*SS*	*df*	*MS*	*F*	*P-value*	*F crit*
Between Groups	4,671622	2	2,335811	116145,3	1,72E-14	27
Within Groups	0,000121	6	2,01E-05			
Total	4,671743	8				

SUMMARY

Groups	*Count*	*Sum*	*Average*	*Variance*
HD Control	3	7,261	2,420333	3,03E-05
HD Etoposide	3	5,26	1,753333	0,00053
HD TMZ	3	5,384	1,794667	4,43E-05

ANOVA

Source of Variation	*SS*	*df*	*MS*	*F*	*P-value*	*F crit*
Between Groups	0,838056	2	0,419028	2077,825	3E-09	27
Within Groups	0,00121	6	0,000202			
Total	0,839266	8				

SUMMARY

Groups	*Count*	*Sum*	*Average*	*Variance*
3D Control	3	5,338	1,779333	9,03E-05
3D Etop	3	5,015	1,671667	0,000137
3D TMZ	3	5,05	1,683333	3,03E-05

ANOVA

Source of Variation	*SS*	*df*	*MS*	*F*	*P-value*	*F crit*
Between Groups	0,020944	2	0,010472	121,7687	1,39E-05	27
Within Groups	0,000516	6	0,000086			
Total	0,02146	8				